Superperturbation theory for correlated fermions

Dissertation

zur Erlangung des Doktorgrades

des Fachbereiches Physik

der Universität Hamburg

vorgelegt von

Christoph Jung

aus Limburg an der Lahn

Hamburg

2010

Gutachter der Dissertation:
Prof. Dr. A. Lichtenstein
J. Prof. Dr. F. Lechermann

Gutachter der Disputation:
Prof. Dr. A. Lichtenstein
Prof. Dr. A. Rubtsov

Datum der Disputation:
15.12.2010

Vorsitzender des Prüfungsausschusses:
Dr. A. Chudnovskiy

Vorsitzender des Promotionsausschusses:
Prof. Dr. J. Bartels

Dekan der MIN-Fakultät:
Prof. Dr. Heinrich Graener

Abstract

This thesis is devoted to new numerical approaches for the treatment of strongly correlated systems: The dual fermion perturbation theory is generalized to much broader scope, which is not limited to the treatment of correlated lattice models. By considering three different problems, it is shown that the dual fermion scheme is a formalism, which allows to perform a perturbation expansion around an exactly solvable reference system, which has been optimized for the investigation of the particular physical situation. The three examples are:

- The superperturbation impurity solver for quantum impurity problems. Here a finite size system, which can be solved using exact diagonalization, is used to approximate a bath with a continuous energy spectrum. Several exact limits of the approach are discussed and a way to directly compute the density of states on the real axis is introduced. The meaning of the reference system is analyzed in terms of the Kondo problem and a possible application as a solver for the DMFT is discussed. At the end of the chapter a renormalization procedure is formulated, which alleviates the non-causality problem, that can occur at low temperatures.

- The variational lattice approach (VLA). The VLA is a variant of the classical dual fermion approach, which also utilizes exact diagonalization as an impurity solver for the reference system. Using this approach the Mott metal insulator transition is analyzed and the results are compared to a previous CDMFT study. By employing Padé analytic continuation the pseudogap formation in the bad-metal regime is investigated.

- The superperturbation impurity solver for quantum impurity problems out of equilibrium. At the end of the thesis the dual approach is generalized to systems out of equilibrium within the Keldysh framework. A discretization scheme for the numerical treatment is discussed and first results are presented.

Kurzzusammenfassung

Diese Arbeit ist neuen numerischen Ansätzen für die Behandlung von stark korrelierten Systemen gewidmet. Die Methode der dualen Fermionen wird in ihrem Bedeutungsrahmen erweitert, der nicht auf die Behandlung von korrelierten Gittermodellen begrenzt sein muss. Anhand von drei Problemstellungen wird gezeigt, dass die duale Störungstheorie ein Formalismus ist, der es erlaubt eine Störungsentwicklung um ein exakt lösbares Bezugssystem zu formulieren, welches für die Untersuchung des vorliegenden physikalischen Problems optimiert wurde. Die drei Beispiele sind:

- Das Superperturbations Verfahren zur Lösung von quantenmechanischen Störstellenproblemen. Hierbei wird eine Näherung für eine Störstelle in einem Bad mit kontinuierlichem Energiespektrum mit Hilfe eines Bades endlicher Größe konstruiert, welches dann durch exakte Diagonalisierung gelöst werden kann. Danach werden mehrere exakte Grenzfälle der Theorie erörtert und eine Methode zur direkten Berechnung der Zustandsdichte auf der reellen Achse vorgestellt. Die Bedeutung des Referenzsystems wird im Kontext des Kondo Problems analysiert und eine Anwendung der Methode als Lösungsverfahren für die dynamische Molekularfeldtheorie diskutiert. Am Ende des Kapitels wird ein Renormierungsverfahren eingeführt, das Nicht-Kausalitätsprobleme, die bei tiefen Temperaturen auftreten können, behebt.

- Die Variations-Gitter Näherung (VLA). VLA ist eine Variante des klassischen Ansatzes dualer Fermionen, welche auch exakte Diagonalisierung zum Lösen des Störstellenproblems einsetzt. Mit Hilfe dieser Methode wurde der Mott Übergang analysiert und mit den Ergebnissen früherer CDMFT Untersuchungen verglichen. Um die Pseudo-Bandlücke im metallischen Regime zu untersuchen, wurde eine analytische Fortsetzung mit Hilfe von Padé auf die reelle Achse durchgeführt.

- Das Superperturbations Verfahren zur Lösung von quantenmechanischen Störstellenproblemen im Nichtgleichgewicht. Am Ende der Arbeit wird der Ansatz der dualen Fermionen auf Nichtgleichgewichts Systeme verallgemeinert. Dies wird

mit Hilfe der Keldysh Theorie bewerkstelligt. Ein Schema zur numerischen Behandlung der auftretenden Größen wird eingeführt und erste Ergebnisse werden präsentiert.

"I may not have gone where I intended to go, but I think I have ended up where I needed to be."

Douglas Adams
English humorist & science fiction novelist (1952 - 2001)

Contents

Chapter 1

Introduction

Understanding and controlling the physical properties of solid state materials is an aspect of condensed matter physics, which pervades everyday life. The development of transistors and semiconducting devices on the nanoscale level affected the progress in modern telecommunication techniques with such a strong impact that the change in our society is comparable to that caused by the invention of the steam-engine in the 18th century.

Today, personal computers can be found in nearly every household and almost every machine is controlled by this kind of device. This historical success has two main ingredients: Understanding of the underlying physical concepts and, deduced from this knowledge, the ability to control these features.

A subclass of modern materials, which can be efficiently controlled by external parameters, are strongly correlated compounds. In this case the term correlated means that the electrons in the system can no longer be described in an effective single particle picture, but one has to rely on methods which take into account the effect of electron-electron interaction on the quantum nature of the particles itself. These compounds are often made of atoms with open d- or f-shells, which leads to a sensitive equilibrium of two fundamental properties of the electrons, their particle- and wavelike character. If the Coulomb interaction is of the same order as the kinetic energy of the conducting electrons, a strong competition between a growing localization and the tendency towards

a free motion dominates the physical properties of these materials. This fragile balance can be easily changed by adjusting external control parameters such as pressure or temperature. Consequently, strongly correlated materials fulfill the first requirement for future applications: Their behavior can be technically controlled very easily.
The second ingredient, understanding the properties of correlated systems is a not so easy task to accomplish. In principle all properties of an electron system are described by a N-electron Hamilton operator in the Born-Oppenheimer approximation

$$H = \sum_{i=1}^{N} \left(\frac{\hbar^2}{2m} \nabla^2 + V(r_i) \right) + e^2 \sum_{i<j} \frac{1}{|r_i - r_j|}, \tag{1.1}$$

but since N is of the order of 10^{23} a full solution of the corresponding Schrödinger equation is not possible. The situation can be compared to the analysis of the human genome: The structure of the DNA is known, but the practical meaning of the genetic code is often obscure, because the amount of information embedded in the DNA is extremely huge. In equation (1.1) the situation is the same: The main ingredients, the expression for the interaction and the kinetic energy are known, but the complexity of the problem makes it impossible to find a solution which depends on all 10^{23} degrees of freedom. Therefore proper approximation schemes to the correlated many body problem have to be found.
In the case of weak correlations several notable approaches such as the Landau Fermi-liquid theory or the density functional theory (DFT) have been introduced. The DFT for example is nowadays a very common tool for the description of realistic materials and is able to reproduce experimental results to a very high accuracy. The basic idea of the approach originates from two theorems by Kohn and Hohenberg, which state that the ground state energy of an electronic system minimizes an universal functional of the ground state density, which only depends on three spatial coordinates. This reduction from 10^{23} degrees of freedom to 3 is the main reason for the success of the density functional theory and related approaches.
Although the DFT is a very successful theory, it fails to describe systems where strong correlations are the important ingredient, as for example the Mott metal-insulator transition. In these cases another route is taken: The problem is mapped onto a minimal

model, which exhibits the same characteristic features. One of the simplest descriptions of correlated fermions on a lattice offers the Hubbard model:

$$H = -t \sum_{\langle ij \rangle, \sigma} (c^*_{i,\sigma} c_{j,\sigma +\text{ h.c.}}) + U \sum_{i=1}^{N} n_i^{\uparrow} n_j^{\downarrow}, \tag{1.2}$$

where $\langle ij \rangle$ indicates a sum over nearest neighbors. Even though the latter Hamiltonian is a strong simplification in comparison to Eq. (1.1), the complexity is still very high and an approximation has to be applied in order to find a solution. A very simple approach is perturbation theory: A solution is searched in a region where either the interaction U or the hopping t is small. The starting point of such a perturbation expansion is consequently the free lattice or the interacting atom. But one can imagine that it is extremely hard for a perturbation expansion to reach the other limiting case, therefore perturbative approaches often fail in the intermediate regime where a phase transition takes place.

A way out of this dilemma was the invention of the dynamical mean field theory (DMFT). Here the basic idea is to replace the correlated lattice by an impurity embedded in an effective medium plus a self-consistency condition. Nowadays such an impurity problem can be solved exactly with the help of continuous-time quantum Monte Carlo. The efficiency of these solvers had a very strong impact on the promotion of this theory.

One important feature of the DMFT is that the theory is exact in both of the above described limits and offers therefore a more adequate description of correlated systems in the intermediate regime. Additionally it was shown by Metzner and Vollhardt that the DMFT is also exact in an infinite coordination number limit. In lower dimensions the DMFT still catches local temporal quantum fluctuations, but spatial correlations are neglected. Several cluster extensions of the DMFT have been discussed in the literature, which were able to alleviate the problem as long as only short ranged non-local correlations were concerned.

An important extension to the DMFT was brought up by Rubtsov and coworkers, who were able to construct a perturbation expansion around an arbitrary impurity problem by applying a fermionic Hubbard-Stratonovich transformation to new so-called dual variables. The approach, called dual fermion, has been successfully applied to several

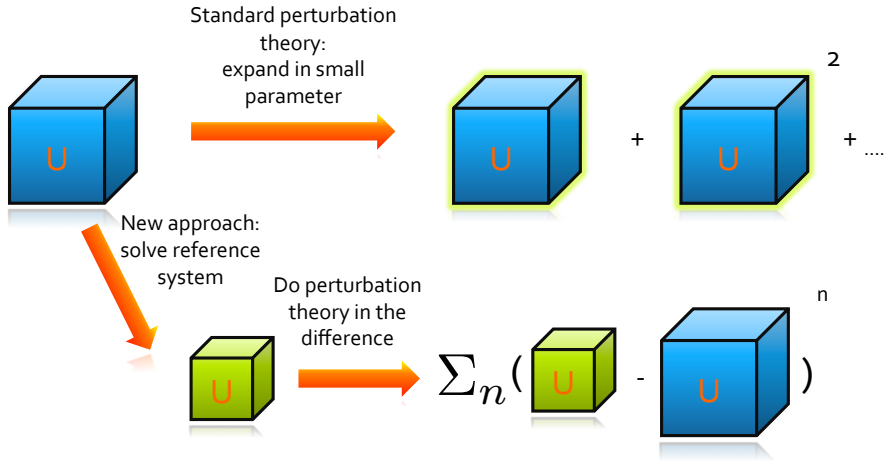

FIGURE 1.1: General concept of the dual perturbation theory: Instead of expanding a large interacting system (blue box) in a small parameter (horizontal arrow), a reference system (green box) is constructed, which contains as much of the essential physics as possible. A transformation to new fermionic variables allows to formulate a perturbation expansion in the difference between both systems.

strongly correlated problems.

This thesis intends to show that the perturbation theory introduced by Rubtsov is an approach of a much broader scope and that the theory can be easily adapted to very different physical problems. The basic idea is illustrated in figure 1.1. Suppose the solution of an interacting fermionic problem (blue box) is required, but the amount of correlated degrees of freedom makes a numerical or analytic treatment impossible. As described earlier a standard approach would be to expand in a hopefully small parameter and to find an approximate solution (horizontal arrow), which often ends up in the earlier described problems. An alternative scheme (lower arrow) is to construct a reference system (green box), which already contains as much of the essential physics as possible and to solve this system exactly. The dual approach then allows to perform a perturbation expansion in the difference between the reference and the full system. In this thesis three possible variants of the scheme are discussed: The superperturbation solver for the Anderson impurity model, which uses a finite-size reference system to approximate

a continuous bath, the variational lattice approach (VLA) for correlated lattices, a variant of the original dual fermion, which is also based on exact diagonalization, and the superperturbation solver for time dependent problems, which is able to treat systems out of equilibrium.

1.1 Structure of the thesis

This thesis is organized as follows: In the first chapters we review the theoretical background of the dual fermion perturbation theory. This includes a discussion of the Anderson impurity model, as the prototype of a reference system (chapter 2), and a survey of efficient numerical methods to solve this model (chapter 3).
In chapter 4 the dual theory for the equilibrium case is deduced. In comparison to earlier derivations the formulation will be general enough to hold for all equilibrium variants of the dual theory: the superperturbation, the VLA and the lattice dual fermion.
In chapters 5 and 6 the superperturbation solver and the VLA will be introduced. Given that the dual theory has been already discussed in chapter 4 those sections will mainly focus on the results, but they will contain enough background information to read them separately from the rest of the thesis.
Chapter 7 has an exceptional position in this thesis. The superperturbation solver will be generalized to non-equilibrium phenomena, therefore it is necessary to review the Keldysh theory for systems out of equilibrium and to reformulate the dual theory in this formalism. In the last chapter the results are summarized and several possibilities for future projects are discussed.

Chapter 2

Anderson Impurity model

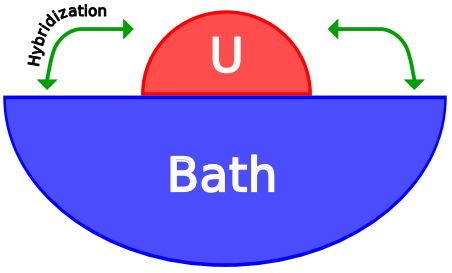

FIGURE 2.1: The Anderson impurity model describes an interacting impurity coupled to a free electronic bath.

As already mentioned in the introduction, it is the main intention of this thesis to show that the recently developed dual fermion approach can be understood as a general framework to do a perturbation expansion of a large interacting fermionic system around a non-trivial starting point. In the following chapter we would like to present the prototype of such an initial reference system: the Anderson impurity model (AIM).
The AIM was introduced by Anderson [1] to describe the behavior of a magnetic moment in a metallic host. The system is described by an interacting impurity, embedded in a bath of free electrons. The bath electrons are allowed to hop on and off the impurity and if two electrons with opposite spin occupy the impurity at the same time, they have

to pay the price of a local Hubbard U. This combination of time depended retardation effects and fermionic interaction can lead to interesting new many body phenomena such as a Kondo resonance [2]. Despite the zero dimensional nature of the problem, the numerical solution of the model is a quite challenging task. Nevertheless, there a many highly efficient solvers available [3–5], so that it is possible to use the AIM as a starting point for our perturbation theory.
In the following we start by introducing the Hamiltonian of the AIM and derive the equilibrium action formulation of the system in its discretized version. In doing so we try to indicate the possible differences to the AIM on the Keldysh contour, described in chapter 7.

2.1 From the Hamiltonian to a coherent state path integral formulation

The Hamiltonian of a general AIM can be written in the following form:

$$H = \sum_{k\alpha} \epsilon^b_{k\alpha} b^\dagger_{k\alpha} b_{k\alpha} + \sum_{\alpha} \epsilon^c_\alpha c^\dagger_\alpha c_\alpha + H_{\mathrm{loc}}[c^\dagger, c] + \sum_{k\alpha\beta} \left(V_k^{\alpha\beta} c^\dagger_\alpha b_{k\beta} + V_k^{*\beta\alpha} b^\dagger_{k\alpha} c_\beta \right). \quad (2.1)$$

In this expression Greek letters are used as a combined index for orbital and spin degrees of freedom, $b^\dagger$ and b are the bath, $c^\dagger$ and c the impurity creation and annihilation operators.
The first term describes the dispersion of the free electronic bath. States with different momentum have been labelled by an additional index k. The interacting impurity is characterized by the second and third expression. The second one defines the free energy spectrum of the impurity and H_{loc} is some local electron-electron interaction. The last part describes the hoping of an electron from the bath to an impurity state and the reverse process.
Most of the approaches to solve the AIM discussed in this thesis rely on the coherent state path integral formulation of the problem. In the following this representation of the AIM is deduced. Therefore the partition function is written as a trace over coherent

states:

$$Z = \mathrm{Tr}\, e^{-\beta H} = \int \prod_{\alpha} d(c_\alpha^*, c_\alpha)\, e^{-\sum_\alpha c_\alpha^* c_\alpha} \langle -c| e^{-\beta H} |c\rangle. \tag{2.2}$$

The key idea to reformulate the last expression in a path integral manner is to rewrite the expectation value of the partition operator as an integral over an imaginary time evolution operator $U(\tau, \tau') = \exp(-(\tau - \tau')H)$ on the interval $\big[0, \beta\big)$. Afterwards the integral is linearized by insertion of coherent state unity matrices on a infinitesimal dense time grid and by utilization of the composition property of the imaginary time evolution operator. The minus sign in the bra vector of Eq. (2.2), a direct consequence of the anti-commuting character of the fermionic operators, will define the boundary conditions on the imaginary time interval. The completeness relation for coherent states reads:

$$\mathbb{1}_{\mathcal{F}} = \int \prod_{\alpha} d(c_\alpha^*, c_\alpha)\, e^{-\sum_\alpha c_\alpha^* c_\alpha} |c\rangle\langle c|. \tag{2.3}$$

Applying the described steps, the partition function can be written in the following form:

$$Z = \lim_{M\to\infty} \int \prod_{k=1}^{M} \prod_{\alpha} d(c_{\alpha k}^*, c_{\alpha k}) e^{-\sum_\alpha c_{\alpha k}^* c_{\alpha k}} \langle -c_1| e^{-\Delta\tau H} |c_M\rangle \ldots \langle c_2| e^{-\Delta\tau H} |c_1\rangle \tag{2.4}$$

$$\begin{aligned} = \lim_{M\to\infty} \int \prod_{k=1}^{M} \prod_{\alpha} d(c_{\alpha k}^*, c_{\alpha k}) e^{-\sum_\alpha c_{\alpha k}^* c_{\alpha k}} e^{-c_1^* c_M - \Delta\tau H(-c_1^* c_M)} \times \\ \ldots \times e^{c_3^* c_2 - \Delta\tau H(c_3^* c_2)} \times e^{c_2^* c_1 - \Delta\tau H(c_2^* c_1)} \end{aligned} \tag{2.5}$$

$$= \lim_{M\to\infty} \int \prod_{k=1}^{M} \prod_{\alpha} d(c_{\alpha k}^*, c_{\alpha k}) e^{-S(c_{\alpha k}^*, c_{\alpha k})}, \tag{2.6}$$

with the following expression for the discretized action:

$$\begin{aligned} S(c_{\alpha k}^*, c_{\alpha k}) =& \Delta\tau \sum_{k=2} \Big[\sum_\alpha c_{\alpha k}^* \big(\frac{c_{\alpha k} - c_{\alpha k-1}}{\Delta\tau} \big) + H(c_{\alpha k}^*, c_{\alpha k-1}) \Big] \\ &+ \Delta\tau \Big[\sum_\alpha c_{\alpha 1}^* \big(\frac{c_{\alpha 1} + c_{\alpha M}}{\Delta\tau} \big) + H(-c_{\alpha 1}^*, c_{\alpha M}) \Big]. \end{aligned} \tag{2.7}$$

$$S(c^*_{\alpha k}, c_{\alpha k}) = \sum_{j,k=1}^{M} c^*_j S^{(\alpha)}_{jk} c_k$$

$$S^{(\alpha)}_{jk} = G_0^{-1} = \begin{pmatrix} G^{-1}_{\text{imp}} & \hat{V} \\ \hat{V} & G^{-1}_{\text{bath}} \end{pmatrix} = \left(\begin{array}{ccc|ccc} 1 & 0 & +a_i & 0 & 0 & -v \\ -a_i & 1 & 0 & v & 0 & 0 \\ 0 & -a_i & 1 & 0 & v & 0 \\ \hline 0 & 0 & -v & 1 & 0 & +a_b \\ v & 0 & 0 & -a_b & 1 & 0 \\ 0 & v & 0 & 0 & -a_b & 1 \end{array}\right)$$

EXAMPLE 2.1: Example of an interaction free two site model. The Hamiltonian is given by $H = \epsilon_i c^\dagger c + \epsilon_b b^\dagger b + (V c^\dagger b + \text{h.c.})$. In this special case the discretized action can be represented as a matrix, which is diagonal in time but nondiagonal in orbital indices. Terms in the right upper edges (red) are a direct consequence of the antiperiodic bounding conditions on the imaginary time contour. These terms correspond to ρ terms in Kledysh theory. The following abbreviations have been used: $v = V\Delta\tau$, $a_{i/b} = 1 - \Delta\tau\epsilon_{i/b}$.

The last line of Eq. (2.7) corresponds to a boundary condition term caused by the anti-commuting properties of the fermionic operators[1], which states that the system should be anti periodic on the imaginary time interval. An example for a discretized action is given in Ex. 2.1.

Taking the limit $\Delta\tau \to 0$, the action can be written in a continuous form:

$$\begin{aligned} S = \int_0^\beta \Bigg(& \sum_\alpha c^*_\alpha(\tau)(\partial_\tau - \mu + \epsilon^c_\alpha) c_\alpha(\tau) + \sum_{k\alpha} b^*_{k\alpha}(\tau)(\partial_\tau - \mu + \epsilon^b_{k\alpha}) b_\alpha(\tau) \\ & + H_{loc}[c^*, c] + \sum_{k\alpha\beta} \left(V_k^{\alpha\beta} c^*_\alpha b_{k\beta} + V_k^{*\beta\alpha} b^*_{k\alpha} c_\beta \right) \Bigg) d\tau. \end{aligned} \tag{2.8}$$

Here the reader should be aware that the boundary term of Eq. (2.7) is implied. In addition to that it has to be clear that Eq. (2.7) is the only discretization of expression (2.7) which will give the right physics. This is important if for some reason a discretization is necessary.

In the next step the action is reduced to a form, which only depends on impurity degrees

[1] In comparison to the Keldysh formalism introduced in chapter 7, this term is replaced by an analogous expression containing the density matrix at the starting time.

of freedom. This is done by integrating out the Gaussian bath by application of the following identity for Grassmann numbers:

$$\int \prod_{i=1}^{n} d(b_i^*, b_i) \exp\left(-b_i^*(G_0^{-1})_{ij} b_j + c_i^* \hat{V}_{ij} b_j + b_i^* \hat{V}_{ij}^\dagger c_j\right) = \det G_0^{-1} \exp(c_i^* \left[\hat{V}(G_0^{-1})^{-1}\hat{V}^\dagger\right]_{ij} c_j). \quad (2.9)$$

With this the action can be written in its final version, only depending on impurity indices, but with an additional integration variable τ', which is caused by the Gaussian part being no longer diagonal in time:

$$\begin{aligned} S = \iint_0^\beta \Bigg(\sum_{\alpha\beta} c_\alpha^*(\tau) \Big[&(\partial_\tau - \mu - \epsilon_\alpha^c)\delta_{\alpha\beta}\delta(\tau - \tau') \\ &+ \left(\hat{V}(\partial_\tau - \mu - \epsilon_\alpha^b)^{-1}\hat{V}^\dagger\right)_{\alpha\beta} \Big] c_\beta(\tau') + H_{\text{loc}}[c^*, c] \Bigg) d\tau d\tau' \end{aligned} \quad (2.10)$$

$$\begin{aligned} = \iint_0^\beta \Bigg(\sum_{\alpha\beta} c_\alpha^*(\tau) \Big[&(\partial_\tau - \mu - \epsilon_\alpha^c)\delta_{\alpha\beta}\delta(\tau - \tau') + \Delta_{\alpha\beta}(\tau - \tau') \Big] c_\beta(\tau') \\ &+ H_{\text{loc}}[c^*, c] \Bigg) d\tau d\tau', \end{aligned} \quad (2.11)$$

with $\Delta_{\alpha\beta}(\tau - \tau') = (\hat{V}(\partial_\tau - \mu - \epsilon_\alpha^b)^{-1}\hat{V}^\dagger)_{\alpha\beta}$. In the case at hand, the problem can be further simplified by introducing Matsubara frequencies, which automatically take care of the antiperiodic boundary conditions.[2] The Fourier transform is defined in the following way:

$$c(\tau) = \frac{1}{\beta} \sum_{\omega_n} c(\omega_n) e^{-i\omega_n \tau} \quad (2.12)$$

$$c^*(\tau) = \frac{1}{\beta} \sum_{\omega_n} c^*(\omega_n) e^{+i\omega_n \tau}. \quad (2.13)$$

[2] In the Keldysh theory, there is no frequency representation, which automatically takes care of the boundary conditions. This is one of the major difficulties one encounters when working on the Keldysh contour.

After performing the Fourier transform the final result reads:

$$S = -\frac{1}{\beta}\left(\sum_{\substack{\alpha\beta\\ \omega_n}} c^*_\alpha(\omega_n)\Big((i\omega_n + \mu - \epsilon^c_\alpha)\delta_{\alpha\beta} - \Delta_{\alpha\beta}(i\omega_n)\Big)c_\beta(\omega_n)\right) + H_{loc}[c^\dagger, c] \tag{2.14}$$

$$= -\frac{1}{\beta}\left(\sum_{\substack{\alpha\beta\\ \omega_n}} c^*_\alpha(\omega_n)\Big((G_0)^{-1}_{\alpha\beta}\Big)c_\beta(\omega_n)\right) + H_{loc}[c^\dagger, c], \tag{2.15}$$

with

$$\Delta_{\alpha\beta} = \sum_{k,\gamma} \frac{V_{k\alpha\gamma}V^*_{k\gamma\beta}}{i\omega - \epsilon_{k\gamma}} \tag{2.16}$$

and

$$(G_0)^{-1}_{\alpha\beta} = (i\omega_n + \mu - \epsilon^c_\alpha)\delta_{\alpha\beta} - \Delta_{\alpha\beta}(i\omega_n). \tag{2.17}$$

2.2 Dynamical Mean Field Theory

In this paragraph the dynamical mean field theory (DMFT) is reviewed as one application of the AIM. The intention is to show that the description of strongly correlated systems by means of a quantum mean-field, which fully takes into account local fluctuations, has great advantages over a standard perturbation theory and is a good starting point for a general perturbation theory. Today the DMFT is a standard tool for the investigation of strongly correlated lattices [6] and has been applied in the equilibrium and non-equilibrium case to various models and real materials [7–9].

The main concept of the DMFT is to replace the correlated lattice by a single impurity embedded in a self-consistent effective medium. In contrast to a classical mean field approach the effective medium in the DMFT is represented by an energy dependent function and therefore takes fully into account local temporal fluctuations, whereas spatial correlations of the lattice are frozen out. The energy dependence of the Weiss field in combination with a fixed chemical potential allows to automatically calculate quantities in the thermodynamic limit. Additionally the DMFT combines two very different energy scales in one single approach: The method is able to treat large atomic energies, stemming from the impurity, on the same footing with small excitations on the Fermi

level described by the Weiss field. Consequently, it is possible for example to describe the physics of Hubbard satellites and Kondo resonances in the same model.
Furthermore it has been shown that the DMFT is exact in various limits. The method gives the correct results for an interaction-free lattice as well as for a non-coupled compound of atoms. A very special case is the limit of a lattice with an infinite coordination number. It has been observed by Metzner and Vollhardt [10] that in this case the spatial correlations of the lattice vanish and the DMFT equations become exact.
In realistic situations with dimensionality lesser than infinity the DMFT has often proven to be a good approximation. In cases where spatial correlations can not be neglected, various cluster extensions [11] of the DMFT like the CDMFT, DCA and VCA are available, which take into account short ranged spatial correlations.

2.2.1 Cavity construction

There are several ways to derive the DMFT equations, among others the possibility to deduce the DMFT as a zero order approximation of the dual perturbation theory described in this thesis. Here we introduce the so-called cavity construction. The key idea is to focus on one lattice site and to integrate out the effect of the remaining sites. The main concept of this construction is depicted in Fig. 2.2. Here we perform the construction for a one-orbital, spin-diagonal Hubbard model on a hypercubic lattice. The corresponding action can be written in the following form:

$$S = \sum_i S_i^{\mathrm{Site}} + \sum_{\langle ij \rangle} S_{ij}^{\mathrm{hop}}, \tag{2.18}$$

with

$$S_i^{\mathrm{Site}} = \sum_\sigma \int_0^\beta d\tau \, c_{i\sigma}^*(\tau)[\partial_\tau - \mu] c_{j\sigma}(\tau) + S^{\mathrm{NG}}[c_i^*, c_i] \tag{2.19}$$

$$S_{ij}^{\mathrm{hop}} = \sum_\sigma \int_0^\beta d\tau \, [t_{ij} c_{i\sigma}^*(\tau) c_{j\sigma}(\tau) + t_{ji} c_{j\sigma}^*(\tau) c_{i\sigma}(\tau)]. \tag{2.20}$$

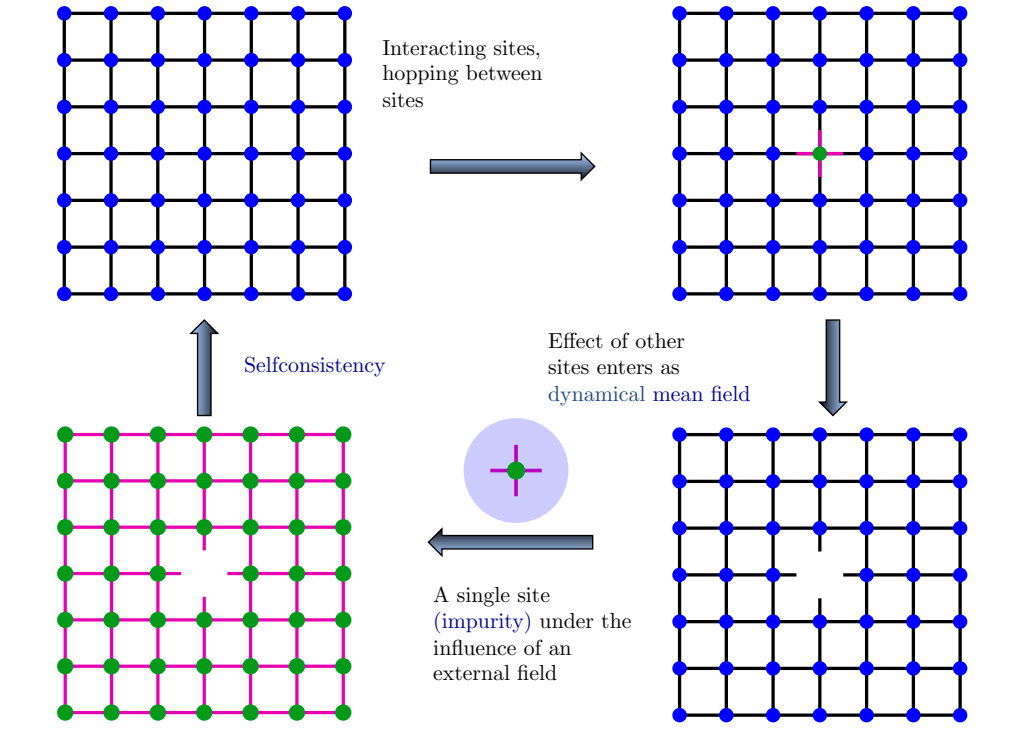

FIGURE 2.2: Illustration of the cavity construction for the DMFT: The interacting lattice (upper left) is replaced by a single site which exchanges particles with an electronic bath (upper right). The bath is given by the cavity, i.e. the lattice with one site missing (lower right). Since the cavity correlators are not known a priori, the problem is solved in a self-consistent manner in the $d = \infty$ limit, when non-local correlations in the cavity can be neglected. In this case the problem can be reduced to the solution of an AIM with a self-consistency condition.

S_i^{Site} is the local contribution for site i containing a non-Gaussian interaction part, which is abbreviated with S^{NG}. S_{ij}^{hop} describes nearest neighbor hopping. To end up with a formulation in which one site is separated from the rest of the lattice, the action in (2.18) is reformulated in the following way:

$$S = S_0^{\text{Site}} + S^{\text{c}} + S^{\Delta}. \tag{2.21}$$

Here S_0^{Site} represents all action components which are local on the separated site, which is called site zero in the following. S^{c} is the action of the cavity, it contains all on-site terms and hoppings of the lattice excluding site zero. S^{Δ} contains all hopping terms

from the cavity to site zero and back. The formal definition of S^{c} and S^{Δ} is given in the following:

$$S^{\mathrm{c}} = \sum_{i\neq 0} S_i^{\mathrm{Site}} + \sum_{\substack{\langle ij\rangle \\ i,j\neq 0}} S_{ij}^{\mathrm{hop}}, \tag{2.22}$$

$$S^{\Delta} = \sum_{j} S_{0j}^{\mathrm{hop}}. \tag{2.23}$$

Now the cavity is integrated out by defining the effective action of site zero as an integral over all remaining degrees of freedom:

$$\frac{1}{Z_{\mathrm{eff}}} e^{-S^{\mathrm{eff}}}[c_0^*, c_0] = \frac{1}{Z} \int e^{-S[c_i^*, c_i]} D[c_{i\neq 0}^*, c_{i\neq 0}]. \tag{2.24}$$

These integrals are evaluated by Taylor expansion of S^{Δ}. The resulting terms are then averaged over S^{c}.

$$Z = \int e^{-S[c_i^*, c_i]} = \int e^{-S_0^{\mathrm{Site}}} \int e^{-S^{\mathrm{c}}} \sum_{n=0}^{\infty} \frac{1}{n!} (S^{\Delta})^n D[c_{i\neq 0}^*, c_{i\neq 0}] D[c_0^*, c_0] \tag{2.25}$$

$$= \int e^{-S^{\mathrm{Site}}} D[c_0^*, c_0] Z^{\mathrm{c}} \sum_{n=0}^{\infty} \frac{1}{n!} \langle (S^{\Delta})^n \rangle_{\mathrm{c}} \tag{2.26}$$

The first non-trivial term in this expansion is given by:

$$\frac{1}{2!} \langle (S^{\Delta})^2 \rangle_{\mathrm{c}} = \sum_{\sigma} \iint_0^{\beta} d\tau d\tau' \, c_{0\sigma}^*(\tau) \sum_{ij} t_{0i} t_{j0} \langle c_{i\sigma} c_{j\sigma}^* \rangle_{\mathrm{c}} \, c_{0\sigma}(\tau'). \tag{2.27}$$

This expression describes a sequential hopping process, where an electron hops from site zero to site i and propagates in the cavity from i to j via the correlator $\langle c_{i\sigma} c_{j\sigma}^* \rangle_{\mathrm{c}}$ and hops back to site zero. The general result for Eq. (2.26) involves all orders of correlation functions of the cavity and takes the following form:

$$\begin{aligned} S^{\mathrm{eff}} = S_0^{\mathrm{Site}} + \sum_{n=0}^{\infty} \sum_{\sigma} \sum_{i_1 \ldots j_n} \int \cdots \int_0^{\beta} d\tau_1 d\tau_1' \ldots d\tau_n d\tau_n' \, t_{0i_1} t_{j_1 0} \ldots t_{0i_n} t_{j_n 0} \\ \times c_{0\sigma}^*(\tau_1) c_0(\tau_1') \ldots c_{0\sigma}^*(\tau_n) c_0(\tau_n') G_{i_1 j_1 \ldots i_n j_n}^{\mathrm{c}\,\sigma}(\tau_1, \tau_1', \ldots, \tau_n, \tau_n'). \end{aligned} \tag{2.28}$$

The last equation is no simplification in comparison to the initial action formulation in Eq. (2.18), since the correlators of the cavity are not known. It was the observation of Metzner and Vollhardt [10] that Eq. (2.28) strongly simplifies in the limit of infinite coordination number. In this case the hopping amplitude t_{ij} has to be rescaled by a factor of $1/\sqrt{z}$, wherein z is the coordination number. This necessity could be best understood by reviewing Eq. (2.27). In this case the summands have to be proportional to $1/z^2$ in order to keep the two dimensional sum over nearest neighbors finite. Since the single particle Green's function is in the lowest order proportional to $t^{|i-j|}$, with $|i-j|$ being the Manhattan distance of the lattice, the total summand is proportional to t^4 on a hyper-cubic lattice. Hence a scaling $t_{ij} \to \tilde{t}_{ij}/\sqrt{z}$ will keep the lowest order term finite. All terms which involve higher order Green's function vanish in the $z \to \infty$ limit, because they are proportional to $(1/z)^{n-2}$, with n being the expansion order of Eq. (2.28). Consequently, only the contribution of Eq. (2.27) survives. This leads to the following definition for the effective action in the infinite coordination number limit:

$$S^{\text{eff}} = \sum_{\sigma} \int_0^\beta d\tau \int_0^\beta d\tau'\, c^*_{0\sigma}(\tau) \left[\partial_\tau - \mu - \epsilon_0 - \sum_{\langle ij \rangle} t_{0i} G^{\text{c}\,\sigma}_{ij} t_{j0} \right] c_{0\sigma}(\tau') + S^{\text{NG}}[c^*_0, c_0] \tag{2.29}$$

$$= \sum_{\sigma} \int_0^\beta d\tau \int_0^\beta d\tau' \left[-c^*_{0\sigma}(\tau) (\mathcal{G}^\sigma(\tau - \tau'))^{-1} c_{0\sigma}(\tau') + S^{\text{NG}}[c^*_0, c_0] \right]. \tag{2.30}$$

Here the Weiss function $\mathcal{G}^\sigma$ has been defined in the following way:

$$(\mathcal{G}^\sigma(i\omega))^{-1} = (i\omega + \mu - \epsilon_0) - \sum_{\langle ij \rangle} t_{0i} G^{\text{c}\,\sigma}_{ij} t_{j0}. \tag{2.31}$$

This equation is extremely important, because it connects $\mathcal{G}^\sigma$ with the cavity Green's function $G^{\text{c}\,\sigma}_{ij}$. The last step to receive a closed set of equations is to relate the cavity Green's function to the Green's function of the original lattice. In general this step is more involved but takes a very simple form on the Bethe lattice [12] in infinite dimensions. A mathematical representation of this lattice is a Cayley tree with infinite connectivity. A Cayley tree of connectivity 3 is depicted in Fig. 2.3. In this special geometry nearest neighbors of site zero are disconnected in the cavity, if site zero is removed. Consequently,

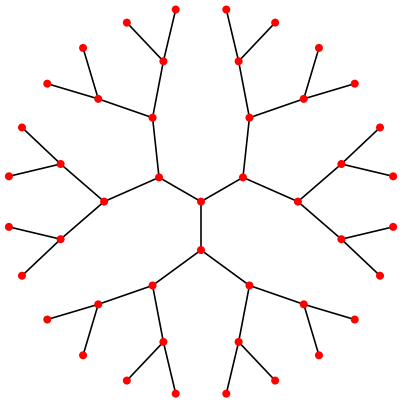

FIGURE 2.3: Cayley tree for coordination number $z = 3$.

the cavity Green's function is diagonal in nearest neighbor indices: $G^{c\,\sigma}_{ij} = G^{c\,\sigma}_{ii}\delta_{ij}$. Additionally, the cavity Green's function is equal to the Green's function of the full lattice G, since the removal of site zero doesn't matter in the limit of infinite coordination number. For the Bethe lattice the final DMFT equation, which connects the Weiss function to the Green's function of the full lattice, reads:

$$(\mathcal{G}^{\sigma}(i\omega))^{-1} = (i\omega + \mu - \epsilon_0) - tG^{\sigma}(i\omega)t. \tag{2.32}$$

This non-linear equation is technically solved by a self-consistent iteration with a guess for the initial Weiss function. So normally the scheme is started by either taking the free or the atomic limit.

In the following we will briefly review the self-consistency loop in its general form. This loop is depicted in Fig. 2.4. To start the iteration, a guess for the Weiss field $\mathcal{G}$ is generated by employing the atomic Green's function or by just setting the self-energy to zero. With this initial assumption for $\mathcal{G}$ the AIM is well defined and can be solved by various methods, which will be described in the next chapter. The result of the numerical evaluation is the impurity Green's function, which is abbreviated by g. Using this function and the input Weiss field $\mathcal{G}$, it is possible to extract the self-energy by applying Dyson equation:

$$\Sigma(i\omega) = \mathcal{G}^{-1}(i\omega) - g^{-1}(i\omega). \tag{2.33}$$

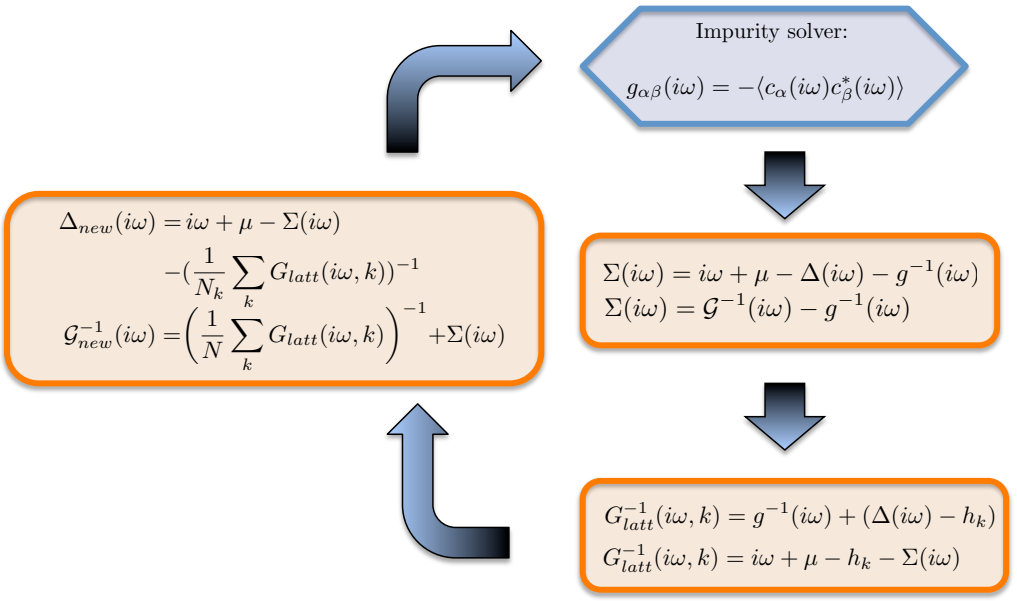

FIGURE 2.4: Illustration of the standard DMFT cycle (upper equations are formulated in terms of the hybridization function Δ, lower equations in terms of $\mathcal{G}$): The self-consistency loop is started in the left box with an initial guess for the Weiss field, which specifies the AIM. In the next step the impurity problem is solved and an impurity Green's function is determined. From this quantity the local self-energy is obtained. Afterwards the self-energy is used to construct the lattice Green's function and a new Weiss field. With the new Weiss field the self-consistency loop is started again. Self-consistency is reached when the local Green's function is equal to the impurity Green's function.

In a next step Σ is used to construct an expression for the lattice Green's function. This is done by assuming that the temporal correlations of each site in the lattice can be described by the self-energy of the AIM:

$$G^{-1}_{latt}(i\omega, k) = i\omega + \mu - h_k - \Sigma(i\omega). \tag{2.34}$$

To obtain a new expression for the Weiss field, the lattice Green's function is integrated over k to construct its local counterpart. From this expression the self-energy is removed

by again using a Dyson like equation:

$$\mathcal{G}^{-1}_{new}(i\omega) = \left(\frac{1}{N} \sum_k G_{latt}(i\omega, k) \right)^{-1} + \Sigma(i\omega). \tag{2.35}$$

The described scheme is then iterated until the local part of the lattice Green's function is equal to the impurity Green's function:

$$\frac{1}{N} \sum_k G_{latt}(i\omega, k) = g(i\omega). \tag{2.36}$$

Normally the convergence in the number of iterations is quite fast but can be exponentially hard near a phase transition. In those cases it might be necessary to introduce an additional mixing between different iterations.

Chapter 3

Impurity Solvers

A crucial part of this thesis is the development and application of efficient quantum impurity solvers. The possibility to construct a perturbation theory such as dual fermion, which is basically defined as an expansion around some optimized impurity problem, is based on the fact that a solution to these impurity problems can found very efficiently. We therefore review the basic principles of modern impurity solvers in this chapter and explain their differences.

3.1 Exact Diagonalization

In this section we outline the exact diagonalization approach as a solver for the Anderson impurity model introduced in the last chapter. The main idea behind this method is to access the eigenvalues and eigenvectors of the system by diagonalization of an effective Hamilton matrix. Since the Hilbert space of an interacting fermionic system grows exponentially with the system size, this method requires a suitable approximation to the full system, which allows to describe an infinitely large system by a matrix of finite dimension. The Hamilton matrix scales with the number of sites N as

$$\dim H_N = 4^N = 2^{2N}. \tag{3.1}$$

As a consequence, the number of sites in a full diagonalization scheme is limited to a range of $6-9$ sites, depending on the symmetries used. If only the low lying energies are needed an iterative solver such as the Lanczos method [13] can be employed. Here the maximum number of sites lies in a range of $11-16$ sites. The world record is held by Yamada et al. [14], who calculated 12 fermions on a 24 site lattice. But compared to the number of sites one is normally interested in 24 sites is still rather small.
The Hamilton operator of the AIM can be written in the following form:

$$H = \sum_{k}^{N_b} \epsilon_k^b b_k^\dagger b_k + \epsilon^c c^\dagger c + H_{loc}[c^\dagger, c] + \sum_{k}^{N_b} \left(V_k c^\dagger b_k + V_k^* b_k^\dagger c \right). \tag{3.2}$$

The corresponding action is given by:

$$S = -\frac{1}{\beta} \left(\sum_{\omega_n} c^*(\omega_n) \big((i\omega_n + \mu - \epsilon^c) - \Delta(i\omega_n) \big) c(\omega_n) \right) + H_{loc}[c^\dagger, c]. \tag{3.3}$$

The dimension of the Hamilton matrix corresponding to Eq. (3.2) is mainly determined by the number of bath sites N_b. If a continuous density of states for the bath is assumed, N_b is infinitely large. At first sight, an obvious approximation would be to truncate the sum in Eq. (3.2) and thereby limit the number of bath sites. The problem with that approach is the lack of a good criteria to determine which bath levels should enter the actual simulation.
Caffarel et al. [5] proposed a different method. Instead of limiting the calculation to a finite subset of bath sites, the exact hybridization function Δ in Eq. (3.3) is approximated by a function Δ^n. This function Δ^n is constructed with the help of an effective system with lesser bath sites H^N.

$$H^N = \sum_{k}^{N} \tilde{\epsilon}_k b_k^\dagger b_k + \epsilon^c c^\dagger c + H_{loc}[c^\dagger, c] + \sum_{k}^{N} \left(\tilde{V}_k c^\dagger b_k + \tilde{V}_k^* b_k^\dagger c \right). \tag{3.4}$$

The corresponding effective action reads:

$$S^N = -\frac{1}{\beta} \left(\sum_{\omega_n} c^*(\omega_n) \big((i\omega_n + \mu - \epsilon^c) - \Delta^N(i\omega_n) \big) c(\omega_n) \right) + H_{loc}[c^\dagger, c]. \tag{3.5}$$

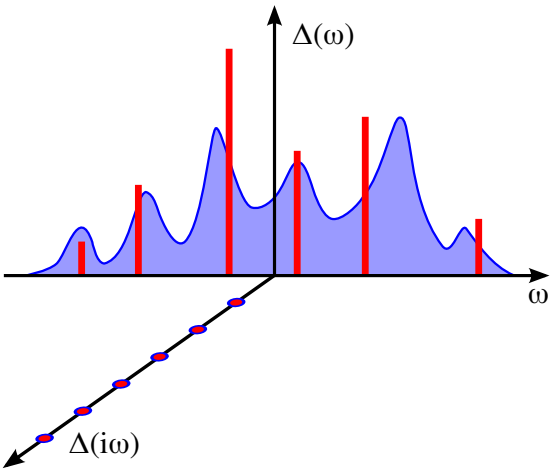

FIGURE 3.1: Illustration of the fitting procedure used by Caffarel et al. [5]. The smooth hybridization function $\Delta(\omega)$ is represented by a collection of auxiliary energies $\tilde{\epsilon}$ and weights $\tilde{V}$. The approach involves minimization on the imaginary axis.

The function Δ^N can be calculated using Gaussian integration:

$$\Delta^N(i\omega_n) = \sum_k^N \frac{\tilde{V}_k \tilde{V}_k^*}{i\omega_n - \tilde{\epsilon}_k}. \tag{3.6}$$

It is important to note that the bath sites occurring in the system H^N need not to occur in the former system H, but the parameters $\tilde{\epsilon}_k^b$ and $\tilde{V}_k$ are chosen in a way to minimize the difference between Δ and Δ^N. This difference is measured by a predefined distance function:

$$d = \frac{1}{N_\omega} \sum_{\omega_n}^{N_\omega} \omega_n^{-s} |\Delta^n(i\omega_n) - \Delta(i\omega_n)|^2. \tag{3.7}$$

Note that the distance between Δ and Δ^n is measured on the imaginary axis as depicted in Fig. 3.1. The actual details of the distance function play only a minor role. They just define in which region on the imaginary axis the distance between Δ^N and Δ should receive a higher weight. If N_ω is small and s is large the agreement on small frequencies will be enhanced. On the contrary if N_ω is large and $s = 0$ the agreement is shifted to large frequencies, which leads to a good coincidence in the asymptotic region. Numerically the multidimensional minimization is done using a conjugate gradient method

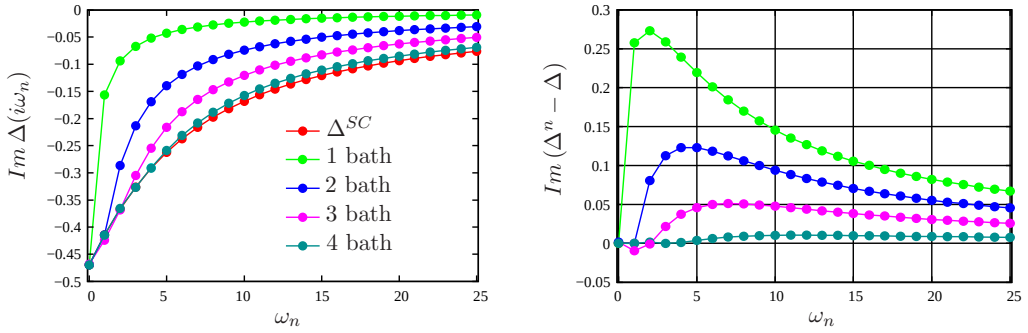

FIGURE 3.2: Convergence of Δ^N to Δ with increasing number of bath sites. *Left:* Imaginary part of the hybridization function for different number of bath sites. The parameters of H^N were fixed in such a way that the first N frequencies are equal. *Right:* Distance between Δ and Δ^N

taken from the GNU scientific library [15]. A detailed introduction to the fitting procedure on the imaginary axis can be found in [6, 16].

In the following an example for the single impurity Anderson model is discussed: A single orbital impurity in a semicircular density of states. The interaction strength is $U/D = 1$ where D is half the bandwidth $D = 2t$ with $\beta = 50$.

Fig. 3.2 shows the convergence of Δ^N to Δ with increasing number of bath sites. In these calculations the parameters $\tilde{\epsilon}_k$ and $\tilde{V}_k$ of the reference system H^N have been determined in such a way that on the first N frequencies Δ^N equals to Δ. Thus the difference between both hybridization functions is zero at the beginning. The resulting Green's function compared to the exact result obtained from a continuous-time quantum Monte Carlo simulation is shown in Fig. 3.3(a). Already with 3 bath sites the difference to the exact result is only visible if a strong zoom is applied to the figure. The reason for this strong convergence is the exponential drop of the distance function with increasing number of bath sites as shown in Fig . 3.3(b).

The results on the real axis shown in Fig. 3.4 are hard to compare with those obtained from Monte Carlo. The reason for this is the fact that in exact diagonalization the density of states can be calculated exactly from the Lehmann representation of the Green's function. In a continuous-time quantum Monte Carlo simulation the density of states is obtained by analytic continuation using the maximum entropy method. This procedure gives only a qualitative result, because the problem of finding the density of states from

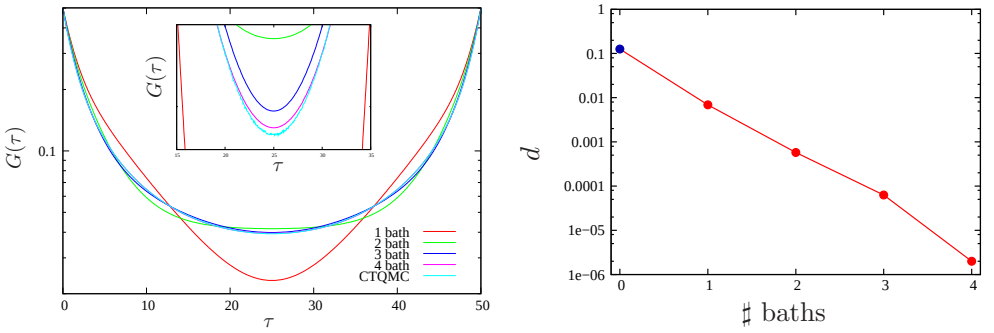

(a) (b)

FIGURE 3.3: (a) Convergence of $G(\tau)$ with increasing number of bath sites. (b) Dependence of the distance function on the number of bath sites. The blue dot shows the norm of Δ, i.e. the norm with no bath site. For the norm we have chosen $N_\omega = 200$ and $s = 2$.

noisy Monte Carlo data is an ill conditioned problem. Nevertheless one can see that with an increasing number of bath sites the exact diagonalization results approach the Monte Carlo curve.

In the following sections we briefly review how one can extract physical information from the eigenvalues and eigenvectors, i.e. how to calculate the one particle Green's function and higher order correlators.

3.1.1 Full Diagonalization

As the name indicates the full diagonalization method is designed to compute the full spectrum and all corresponding eigenvectors from a Hamilton matrix H. Since various numerical algorithms are known for such a purpose, the actual step of diagonalizing the matrix is not the crucial part of the scheme. In the past, several algorithms, such as the Jacobi method [17, 18] or the QL QR method [17, 19] have been proposed. In addition to that many of these algorithms have been successfully implemented in several programming languages and are available as open source code [15, 20].

As explained in the last section the main bottleneck of the approach is the matrix size of the Hamiltonian. The actual art of the technique is to reduce the matrix size by utilizing every possible symmetry present. In the following we give a short list of symmetries for

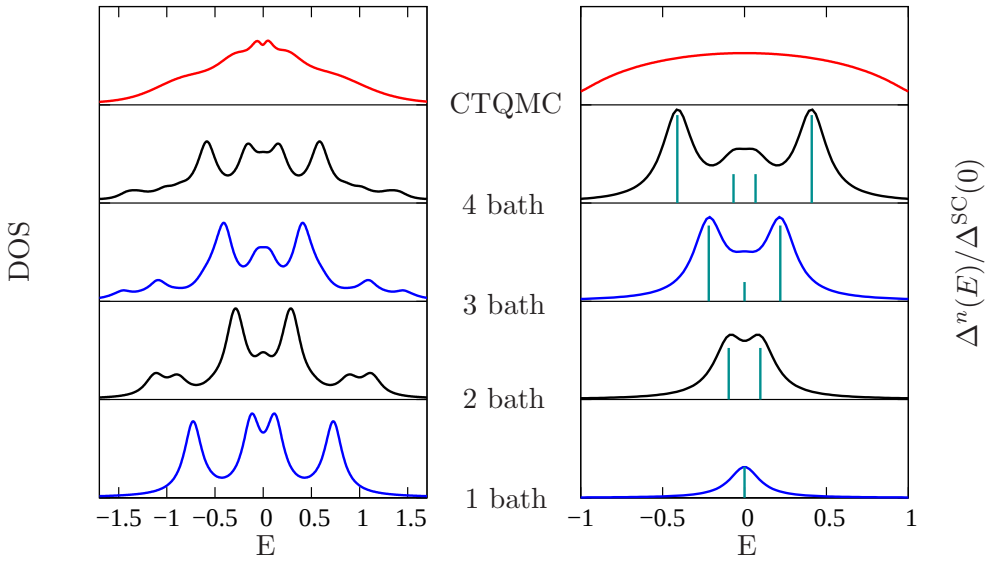

FIGURE 3.4: *Left:* Convergence of the density of states with increasing number of bath sites on the real axis. For the exact diagonalization the data have been achieved using the Lehmann representation, for the Monte Carlo using the maximum entropy method. *Right:* Convergence of Δ^N on the real axis. The vertical lines indicate the height of a single Lorentzian defined by the parameters $\tilde{\epsilon}$ and $\tilde{V}$, $\Delta_k^N(\tilde{\epsilon}) = V^2/(\pi\delta)$. *Parameters:* $\beta = 50$, $U/D = 1$.

the single impurity Anderson model, which have been used for the calculations in this thesis.

Particle number conservation: H commutes with the total particle number

$$[\, H, N_{tot} \,] = 0, \qquad N_{tot} = \sum_{i,\sigma} n_{i,\sigma}.$$

SU(2) spin symmetry: H commutes with all components of the total spin

$$[\, H, S^\alpha \,] = 0, \qquad S^\alpha = \frac{1}{2} \sum_{i,\nu\mu} c_{i\mu}^\dagger \sigma_{\mu\nu}^\alpha c_{i\nu}.$$

where σ^α denotes the Pauli matrices, and $\mu, \nu \in \{\uparrow, \downarrow\}$.

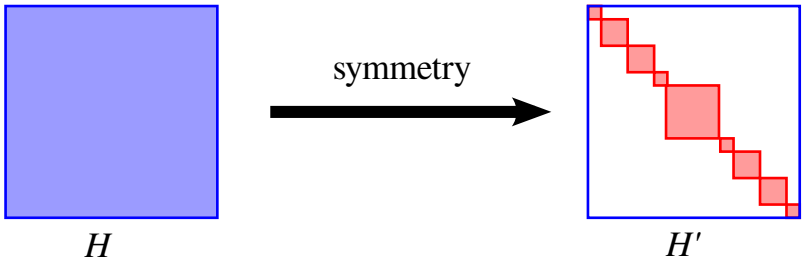

FIGURE 3.5: The usage of symmetries in the construction of a Hamiltonian leads to a block structure in the corresponding Hamilton matrix. The advantage of this block structure is that each block can be diagonalized separately.

The combination of both symmetries leads to the conservation of the total number of spin up and spin down electrons. As a consequence, the Hamilton matrix acquires a block diagonal form, if the basis states are sorted according to N_σ. Therefore the numerical effort to diagonalize the matrix is strongly reduced.

3.1.2 Calculating correlators

An n-particle correlator is defined as a time ordered expectation value of n creation and n annihilation operators.

$$F(\tau_1, \ldots, \tau_n) = \langle T c(\tau_1) c^\dagger(\tau_2) \ldots c(\tau_{n-1}) c^\dagger(\tau_n) \rangle \tag{3.8}$$

$$= \langle T \hat{O}_1 \hat{O}_2 \ldots \hat{O}_{n-1} \hat{O}_n \rangle \tag{3.9}$$

Here time ordering means that operators with larger imaginary time τ stand to the left. With this in mind Eq. (3.9) can be transformed to a sum over all possible permutations of the involved operators. The hat over the operator indicates that $\hat{O}$ is an operator in the Heisenberg form with all its time dependence. The index $i = 1 \ldots n$ is a combined index and stands for time, spin and orbital degrees of freedom.

$$F(\tau_1, \ldots, \tau_n) = \sum_{\pi \in S_n} (-1)^\pi \theta(\tau_{\pi_1} > \cdots > \tau_{\pi_n}) \langle \hat{O}_{\pi_1} \ldots \hat{O}_{\pi_n} \rangle \tag{3.10}$$

Now the only thing left is to find an efficient way to calculate the τ dependent expectation value of $2n$ fermionic operators. As long as the Hamiltonian of the system does not explicitly depend on time[1] the imaginary time evolution operator can be written as $U = \exp(-\tau H)$. In addition to that the expectation value can be expressed as a trace over eigenstates, which is essentially the Lehmann representation of the correlator:

$$\begin{aligned} F(\tau_1, \ldots, \tau_n) = \sum_{\pi \in S_n} (-1)^\pi \theta(\tau_{\pi_1} > \cdots > \tau_{\pi_n}) \\ \times \frac{e^{-\beta E_n}}{Z} \sum_n \langle n | e^{H\tau_{\pi_1}} O_{\pi_1} e^{-H\tau_{\pi_1}} \ldots e^{H\tau_{\pi_n}} O_{\pi_n} e^{-H\tau_{\pi_n}} | n \rangle. \end{aligned} \tag{3.11}$$

Now O is an operator in the Schrödinger picture without any time dependence left. The open question now is how to calculate the exponent of $H\tau$. In principle the exponent of a matrix is defined as its Taylor expansion, but there are several other techniques known to calculate the exponential in more efficient ways [21]. In the following it will be shown that the matrix exponential can be calculated if the problem is expressed in the eigenbasis.

Another quite promising way mentioned in the literature is to calculate the exponential in the so called Krylov-space [21, 22]. This method has been already used in the context of the hybridization expansion quantum Monte Carlo [23], and is now subject of an ongoing diploma thesis in the context of the Lanczos method. This approach might be still useful if the dimension of the Hilbert space is large and a calculation of the exponential in the eigenbasis would be unfeasible. In section 3.1.3 the basics of this quite promising technique will be explained.

In order to calculate the exponent in Eq. (3.11) in the eigenbasis, identity matrices $\mathbb{1} = |m\rangle\langle m|$ are inserted between the creators and annihilators.

$$\begin{aligned} F(\tau_1, \ldots, \tau_n) = \sum_{\pi \in S_n} (-1)^\pi \theta(\tau_{\pi_1} > \cdots > \tau_{\pi_n}) \\ \times \frac{e^{-\beta E_n}}{Z} \sum_{n,m \ldots k} \langle n | e^{E_n \tau_{\pi_1}} O_{\pi_1} | m \rangle \langle m | e^{-E_m \tau_{\pi_1}} \ldots | k \rangle \langle k | e^{E_k \tau_{\pi_n}} O_{\pi_n} e^{-E_n \tau_{\pi_n}} | n \rangle \end{aligned} \tag{3.12}$$

[1] The case of a time dependent Hamiltonian will be treated in chapter 7.

So Eq. (3.9) has been reduced to a representation, which only contains the matrix elements of all creation and annihilation operators in the eigenbasis and all eigenenergies. The main drawback of this formulation is the multidimensional sum in front of the matrix elements. Since the Hilbert space grows exponentially one might have a chance to diagonalize the problem, but the repeated summation over all states might become an impossible task. As long as one is only interested in observables, which depend on τ only, the multidimensional sum can be converted to a more efficient product of matrices. But if one is interested in a representation on Matsubara frequencies the direct evaluation of nested sums is unavoidable. Even for a cluster of 4 sites in total as described in Fig. 3.6(b), this task can take half a day on a modern 8 CPU cluster.
To optimize the calculation of correlators, which require the evaluation of nested sums, the following standard procedures were applied:

Precalculation of exponential factors: In a nested loop the calculation of an exponential factor is most expensive. Although the number of eigenenergies is large, they can be easily stored. So it is possible to precalculate the factors $\exp(-\beta E_i)$ or even the numerical expression for $\exp(-\beta E_i \tau_j)$ if one works on a finite τ-mesh. Normally such a simplification can speed up the calculation time by 2 orders of magnitude.

Truncation of sums: In principle there are two possible ways to truncate the multi index sum in Eq. (3.12). If all energies lie above a predefined threshold the exponential factors will be small and can be neglected to a certain accuracy. This approximation corresponds to the fact that transitions in the high energy regime play only a minor role. This procedure involves the risk, that if the threshold is not chosen with care one loses easily essential physics. A second truncation scheme is to limit the outer summation, which is damped by the statistical factor $\exp(-\beta E_n)$ and to fully account all other index summations. This approximation is not as severe as the one mentioned before, since the basic transitions in every energy range are included.

Employing symmetries: Since the basis has been constructed in such a way, that all eigenenergies correspond to a certain spin and particle number N^σ, the expectation

value of Eq. (3.12) will only be non-zero if N^σ for the starting state is the same as for the ending state. So it is checked if applying all creators and annihilators will end in the same symmetry sector.

So far only the formulas for correlators in τ-representation were given, but very often one is interested in its Fourier transform on Matsubara frequencies. These quantities are heavily used throughout this thesis in the context of the dual perturbation technique, although the dual perturbation is not limited to the Matsubara case, as we will see in chapter 7. The Fourier transform of an $n-$particle correlator is introduced by defining

$$c(\tau) = \frac{1}{\beta} \sum_{\omega_n} e^{-i\omega_n \tau} c(\omega_n) \tag{3.13}$$

$$c(\omega_n) = \int_0^\beta d\tau e^{+i\omega_n \tau} c(\tau) \tag{3.14}$$

$$c^\dagger(\tau) = \frac{1}{\beta} \sum_{\omega_n} e^{+i\omega_n \tau} c^\dagger(\omega_n) \tag{3.15}$$

$$c^\dagger(\omega_n) = \int_0^\beta d\tau e^{-i\omega_n \tau} c(\tau). \tag{3.16}$$

In principle the transformation from τ to ω_n and back can be done numerically, but since we already have an analytic expression for the τ-representation of the correlators in Eq. (3.12) it is possible to derive explicit formulas for the Fourier transform of $n-$particle correlators. In the next two paragraphs the definition and formulas for the one-particle and two particle Green's function are given.

3.1.2.1 One particle Green's function

The one particle Green's function is defined as

$$g_{\alpha\beta}(\tau_1, \tau_2) = -\langle T c_\alpha(\tau_1) c^\dagger_\beta(\tau_2) \rangle. \tag{3.17}$$

Where α and β are combined indices for spin and orbital degrees of freedom. Using the cyclic invariance of the correlator, Eq. (3.17) can be rearranged in such a way, that the

Green's function only depends on the time difference:

$$g_{\alpha\beta}(\tau_1 - \tau_2) = -\langle c_\alpha(\tau_1 - \tau_2) c_\beta^\dagger(0)\rangle. \tag{3.18}$$

In the last step it has been used that the Green's function is always time ordered, if the last time is set to zero. Using the Hamiltonian eigenbasis, this expression can be written in the following way:

$$g_{\alpha\beta}(\tau_1 - \tau_2) = g_{\alpha\beta}(\tilde{\tau}) = \frac{1}{Z}\sum_{n,m}\langle n|c_\alpha|m\rangle\langle m|c_\beta^\dagger|n\rangle e^{-\beta E_n} e^{\tilde{\tau}(E_n - E_m)}. \tag{3.19}$$

The expression for the Fourier transformed Green's function reads:

$$g_{\alpha\beta}(i\omega_n) = \frac{1}{Z}\sum_{n,m}\frac{\langle n|c_\alpha|m\rangle\langle m|c_\beta^\dagger|n\rangle}{i\omega_n + E_n - E_m}\left(e^{-\beta E_n} + e^{-\beta E_m}\right). \tag{3.20}$$

3.1.2.2 Two particle Green's function and vertex

The two particle Green's function is defined as:

$$\chi_{1234}(\tau_1, \tau_2, \tau_3, \tau_4) = \langle T c_1(\tau_1) c_2^\dagger(\tau_2) c_3(\tau_3) c_4^\dagger(\tau_4)\rangle. \tag{3.21}$$

Again one can use the cyclic invariance to eliminate the dependence on the last time:

$$\chi_{1234}(\tilde{\tau}_1, \tilde{\tau}_2, \tilde{\tau}_3) = \langle T c_1(\tilde{\tau}_1) c_2^\dagger(\tilde{\tau}_2) c_3(\tilde{\tau}_3) c_4^\dagger(0)\rangle. \tag{3.22}$$

$$= \langle T O_1 O_2 O_3 c_4^\dagger(0)\rangle \tag{3.23}$$

Here $\tilde{\tau}_i$ is just the difference between τ_i and τ_4. Since the last time is set to zero the time ordering operator only acts to the first three times. The reader should be aware of the fact that, with fixing the last time to be zero, the condition of energy conservation in terms of Matsubara frequencies has also been fixed to $\omega_1 - \omega_2 = \omega_4 - \omega_3$. Repeating the steps mentioned in the last section the expression of the two particle Green's function is

given by:

$$\chi_{1234}(\tilde{\tau}_1,\tilde{\tau}_2,\tilde{\tau}_3) = \sum_{\pi\in S_n}(-1)^\pi\theta(\tilde{\tau}_{\pi_1}>\tilde{\tau}_{\pi_2}>\tilde{\tau}_{\pi_3})\sum_{ijklm}\langle n|O_{\pi_1}|k\rangle\langle k|O_{\pi_2}|l\rangle\langle l|O_{\pi_3}|m\rangle\langle m|c_4^\dagger|n\rangle \times e^{-\beta E_n}e^{\tilde{\tau}_{\pi_1}(E_n-E_k)}e^{\tilde{\tau}_{\pi_2}(E_k-E_l)}e^{\tilde{\tau}_{\pi_3}(E_l-E_m)}. \tag{3.24}$$

To derive a representation on Matsubara frequencies the last equation will be Fourier transformed analytically.

$$\begin{aligned}\chi_{1234}(\omega_1,\omega_2,\omega_3) &= \int_0^\beta d\tilde{\tau}_1\int_0^\beta d\tilde{\tau}_2\int_0^\beta d\tilde{\tau}_3\sum_{\pi\in S_n}e^{i(\tilde{\omega}_{\pi_1}\tilde{\tau}_{\pi_1}+\tilde{\omega}_{\pi_2}\tilde{\tau}_{\pi_2}+\tilde{\omega}_{\pi_3}\tilde{\tau}_{\pi_3})} \\ &\quad\times(-1)^\pi\theta(\tilde{\tau}_{\pi_1}>\tilde{\tau}_{\pi_2}>\tilde{\tau}_{\pi_3})\langle O_{\pi_1}O_{\pi_2}O_{\pi_3}c_{\pi_4}^\dagger(0)\rangle\end{aligned} \tag{3.25}$$

$$\begin{aligned}&= \sum_{\pi\in S_n}\sum_{1,2,3,4}\phi(E_1,E_2,E_3,E_4,\tilde{\omega}_{\pi_1},\tilde{\omega}_{\pi_2},\tilde{\omega}_{\pi_3}) \\ &\quad\times(-1)^\pi\langle 1|O_{\pi_1}|2\rangle\langle 2|O_{\pi_2}|3\rangle\langle 3|O_{\pi_3}|4\rangle\langle 4|c_4^\dagger|1\rangle\end{aligned} \tag{3.26}$$

In the last step it was necessary to account for the correct sign of the Matsubara frequencies: Since a time $\tilde{\tau}_{\pi_i}$ and the corresponding frequency $\tilde{\omega}_{\pi_i}$ stay with the permuted operator, it is possible that the corresponding frequency enters with positive or negative sign, depending on O_{π_i} being a creator or annihilator. Consequently the frequency is $\tilde{\omega}_{\pi_i} = -\omega_{\pi_i}$ for creators and $\tilde{\omega}_{\pi_i} = +\omega_{\pi_i}$ for annihilators. The function ϕ is the Fourier transform of the time evolution operators in the eigenbasis plus the statistical weight:

$$\begin{aligned}\phi(E_1,E_2,E_3,E_4,\tilde{\omega}_{\pi_1},\tilde{\omega}_{\pi_2},\tilde{\omega}_{\pi_3}) &= \int_0^\beta d\tilde{\tau}_1\int_0^\beta d\tilde{\tau}_2\int_0^\beta d\tilde{\tau}_3\, e^{i(\tilde{\omega}_{\pi_1}\tilde{\tau}_{\pi_1}+\tilde{\omega}_{\pi_2}\tilde{\tau}_{\pi_2}+\tilde{\omega}_{\pi_3}\tilde{\tau}_{\pi_3})} \\ &\quad\times e^{-\beta E_1}e^{E_{12}\tilde{\tau}_{\pi_1}}e^{E_{23}\tilde{\tau}_{\pi_2}}e^{E_{34}\tilde{\tau}_{\pi_3}}.\end{aligned} \tag{3.27}$$

Here E_{ij} is a short-hand notation for $E_i - E_j$. The Fourier transform can be done analytically, but special attention has to be paid to possible degeneracies. For the final result one gets:

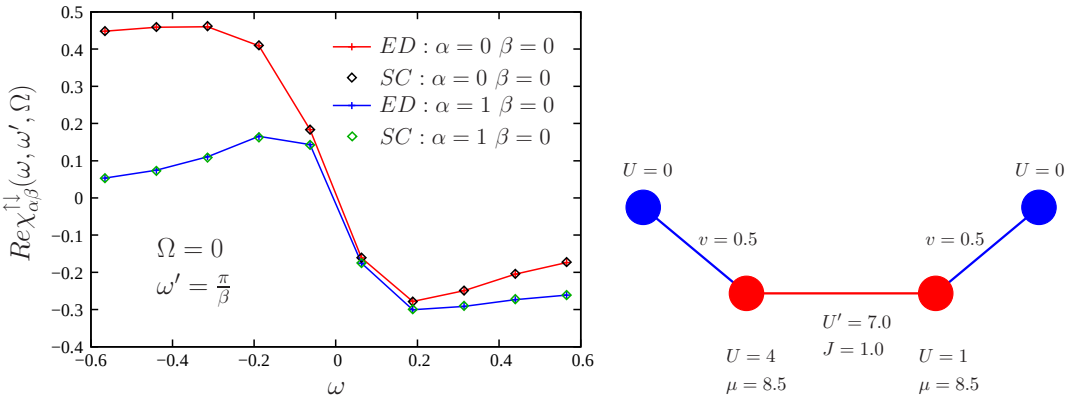

FIGURE 3.6: Two-particle Green's function $\chi^{\uparrow\downarrow}_{\alpha\beta}(\omega_1, \omega_2, \Omega)$ in dependence of ω_1 for fixed Ω and ω_2. The results are shown in (a). The underlying model (b) has been chosen as asymmetric as possible for testing purposes. Different curves correspond to a specific choice of orbital indices. $\beta = 50$

$$\phi(E_1, E_2, E_3, E_4, \tilde{\omega}_{\pi_1}, \tilde{\omega}_{\pi_2}, \tilde{\omega}_{\pi_3}) = \frac{1}{i\tilde{\omega}_{\pi_3} + E_{34}} \tag{3.28}$$
$$\times \Bigg[\frac{1 - \delta^{E_{24}}_{\tilde{\omega}_{23}}}{i(\tilde{\omega}_{\pi_2} + \tilde{\omega}_{\pi_3}) + E_{24}} \left(\frac{e^{-\beta E_1} + e^{-\beta E_2}}{i\tilde{\omega}_{\pi_1} + E_{12}} - \frac{e^{-\beta E_1} + e^{-\beta E_4}}{i(\tilde{\omega}_{\pi_1} + \tilde{\omega}_{\pi_2} + \tilde{\omega}_{\pi_3}) + E_{14}} \right)$$
$$+ \delta^{E_{24}}_{\tilde{\omega}_{23}} \left(\frac{e^{-\beta E_1} + e^{-\beta E_2}}{(i\tilde{\omega}_{\pi_1} + E_{12})^2} - \beta \frac{e^{-\beta E_2}}{i\tilde{\omega}_{\pi_1} + E_{12}} \right)$$
$$- \frac{1}{i\tilde{\omega}_{\pi_2} + E_{23}} \left(\frac{e^{-\beta E_1} + e^{-\beta E_2}}{i\tilde{\omega}_{\pi_1} + E_{12}} - (1 - \delta^{E_{13}}_{\tilde{\omega}_{12}}) \frac{e^{-\beta E_1} - e^{-\beta E_3}}{i(\tilde{\omega}_{\pi_1} + \tilde{\omega}_{\pi_2}) + E_{13}} + \beta e^{-\beta E_1} \delta^{E_{12}}_{\tilde{\omega}_{12}} \right) \Bigg].$$

Here again a short-hand notation for the Kronecker deltas has been introduced: $\delta^{E_{kl}}_{\tilde{\omega}_{ij2}} = \delta_{\tilde{\omega}_{\pi_i}, -\tilde{\omega}_{\pi_2}} \cdot \delta_{E_1, E_2}$. These Kronecker deltas have to be understood in such a way that the expression in brackets behind the Kronecker delta vanishes if $\delta^{E_{kl}}_{\tilde{\omega}_{ij2}} = 0$, even though in most cases the corresponding denominator diverges.

In Fig. 3.6 a continuous-time quantum Monte Carlo calculation of the two-particle Green's function is compared to the result of an exact diagonalization simulation of the same model. The underlying model has been chosen in the most asymmetric way to have a reliable test for both methods. A sketch of the employed geometry with all corresponding parameters is depicted in figure 3.6(b). To compare both results a

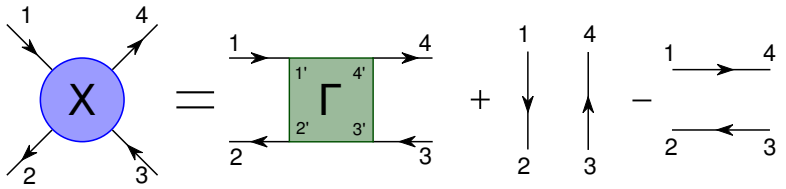

FIGURE 3.7: Composition of the two-particle Green's function. The two main building blocks are the fully irreducible vertex part and the trivial reducible part, consisting of two fermionic propagators.

representation of the two-particle Green's function in dependence on two fermionic and one bosonic frequency is chosen $\chi(\omega, \omega', \Omega)$. Here the condition of energy conservation reduces to the conservation of the transferred bosonic frequency $\Omega = \omega_1 - \omega_2$. For the connection between three fermionic frequencies and the representation in Fig. 3.6(a) one has:

$$\omega_1 = \omega + \Omega \qquad \omega_2 = \omega \tag{3.29}$$

$$\omega_3 = \omega' \qquad \omega_4 = \omega' + \Omega. \tag{3.30}$$

Since the exact diagonalization as well as the the continuous-time quantum Monte Carlo give exact results for the described model the results are indistinguishable.

The key quantity in this thesis is not the two-particle Green's function, but the full irreducible vertex part of it. This part will serve as the interaction of the auxiliary fermions introduced to formulate the dual perturbation theory as we will see later. The two-particle Green's function can be separated into two parts: One part, the vertex, which contains all irreducible diagrams, and a trivial reducible part. Here reducibility means that a diagram can be cut by severing two fermion lines. This situation is shown in Fig. 3.7. The formal definition of the vertex reads:

$$\gamma_{1'2'3'4'} = g^{-1}_{1'1} g^{-1}_{3'3} (\chi_{1234} - g_{12} g_{34} + g_{14} g_{32}) g^{-1}_{22'} g^{-1}_{44'}. \tag{3.31}$$

3.1.3 Lanczos Method

The Lanczos method is a widely used scheme to calculate iteratively the extremal eigenvalues of sparse matrices. The key idea is to represent the Hamilton operator in the so-called Krylov space. This vector space is spanned by a basis set, which originates from successive application of the Hamiltonian on a random starting vector ϕ_0.

$$K_m(H, \phi_0) = \text{span}\{\phi_0, H\phi_0, \ldots, H^m\phi_0\} \tag{3.32}$$

The representation of H in the Krylov space H_m has the key feature that its low lying spectrum converges towards the spectrum of the original Hamiltonian H with increasing dimension of the Krylov space. The method is designed in such a way, that the procedure can be applied iteratively. The dimension of H_m is successively increased until the low eigenvalues are converged to the wanted accuracy. The convergence is rather fast and is one of the reasons for the great success of the Lanczos approach. In practice the size of H_m is of the order $100-400$ whereas the size of the original Hamiltonian is exponentially large as described in the introduction. In addition to that the technique is only based on the multiplication of sparse matrices with vectors, which can be implemented very efficiently.
A way to construct an orthonormal basis of the Krylov space is the Arnoldi algorithm, which is presented in the following:

1. set $\phi_1 = \phi_0 / ||\phi_0||$, this is the first basis vector and starting point of the iteration.
2. compute $z = H\phi_i$, to enlarge the Krylov space.
3. calculate the projections of z onto the other basis vectors: $h_{ij} = \phi_i^T z$.
4. subtract the projections from z to gain the linear independent part of z: $\tilde{z} = z - h_{ij}\phi_i$.
5. normalize $\tilde{z}$ to obtain the new basis vector.
6. jump to 2.

3.1.3.1 Approximation of matrix functions in the Krylov framework

Besides its great success in calculating the extremal eigenvalues of a Hamiltonian, the presented approach is also capable of constructing good approximations of matrix functions. The reason for this is that the representation of H in the Krylov space H_m has not only the same extremal eigenvalues, but also agrees in the first m moments with the original Hamiltonian. In other words: Any polynomial function q_{m-1} of order $m-1$ can be represented exactly in the Krylov space.

$$q_{m-1}(H)\phi_0 = \phi_m q_{m-1}(H_m)e_1 \tag{3.33}$$

Here e_1 is the unit vector in the Krylov space. As a consequence the Hamilton matrix on the Krylov space H_m can be used to construct a polynomial approximation to any function of the original Hamilton operator. This approximation will be exact up to order $m-1$. If $f(H)$ is the function to approximate one gets:

$$f(H)\phi_0 \approx \phi_m f(H_m)e_1. \tag{3.34}$$

The two main applications of this procedure are the calculation of the one particle Green's function and the computation of the time evolution operator in higher order correlators. The latter has already been useful in terms of the hybridization expansion quantum Monte Carlo and could be quite promising in the Keldysh framework, where most of the computational time is spent to compute the matrix exponentials in the eigenbasis.
The procedure could also be applied to compute the Fourier transform of the two particle Green's function in the equilibrium context. But in this case a direct expression of the two particle correlator in terms of H is not known yet. One would have to calculate the correlator in dependence on three imaginary times and then to Fourier transform numerically. At the moment it is not clear, if this procedure is advantageous, since the numerical Fourier transform is a hard task.

3.2 Monte Carlo

The term Monte Carlo summarizes various algorithms, which are applied in nearly all fields of sciences. They all have in common, that they are used to solve problems of high dimensionality. The large phase space of these problems often arises, when large degrees of freedom interact with each other and a picture of decoupled degrees of freedom is insufficient.

The method has become a standard tool in physics [24–27], pure mathematics [28], optimization problems [29], chemistry [30], and even social sciences [31]. All these problems need at some point the numerical treatment of large sums or integrals. In one dimension there are standard quadrature rules such as the Simpson formula [17] or the Gauss-Kronrod procedure [17] available to handle such integrals. All these methods in their non-adaptive formulation divide the integration area in equal spaced nodes and evaluate the integral over this grid. If an algorithm employs N nodes, which leads to a grid spacing of h, the error will be of the order $\mathcal{O}(h^p)$, where p is the order of the algorithm. If the dimensionality of the problem is now enlarged d times, the number of points needed to keep the grid spacing unchanged increases to N^d. For 100 points in the one dimensional unit interval, this would require 10^{20} points in 10 dimensions. It can easily be shown that the numerical solution of the above problems with the help of quadrature rules would often exceed the lifetime of the universe, even if the grid size is chosen in a moderate way. The exponential growth of the numerical effort with larger dimensionality has been named by Bellmann [32] the curse of dimensionality.

This strong dependence on the details of the grid has led to the search for algorithms that are independent of dimensionality. This requirement is fulfilled by Monte Carlo methods.

The crucial idea is that most high dimensional integrals or sums are taken over functions, which are strongly peaked in the integration area. Consequently most nodes used for a standard quadrature rule integration would in most cases have zero contribution to the total integral. The basic idea of Monte Carlo is to stochastically sample the parameter space and only evaluate those nodes which have a strong contribution to the integral. This procedure is called importance sampling. The main concept can be understood by

looking at the following formula:

$$\langle A \rangle = \sum_{x \in \Omega} P(x)\mathcal{A}(x) = \lim_{n \to \infty} \frac{1}{N} \sum_{i=1}^{N} \mathcal{A}(x_i). \tag{3.35}$$

Here Ω is the high dimensional parameter space and $P(x)$ some probability distribution of the function values $\mathcal{A}(x)$. Eq. (3.35) now states that this sum is equal to a large average taken over function values, whose x_i are distributed according to $P(x)$. According to the central limit theorem, which applies if $\mathcal{A}(x)$ is well-behaved, such a procedure converges to the limiting distribution with an error $1/\sqrt{N}$ and is therefore independent of dimensionality. In comparison to Simpson's rule a Monte Carlo algorithm is superior in dimensions $d > 8$. In the following we describe how the concept of Monte Carlo can be applied to the Anderson impurity problem.

3.2.1 Applying Monte Carlo to the Anderson impurity model

The idea behind imaginary time quantum Monte Carlo is to stochastically sample the partition function of the problem, using the action description of the fermionic system:

$$Z = \mathrm{Tr}\, T e^{-S}. \tag{3.36}$$

The action of the Anderson impurity model (AIM) can be written as [33],

$$S = -\int_0^\beta d\tau \int_0^\beta d\tau' \sum_\sigma c_\sigma^\dagger(\tau)\, G_{0,\sigma}^{-1}(\tau - \tau')\, c_\sigma(\tau') + U \int_0^\beta d\tau\, n_\uparrow(\tau)\, n_\downarrow(\tau). \tag{3.37}$$

In this formulation c_σ and $c_\sigma^\dagger$ are anti-commutative fermionic operators and $G_{0,\sigma}(\tau)$ is the time dependent bare Green's function. Its representation in the Matsubara formalism reads

$$G_{0,\sigma}^{-1}(i\omega_n) = i\omega_n + \mu - \Delta(i\omega_n) \tag{3.38}$$

$$\Delta(i\omega_n) = \sum_k \frac{|V_{k,\sigma}|^2}{i\omega_n - \epsilon_{k,\sigma}}. \tag{3.39}$$

Where $\Delta(i\omega_n)$ is the hybridization function. The full impurity Green's function can be defined with the help of Eq. (3.36) as:

$$G(\tau, \tau') = -\frac{1}{Z} \operatorname{Tr} \left[T c(\tau) c^{\dagger}(\tau') e^{-S} \right] \tag{3.40}$$

The starting point of path integral QMC is to partition the problem space in such a way that the partition function can be rewritten as a sum over single configurations of the underlying problem space.

$$Z = \sum_i Z_i \tag{3.41}$$

The difference between the known QMC algorithms is expressed in the way how the partitioning of the problem space is reached. The expectation value of an observable such as the impurity Green's function can then be written as an average of all these configurations:

$$G(\tau, \tau') = \sum_i \frac{Z_i}{Z} G_i(\tau, \tau'). \tag{3.42}$$

The last equation is exactly of the same form as Eq. (3.35). The term Z_i/Z should be interpreted as a probability distribution for the configuration dependent observables G_i. It is straightforward to design a Monte Carlo technique to evaluate Eq. (3.42). The only drawback is that Monte Carlo requires that the underlying probability distribution is well defined, but the anti-commutative properties of fermionic Grassmann numbers can lead to a negative weight for some configurations, $Z_i < 0$. This issue is known as the fermionic sign problem and can be exponentially hard [34]. In the following we describe the underlying concepts of a Monte Carlo algorithm.

3.2.2 Markov chain and the Metropolis-Hastings algorithm

If we want to construct a Monte Carlo algorithm, which is able to numerically calculate an expression like Eq. (3.42), we are facing two problems: First the overall scaling variable Z is unknown and can not be calculated easily and second the parameter space

is often so huge, that an efficient way to generate new configurations Z_i is needed. These two problems are solved with the concept of a Markov chain [35] and the Metropolis-Hastings [36, 37] algorithm.
The idea of sampling the problem space doing a sequence of steps with limited radius is based on the concept of Markov Chains. A sequence of configurations $X_1, \dots X_t$ is called a Markov chain of first order if the occurrence of a new configuration X_{t+1} only depends on the previous chain element X_t, which essentially means that the chain has no memory. The strict mathematical definition is:

$$P(X_{t+1} = S_{t+1}|X_t = S_t, \dots, X_0 = S_0) = P(X_{t+1} = S_{t+1}|X_t = S_t). \tag{3.43}$$

Here S_t denotes a certain configuration. In addition to that the Markov chain has to fulfill two more requirements in order to resemble the probability distribution $P(x)$.

ergodicity: The algorithm must have access to all possible configurations.

detailed balance: The transition probability Π fulfills:

$$P(X_t)\Pi(X_t \to X_{t'}) = P(X_{t'})\Pi(X_{t'} \to X_t). \tag{3.44}$$

In this notation $\Pi(X_t \to X_{t'})$ is the transition matrix from a configuration X_t to a configuration $X_{t'}$. With the following abbreviations, $X_t = a$, $X_{t'} = b$, the transition matrix is normalized such that $\sum_b \Pi_{ab} = 1$ holds.
In order to have a working Monte Carlo algorithm, there is still a criterion missing, which tells us, whether a new configuration should be accepted or refused. Such a criterion has been proposed by Metropolis [36] and was generalized by Hastings [37] afterwards. The Metropolis-Hastings algorithm can be deduced from the detailed balance condition in the following way. In the short notation the detailed balance condition reads:

$$\frac{\Pi_{ab}}{\Pi_{ba}} = \frac{P(b)}{P(a)}. \tag{3.45}$$

Now the matrix elements of the transition matrix are split up in a probability to propose a certain change in the configuration Π^{prop} and a probability to accept such a change

Π^{acc}. The transition matrix then reads $\Pi_{ab} = \Pi_{ab}^{\text{prop}} \cdot \Pi_{ab}^{\text{acc}}$. From equation (3.45) follows:

$$\frac{\Pi_{ab}^{\text{prop}}\Pi_{ab}^{\text{acc}}}{\Pi_{ba}^{\text{prop}}\Pi_{ba}^{\text{acc}}} = \frac{P(b)}{P(a)}. \tag{3.46}$$

This can be changed into the following condition.

$$\frac{\Pi_{ab}^{\text{acc}}}{\Pi_{ba}^{\text{acc}}} = \frac{P(b)\Pi_{ba}^{\text{prop}}}{P(a)\Pi_{ab}^{\text{prop}}} \tag{3.47}$$

It can be easily seen that Eq. (3.47) is fulfilled by the following ansatz for the acceptance probability.

$$\Pi_{ab}^{\text{acc}} = \min(1, \frac{P(b)\Pi_{ba}^{\text{prop}}}{P(a)\Pi_{ab}^{\text{prop}}}) \tag{3.48}$$

This is the general formulation for Π_{ab}^{acc} of Hastings. The great advantage of Eq. (3.48) is that the knowledge of the overall scaling variable Z is no longer required. The decision whether an update is performed or not is only based on the relative weight between the old and the new configuration. In many situations, such as in various spin models, the proposal probability of a new configuration and its reverse are equal. This leads to the following expression:

$$\Pi_{ab}^{\text{acc}} = \min(1, \frac{P(b)}{P(a)}). \tag{3.49}$$

In the remaining part of the chapter we will introduce several Monte Carlo algorithms for the Anderson impurity model. All these methods have in common, that at some point the above described formulas will be used. So in the following part we will not go into further detail how the actual implementation is done, but we will focus on how the partitioning of the problem space is reached.

3.2.3 Hirsch-Fye Quantum Monte Carlo

As the first example of Monte Carlo based solvers for the Anderson impurity model we introduce the algorithm of Hirsch and Fye [38]. It was the first quantum Monte Carlo

solver applied to the DMFT problem [39] and is nowadays still in wide use for realistic structure calculations [40–42].

The key idea of the approach is to discretize the imaginary time domain and to transform the remaining discrete problem of interacting fermions with the help of the Hubbard-Stratonovich transformation [43, 44] to a problem of non-interacting fermions coupled to a time-dependent Ising-like field. The different configurations of the field are then sampled with the help of a Monte Carlo algorithm. The method is exemplified by the single impurity Anderson model:

$$H = \underbrace{\sum_{k\geq 1,\sigma} \epsilon_k b^\dagger_{k\sigma} b_{k\sigma} + \sum_{k\geq 1,\sigma} V_k (d^\dagger_\sigma b_{k\sigma} + b^\dagger_{k\sigma} d_\sigma) + \tilde{\mu} \sum_\sigma n_\sigma}_{H_0} + \underbrace{U[n_\uparrow n_\downarrow - \frac{1}{2}(n_\uparrow + n_\downarrow)]}_{H_i}. \tag{3.50}$$

The Hamiltonian consists of two parts, a Gaussian part H_0 and an interaction term H_i. The chemical potential is chosen in a way that $\tilde{\mu} = 0$ corresponds to half filling. $k = 1, \ldots, n_s$ labels the bath electrons denoted by their annihilation and creation operators b and $b^\dagger$. The impurity site is labelled with d and corresponds to the index $k = 0$, so that $d = b_0$. The corresponding action reads:

$$Z = \mathrm{Tr}\, e^{-\beta(H_0 + H_i)}. \tag{3.51}$$

The first step towards the Hirsch-Fye algorithm is to discretize the imaginary time interval $[0, \beta]$ in N equal time slices of the length $\Delta\tau = \beta/N$. With this Eq. (3.51) is written as

$$Z = \mathrm{Tr} \prod_{n=1}^{N} e^{-\Delta\tau(H_0 + H_i)}. \tag{3.52}$$

The crucial step of the derivation is the Trotter-Suzuki breakup [45, 46] of the partition function, which has the following form:

$$e^{-\Delta\tau(A+B)} = e^{-\Delta\tau A} e^{-\Delta\tau B} + \mathcal{O}(\Delta\tau^2). \tag{3.53}$$

This variant of the Baker-Campbell-Hausdorff expansion introduces an approximation to Eq. (3.52), which is only valid for small $\Delta\tau$. The consequences of this systematic error of the order $\mathcal{O}(\Delta\tau^2)$ are discussed in the later part of this section. With this identity Eq. (3.51) reads:

$$Z \approx Z^{\Delta\tau} \equiv \mathrm{Tr} \prod_{n=1}^{N} e^{-\Delta\tau H_0} e^{-\Delta\tau H_i} + \mathcal{O}(\Delta\tau) \tag{3.54}$$

A formula for the Green's function corresponding to Eq. (3.54) can be achieved in a similar way by discretizing the imaginary time evolution operator and again apply Eq. (3.53): $U^{\Delta\tau} \equiv \exp(-\Delta\tau H_0)\, \exp(-\Delta\tau H_i)$.

$$\begin{aligned} g^{\Delta\tau}_{k,k'}(\tau_{n_1}, \tau_{n_2}) &\equiv \langle b_k(\tau_{n_1}) b^\dagger_{k'}(\tau_{n_2}) \rangle \\ &= \frac{\mathrm{Tr}\, U^{N-n_1}_{\Delta\tau} b_k(\tau_{n_1}) U^{n_1-n_2}_{\Delta\tau} b^\dagger_{k'}(\tau_{n_2}) U^{n_2}_{\Delta\tau}}{\mathrm{Tr}\, U^{N}_{\Delta\tau}} \end{aligned} \tag{3.55}$$

This definition is valid for $n_1 > n_2$ and in accordance with [6] we omit the usual minus sign in the definition of the Green's function. As mentioned above the d-site Green's function is defined as the zeroth component of g: $G^{\Delta\tau}(\tau_{n_1}, \tau_{n_2}) = g^{\Delta\tau}_{00}(\tau_{n_1}, \tau_{n_2})$. The next important step of the derivation is a discrete Hubbard-Stratonovich transformation, which converts the problem of interacting fermions in Eq. (3.54) to a problem of non-interacting fermions exposed to an Ising-like field. The transformation is done on each time slice separately and reads

$$e^{\Delta\tau H_i} = \frac{1}{2} \sum_{s=\pm 1} e^{\lambda s (n_\uparrow - n_\downarrow)} \tag{3.56}$$

$$\lambda = \mathrm{arccosh}(\exp(\Delta\tau U/2)). \tag{3.57}$$

Inserting the result of this transformation in Eq. (3.54) yields:

$$Z^{\Delta\tau} = \frac{1}{2^N} \sum_{s_1,\ldots,s_N=\pm 1} Z^{\Delta\tau}_{s_1,\ldots,s_N} \tag{3.58}$$

with

$$Z^{\Delta\tau}_{s_1,\ldots,s_N} = \prod_{\sigma=\pm 1} \mathrm{Tr}\, e^{-\Delta\tau H_0} e^{V^\sigma(s_1)} e^{-\Delta\tau H_0} e^{V^\sigma(s_2)} \ldots e^{-\Delta\tau H_0} e^{V^\sigma(s_N)}. \tag{3.59}$$

The diagonal matrix V should not be confused with the hybridization matrix, it is rather given by $V^\sigma_{k,k'} = \mathrm{diag}\, V[\exp(\lambda\sigma s_n), 1 \ldots 1]$ and is of the order $n_s \times n_s$. A consequence of the utilized transformation is that all remaining terms in Eq. (3.58) are now bilinear and Wick's theorem is therefore applicable. This in mind $Z^{\Delta\tau}$ can be rewritten as a product of determinants:

$$Z^{\Delta\tau} = \sum_{s_1,\ldots,s_N=\pm 1} \det O^\uparrow(s_1,\ldots,s_N) \det O^\downarrow(s_1,\ldots,s_N). \tag{3.60}$$

The matrices O^σ are connected to the configuration dependent Green's function as $(O^\sigma)^{-1}(s_1 \ldots s_n) = g^\sigma(s_1 \ldots s_n)$. Since all bath states are involved in the derivation, the matrices $O^\sigma(s_1,\ldots,s_n)$ are of the order $n_s N \times n_s N$. Due to the fact that the matrices O^σ need direct manipulation in order to compute $Z^{\Delta\tau}$, the algorithm up to now would be infeasible, because of the large matrix sizes. The main finding Hirsch and Fye did to make their algorithm numerically feasible was that Green's functions of different configurations $S = s_1,\ldots,s_N$ and $S' = s'_1 \ldots s'_n$ are connected via a Dyson-like equation.

$$g' = g + (g - \mathbb{1})(e^{V'-V} - \mathbb{1})g' \tag{3.61}$$

It can be seen rather easily that $(e^{V'-V} - \mathbb{1})$ is a projection operator on the d-site. So Eq. (3.61) also holds for the impurity Green's function.

$$G' = G + (G - \mathbb{1})(e^{V'-V} - \mathbb{1})G' \tag{3.62}$$

These equations represent an enormous reduction of the complexity of the problem and resemble the fact that a non-interacting bath can be always integrated out. Eq. (3.62) is now of the order $N \times N$, which is in most cases no challenge for modern computers. A matrix that changes one configuration to another can be found from Eq. (3.62).

$$\mathcal{T}G' = G, \quad \mathcal{T} \equiv \mathbb{1} + (\mathbb{1} - G)[e^{V'-V} - \mathbb{1}] \tag{3.63}$$

As a consequence the Hirsch-Fye algorithm works in the subspace of impurity orbitals. It starts with a configuration-dependent Green's function with all Ising spins set to zero. The physical Green's function is then calculated by averaging over all possible configurations of the Ising field via local updates using Eq. (3.63). Since the effort to sum up all possible spin arrangements grows exponentially, a Markov chain Monte Carlo sampling is usually used for the task. The Monte Carlo weight of a configuration is directly connected to the matrix $\mathcal{T}$:

$$\prod_{\sigma} \frac{\det O^{\sigma}(S')}{\det O^{\sigma}(S)} = \prod_{\sigma} \frac{\det G^{\sigma}(S')}{\det G^{\sigma}(S)} = \prod_{\sigma} \det \mathcal{T}. \tag{3.64}$$

As long as local updates are concerned, the matrix $\mathcal{T}$ can be updated very efficiently via a Sherman-Morrison formula [47].

As mentioned earlier in this section, the shortcoming of the Hirsch-Fye approach is the systematic error introduced through the discretization of the imaginary time. In the metallic regime the impurity Green's function can exhibit a rapid, non-uniform τ-dependence in the low temperature regime. These strong τ dependencies can only be reproduced, if the imaginary grid is very fine. This leads to huge matrix sizes and therefore to a high numerical cost. In the Hirsch-Fye community a choice of $N = \beta U$ is often used, but there are known examples were a choice of $N = 5\beta U$ is necessary to get the systematic error below the statistical one.

A way to circumvent the problem of finite grid sizes has been proposed recently [48, 49]. In this approach multiple calculations for different grid sizes were performed in parallel and a final result was obtained via extrapolation to zero grid size. At the moment it is not clear if this method is still competitive to the methods of later sections like the continuous-time quantum Monte Carlo.

Like all fermionic quantum Monte Carlo methods the Hirsch-Fye also exhibits a sign problem. But it can be shown that this sign problem is absent for the case of the single band Anderson impurity problem [50].

3.2.4 Continuous-Time quantum Monte Carlo

As mentioned in the last section the Hirsch-Fye method suffers from a systematic error that originates from the discretization of the imaginary time domain. This shortcoming limits the method to relatively high temperatures and makes realistic structure calculations for multi-orbital systems numerically costly. In this paragraph a complementary approach to the Hirsch-Fye method is introduced, the continuous-time quantum Monte Carlo (CTQMC). The main difference between both approaches is that the CTQMC does not depend on a discrete imaginary time grid and is therefore the first Monte Carlo method for the AIM without any systematic error. The main concept behind the CTQMC is to expand the partition function of the problem and to sample the infinite series using a Markov chain Monte Carlo. Up to now there are known two implementations of the CTQMC. First Rubtsov and coworkers [4, 51] developed a CTQMC algorithm based on the expansion in the interaction. This procedure is known as the weak-coupling expansion quantum Monte Carlo. Later Werner [3, 52] introduced a procedure that applied an expansion in the hybridization, the so-called strong-coupling expansion quantum Monte Carlo.
At some point both procedures face the evaluation of an infinite sum, which has its source in the Taylor expansion of an exponential in the partition function:

$$Z = \sum_k \int_0^\beta d\tau_1 \ldots \int_0^\beta d\tau_k \, \rho(\tau_1, \ldots, \tau_k) \tag{3.65}$$

In this formula $\rho(\tau_1 \ldots \tau_k)$ is some probability density and k the order of the expansion. The details of ρ depend on the quantity chosen to expand in. It is easy to see that for any given order the evaluation of the k integrals applying a Monte Carlo procedure is possible. A brute force approach would be to truncate the expansion order at a value $k = k_{max}$ and to evaluate the integrals for every order separately. But this modus operandi would again introduce a systematic discretization error to the procedure. A more adequate integration procedure was introduced by Prokof'ev et al. [53]. They proposed a Monte Carlo method for quantum lattice models, where all orders of a similar expansion are sampled at once. This is done by allowing updates in the configuration space, which lead from one expansion order to another. It is possible to evaluate the

infinite sum in Eq. (3.65) without any additional systematic error. In the case of the Anderson impurity problem, ρ consists of an even number of creation and annihilation operators. To formulate an update that will raise the expansion order means to insert an additional pair of operators into ρ. The removal of two operators would correspond to a lowering of the expansion order. Therefore it is in principle possible to formulate an ergodic Monte Carlo algorithm for the problem at hand. The reason that this procedure is also numerical feasible is that the importance of higher order terms in the sum of Eq. (3.65) are exponentially damped due to an $1/k!$ factor, which arises in the expansion of the exponential. Consequently this procedure will not end up in the summation of infinite high orders. The details of the algorithm can have a great impact on the average perturbation order and can therefore lead to great performance differences [54].
For the above CTQMC variants such as the weak- and strong-coupling expansion one has to show in addition to the ergodicity that the *detailed balance* condition is fulfilled. In the following two paragraphs we briefly describe both methods and illustrate how the detailed balance condition can be fulfilled. In order to derive both methods we will stick to the single orbital case, but elaborate descriptions for the multi orbital case can be found in the literature [51, 52].

3.2.4.1 Hybridization algorithm

In order to derive the strong-coupling expansion algorithm we begin again with the action formulation of the Anderson impurity problem. The action reads

$$S = -\int_0^\beta d\tau \int_0^\beta d\tau' \sum_\sigma c_\sigma^*(\tau) G_{0,\sigma}^{-1}(\tau - \tau') c_\sigma(\tau') + U \int_0^\beta d\tau\, n_\uparrow(\tau) n_\downarrow(\tau), \tag{3.66}$$

and can be split up into an atomic part and a hybridization term describing the coupling to the bath, $S = S_{at} + S_\Delta$.

$$S_{at} = \int_0^\beta d\tau \int_0^\beta d\tau' \sum_\sigma c_\sigma^*(\tau)[\partial_\tau - \mu] c_\sigma(\tau') + U \int_0^\beta d\tau\, n_\uparrow(\tau) n_\downarrow(\tau) \tag{3.67}$$

$$S_\Delta = -\int_0^\beta d\tau \int_0^\beta d\tau' \sum_\sigma c_\sigma(\tau) \Delta(\tau - \tau') c_\sigma^*(\tau') \tag{3.68}$$

In the following we chose the path integral representation for the partition function. This makes the derivation easier, because the time ordering operator does not appear explicitly in the formulas. We begin with the expansion in S_Δ. For simplicity only one spin species is taken into account.

$$Z = \int \mathcal{D}[cc^*] \exp(-S_{at}) \exp(-S_\Delta) \tag{3.69}$$

$$= \int \mathcal{D}[cc^*] \exp(-S_{at}) \sum_k \frac{1}{k!} (-S_\Delta)^k \tag{3.70}$$

$$= \int \mathcal{D}[cc^*] \exp(-S_{at}) \sum_k \frac{1}{k!} (\int_0^\beta d\tau \int_0^\beta d\tau' c(\tau)\Delta(\tau - \tau')c^*(\tau'))^k \tag{3.71}$$

The reader should be aware, that the interchange of creation and annihilation operators in equation (3.68) has saved an additional $(-1)^k$ factor in latter expression. The intermediate result for Z reads:

$$Z = \int \mathcal{D}[cc^*] \exp(-S_{at}) \sum_k \frac{1}{k!} \int_0^\beta \prod_{i=0}^k d\tau_i \int_0^\beta \prod_{i=0}^k d\tau_i' \, c(\tau_i)c^*(\tau_i') \prod_{i=0}^k \Delta(\tau_i - \tau_i'). \tag{3.72}$$

In principle Eq. (3.72) is of the same form as Eq. (3.65). Hence a Monte Carlo sampling of the above formula would be possible. But such a sampling would lead to a grave sign problem, since the terms in Eq. (3.72) can be either of positive or negative weight. The main finding of Werner [3] was that Eq. (3.72) can be regrouped in such a way that a term with positive weight and one with negative contribution are combined into a determinant. To see this we multiply above formula with a factor $1 = k!/k!$.

$$\begin{aligned} Z = \int \mathcal{D}[cc^*] e^{-S_{at}} \sum_k \frac{1}{k!} \int_0^\beta \prod_{i=0}^k d\tau_i \int_0^\beta \prod_{i=0}^k d\tau_i' \\ \times \prod_{i=0}^k c(\tau_i)c^*(\tau_i') \prod_{i=0}^k \Delta(\tau_i - \tau_i') \cdot \frac{k!}{k!} \end{aligned} \tag{3.73}$$

Now $k!$ times the product of Grassmann numbers can be written as a sum over all possible permutations of either the $c(\tau_i)$ or the $c^*(\tau_i')$ in the product, where the order of the remaining species is kept fixed. Depending on the sign of the permutation the

product is multiplied by a minus one factor. In the following we chose the permutations of the c^* operators.

$$\begin{aligned} Z = &\int \mathcal{D}[cc^*] e^{-S_{at}} \sum_k \frac{1}{k!} \int_0^\beta \prod_{i=0}^k d\tau_i \int_0^\beta \prod_{i=0}^k d\tau_i' \\ &\times \prod_{i=0}^k \Delta(\tau_i - \tau_i') \cdot \frac{1}{k!} \sum_{\Pi \in S_n} (-1)^\pi c(\tau_1) c^*(\tau'_{\pi 1}) \dots c(\tau_k) c^*(\tau'_{\pi k}) \end{aligned} \tag{3.74}$$

If we now rename $\tau'_{\pi i} = \tau'_i$, Eq. (3.74) can be equated to

$$\begin{aligned} Z = &\int \mathcal{D}[cc^*] e^{-S_{at}} \sum_k \frac{1}{k!} \int_0^\beta \prod_{i=0}^k d\tau_i \int_0^\beta \prod_{i=0}^k d\tau_i' \prod_{i=0}^k c(\tau_i) c^*(\tau_i') \\ &\times \frac{1}{k!} \sum_{\Pi \in S_n} (-1)^\pi \Delta(\tau_1 - \tau'_{\pi 1}) \dots \Delta(\tau_k - \tau'_{\pi k}). \end{aligned} \tag{3.75}$$

Here the last part represents a determinant of a square $k \times k$ matrix. So we end up with the following formula for Z.

$$Z = \int \mathcal{D}[cc^*] e^{-S_{at}} \sum_k \frac{1}{k!} \int_0^\beta \prod_{i=0}^k d\tau_i \int_0^\beta \prod_{i=0}^k d\tau_i' \prod_{i=0}^k c(\tau_i) c^*(\tau_i') \frac{1}{k!} \det \Delta_{i,j}|_{k\times k} \tag{3.76}$$

$$\begin{aligned} =&Z_{at} \sum_k \frac{1}{k!} \int_0^\beta d\tau_1 \int_0^\beta d\tau_1' \dots \int_0^\beta d\tau_k \int_0^\beta d\tau_k' \langle c(\tau_1) c^*(\tau_1') \dots c(\tau_k) c^*(\tau_k') \rangle_0 \\ &\times \frac{1}{k!} \det \Delta_{i,j}|_{k\times k} \end{aligned} \tag{3.77}$$

$$=Z_{at} \sum_k Z_k \tag{3.78}$$

In the last step the product of Grassmann numbers has been written as an expectation value in the atomic basis $\langle A \rangle_0 = \int \mathcal{D}[cc^*] A e^{-S_{at}} / Z_{at}$. So the partition function has become a sum over configuration depended partition functions Z_k, which are a product of an atomic expectation value, representing the degrees of freedom of the atomic cluster and a hybridization term which corresponds to the bath degrees of freedom.

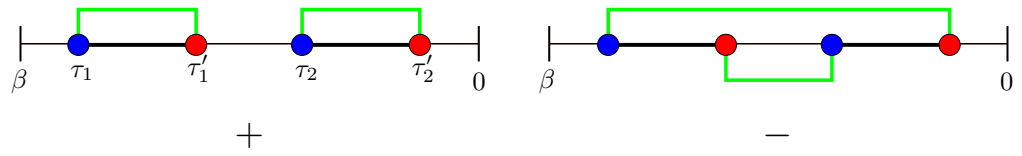

FIGURE 3.8: Complete set of diagrams at $k = 2$ contributing to Eq. (3.80). The left term enters with a positive sign, the right one with a negative sign. Blue dots illustrate an annihilation operator, red ones creation operator. Lower lines represent negative time differences, here Eq. (3.81) should be used.

Diagrammatic representation The partition function of a given order Z_k can be expressed in terms of diagrams. These diagrams have no special physical meaning but illustrate the parametrization of the configuration space and make it easier to understand the process of Monte Carlo updates. To illustrate the diagrammatic representation of Z_k we write Eq. (3.77) for $k = 2$:

$$\begin{aligned} Z_2 =& \frac{1}{4}\int \mathcal{D}[cc^*] \int_0^\beta d\tau_1 d\tau_1' d\tau_2 d\tau_2' \langle c(\tau_1)c^*(\tau_1')c(\tau_2)c^*(\tau_2')\rangle_0 \\ & \times \begin{vmatrix} \Delta(\tau_1-\tau_1') & \Delta(\tau_1-\tau_2') \\ \Delta(\tau_2-\tau_1') & \Delta(\tau_2-\tau_2') \end{vmatrix} \end{aligned} \tag{3.79}$$

$$\begin{aligned} =& \frac{1}{4}\int \mathcal{D}[cc^*] \int_0^\beta d\tau_1 d\tau_1' d\tau_2 d\tau_2' \langle c(\tau_1)c^*(\tau_1')c(\tau_2)c^*(\tau_2')\rangle_0 \Delta(\tau_1-\tau_1')\Delta(\tau_2-\tau_2') \\ & - \langle c(\tau_1)c^*(\tau_1')c(\tau_2)c^*(\tau_2')\rangle_0 \Delta(\tau_1-\tau_2')\Delta(\tau_2-\tau_1')]. \end{aligned} \tag{3.80}$$

The last equation can now be interpreted as an integral over two sorts of τ-dependent diagrams. The atomic expectation value represents a set of two time intervals where a particle is present on the atomic cluster. These intervals are called segments. The hybridization function Δ can now be viewed as a connecting line between these segments. An illustration of a pair of diagrams for the simple case of $k = 2$ can be found in Fig. 3.8. In the evaluation of diagrams, positive and negative time differences are possible in the argument of Δ. But it is only necessary to store Δ for either positive or negative values because the hybridization function is antiperiodic in the imaginary time domain:

$$\Delta(\tau - \tau') = -\Delta(\beta - \tau + \tau'). \tag{3.81}$$

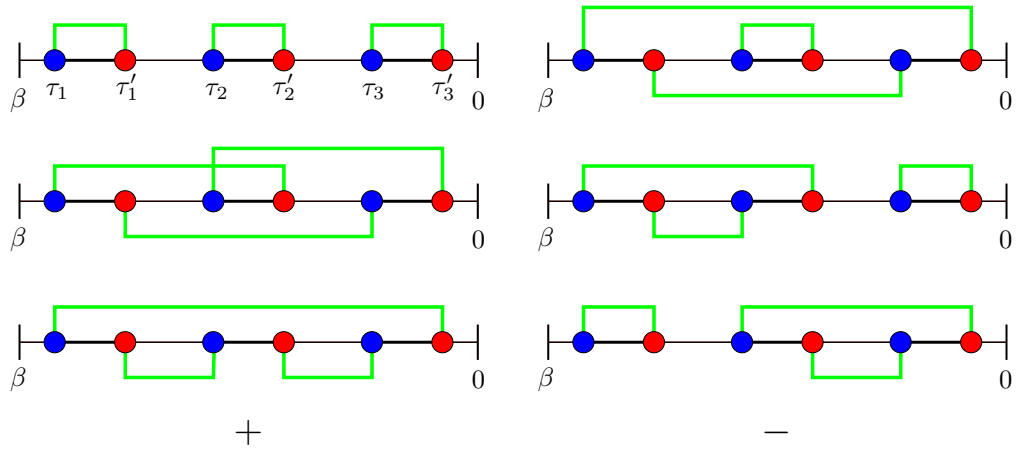

FIGURE 3.9: Diagrams contributing at $k = 3$. Conventions are the same as in Fig. 3.8

The set of diagrams for the case of $k = 3$ is shown in figure 3.9 for the sake of completeness.

Monte Carlo sampling The procedure of Monte Carlo sampling can be understood very easily in the language of diagrams. To ensure ergodicity two sorts of updates are necessary. On the one hand a class of updates that conserves the perturbation order is needed, on the other hand there should be a mechanism, which allows transitions from one order to another. In the first case ergodicity is ensured by allowing a segment to move its position in the imaginary time domain and to change its length. In the latter case the transition to a higher perturbation order is reached by inserting a new segment or, for the reverse step, by removing a segment. These updates ensure ergodicity for the algorithm at hand. Other updates are in principle not needed, but can lead to shorter autocorrelation time [54].

To ensure the detailed balance condition, we make use of the Metropolis Hastings [36, 37] algorithm. A configuration of perturbation order k can be specified by the times of the fermionic creation and annihilation operators, $c_k = \{\tau_1, \tau_1' \ldots \tau_k, \tau_k'\}$. The weight of such a configuration is given by the product of the atomic expectation value and the

determinant of the hybridization function Δ:

$$W_k \approx \langle c(\tau_1)c^*(\tau_1')\dots c(\tau_k)c^*(\tau_k\rangle_0 \times \det\Delta_{ij}. \tag{3.82}$$

The corresponding probability of such a configuration is a product of the weight times a dimensional factor, which conserves the units: $P(c_k) = W_k$ and $P(c_{k+1}) = W_{k+1}d\tau^2$. The last ingredients to the Metropolis Hastings algorithm are the probabilities to propose a move to a higher or lower perturbation order. Since lowering the perturbation order is equivalent to remove a pair of operators and the probability to choose a certain segment is $1/(k+1)$, the probability to propose a transition from order $k+1$ to k is $\Pi^{\text{prop}}_{k+1\to k} = 1/(k+1)$.
The reverse process, raising the perturbation order and inserting a segment, consists of two steps. First a creation operator is inserted at time τ_i' somewhere in the imaginary time domain with probability $d\tau/\beta$. If τ_i' does not fall into an already occupied segment, which is forbidden by the Pauli law, an annihilation operator is placed in a second step between τ_i' and the starting point of the next segment τ_{i-1}'. The probability for this is $d\tau/l_{max}$, where $l_{max} = |\tau_{i-1}' - \tau_i'|$. The overall proposal probability is thus $\Pi^{\text{prop}}_{k\to k+1} = d\tau^2/(\beta l_{max})$. With these definitions the final acceptance criterion reads:

$$\Pi^{\text{acc}}_{k\to k+1} = \min(1, \frac{\beta\, l_{max}}{k+1}\frac{W_{k+1}}{W_k}), \tag{3.83}$$

and the detailed balance condition is implicitly fulfilled.

Segment code In the last paragraph it has become clear, that the main numerical effort of the strong-coupling CTQMC (SCTQMC) lies in the treatment of the determinant of the hybridization function and in the evaluation of the atomic expectation value. If the average expansion order is high, both tasks can be quite elaborate. As we have seen in section 3.2.3 modifications in the hybridization matrix can be again addressed with the help of Sherman Morrison formulas [47]. In principle one is left with the enumeration of the τ-dependent correlator in the atomic basis. To accomplish this task the given atomic cluster is diagonalized and the imaginary time evolution operator $U = \exp(-H\tau)$ is represented in the eigenbasis. With this, one gets a Lehmann-like representation for

the higher order correlators:

$$\langle \ldots \rangle_0 = \frac{1}{Z_{at}} \operatorname{Tr} T_\tau e^{-S_{at}} c_\alpha(\tau_1) c^\dagger_\beta(\tau'_1) \ldots \tag{3.84}$$

$$= \frac{1}{Z_{at}} \sum_{\{n\}} e^{(\tau_1-\beta)E_{n_1}} \langle n_1|c_\alpha|n_2\rangle e^{E_{n_2}(\tau'_1-\tau_1)} \langle n_2|c^\dagger_\beta|n_3\rangle \ldots . \tag{3.85}$$

Here the sequence of operators is not necessarily the one illustrated, but rather the one given by the time ordering operator. For an arbitrary atomic cluster the evaluation of Eq. (3.85) at order k would involve the matrix product of $2k$ matrices. Since the Hilbert space grows exponentially with the number of sites, the enumeration of the atomic expectation value can become the bottleneck of the procedure.

A way to reduce the numerical effort is to follow the route described on page 29 and to take into account the conservation of atomic quantum numbers. In this section we would like to present a special case of the SCQMC known as segment code. This variant of the SCQMC will lead to a very fast way to calculate the atomic expectation value. An alternative implementation to the segment code, which allows to take into account general interactions, is the recently developed Krylov solver. This solver applies the ideas presented in section 3.1.3 in order to speed up the computation of the atomic trace. A detailed introduction can be found in reference [23].

The segment code can be employed if the Hamilton operator of the system can be expressed with the help of density operators only. In this case the Hamiltonian commutes with these operators and the occupation in a given particle number state is a good quantum number. In this case we choose the particle number basis as a natural basis of the problem. As a consequence, there are only two possible values for the product of the matrix elements of the correlator, zero or one. The eigenvalues of the exponential can be expressed with the appropriate combination of density operators. In the end we obtain the following expression for the atomic expectation value:

$$\langle \ldots \rangle_0 = e^{\mu \sum_{n=0}^{N} l_n} e^{-\sum_{m<n} U_{mn} l^O_{mn}}. \tag{3.86}$$

In this notation l_n is a measure for the imaginary time at which an electron is present on the cluster n. l^O_{mn} describes the overlap of occupied segments of orbital m and n.

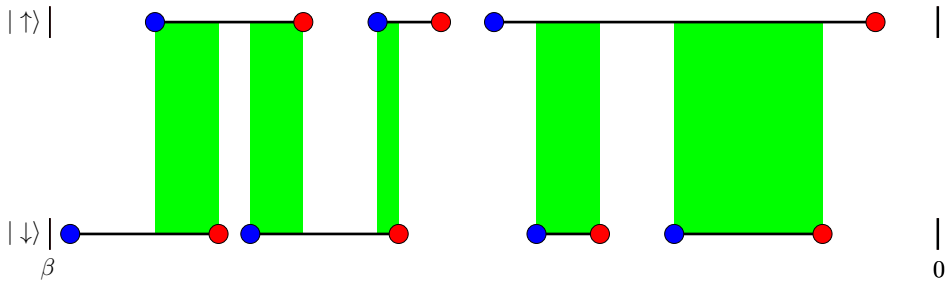

FIGURE 3.10: Conventions are the same as in Fig. 3.8. The green region represents the time interval at which two electrons are present on the impurity and an energy price has to be paid.

In figure 3.10 an example is given for the one orbital case with Hubbard interaction U. If two electrons are present in the same orbital but with different spin, an energy price U has to be paid. So the high dimensional matrix multiplication simplifies to the determination of the overlap of different segments, which is in general a much more easier task.

Measurement of Green's function One of the most important observables in correlated many body problems such as the AIM is the Green's function of the impurity. Once this quantity is calculated, it can be used to determine the density of states on the impurity via analytic continuation. The Green's function is therefore directly related to experimentally accessible quantities and can be written in the following way:

$$G(\tau,\tau') = -\operatorname{Tr} T_\tau c(\tau)c^\dagger(\tau')\exp(-S). \tag{3.87}$$

In order to measure this quantity we follow the main idea of Eq. (3.42) and determine the Green's function as an average over all possible Monte Carlo configurations.

$$G(\tau,\tau') = Z_{at}\sum_k \frac{1}{k!}\int_0^\beta d\tau_1 \ldots \int_0^\beta d\tau_k' G^k(\tau,\tau')\langle c(\tau_1)\ldots c^*(\tau_k)'\rangle_0 \frac{1}{k!}\det\Delta^k \tag{3.88}$$

Here $G^k(\tau,\tau')$ is the configuration dependent Green's function which is defined as follows:

$$G^k(\tau,\tau') = \frac{\langle c(\tau)c^*(\tau')\, c(\tau_1)\ldots c^*(\tau_k')\rangle_0}{\langle c(\tau_1)\ldots c^*(\tau_k)'\rangle_0} = \frac{\langle k+1\rangle_0}{\langle k\rangle_0} \tag{3.89}$$

With the abbreviations for the atomic expectation values in the last equation, the integrand of Eq. (3.88) can be rewritten in the following way:

$$\langle k+1\rangle_0 \det\Delta^k = \frac{\langle k+1\rangle_0}{\langle k\rangle_0}\,\langle k\rangle_0 \det\Delta^k \tag{3.90}$$

$$= \frac{\det\Delta^k}{\det\Delta^{k+1}}\,\langle k+1\rangle_0 \det(\Delta^{k+1}) \tag{3.91}$$

The last two equations give rise to two different definitions of the configuration dependent Green's function. One can either insert two new operators into the atomic expectation value and calculate the ratio of both traces (Eq. (3.90)), or remove a row and a column from the hybridization matrix and calculate the ratio of determinants (Eq. (3.91)). In the language of the formerly discussed segment picture the first would correspond to inserting a pair of unconnected operators into a configuration, the latter to choosing two operators and cutting all the connecting hybridization lines.
Since Eq. (3.90) again involves the manipulation of determinants, it can be coded very efficiently and is therefore the standard definition of the configuration dependent Green's function in modern SCCTQMC codes. The ratio of a matrix's determinant and a determinant of the same matrix, but with one column and one row missing, can be easily computed if one takes into account the following formula from linear algebra:

$$(\Delta^k)^{-1}_{ji} = M^k_{ji} = \frac{(-1)^{i+j}}{\det\Delta_k}\Delta^{k-1}_{ij}, \tag{3.92}$$

where M^k_{ji} is the inverse of the hybridization matrix and the quantity which is stored and manipulated in the codes. Besides the factor $(-1)^{i+j}$ Eq.(3.92) is already the wanted determinant ratio of Eq. (3.91). But this factor is compensated by the fact, that if one chooses a pair of operators to cut all hybridization lines, they have to be commuted to the beginning of the atomic trace, which again gives rise to the same $(-1)^k$ factor. The final measurement of the Green's function in one Monte Carlo configuration is given by

the following equation.

$$G_C^\sigma(\tau,\tau') = \sum_{i,j}^{k} M_{ji}^\sigma \hat{\delta}(\tau-\tau', \tau_i - \tau_j') \text{ with: } \hat{\delta}(\tau,\tau') = \begin{cases} \delta(\tau-\tau') & \tau' > 0 \\ -\delta(\tau-(\tau'+\beta)) & \tau' < 0 \end{cases} \tag{3.93}$$

The measurement of the impurity Green's function can be realized in the following way: If a new Monte Carlo configuration is accepted, the M matrix will be updated and the Green's function can be measured at the time differences occurring in the configuration according to Eq. (3.93).
A similar expression can be derived for the case of the two particle Green's function, which is given here just for completeness.

$$\begin{aligned} \chi_{abcd}^{\sigma\sigma'}(\tau_1,\tau_2,\tau_3,\tau_4) = &\sum_{ab}^{k}\sum_{cd}^{k}(M_{ba}^\sigma M_{dc}^{\sigma'} - \delta_{\sigma\sigma'} M_{da}^{\sigma\sigma} M_{bc}^{\sigma\sigma}) \\ &\times \hat{\delta}(\tau_1-\tau_2,\tau_a-\tau_b')\hat{\delta}(\tau_3-\tau_4,\tau_c-\tau_d')\hat{\delta}(\tau_1-\tau_4,\tau_a-\tau_d')\hat{\delta}(\tau_3-\tau_2,\tau_c-\tau_b') \end{aligned} \tag{3.94}$$

Although the last equation looks like a consequence of Wick's theorem, the reader should be aware that the underlying action is non-Gaussian and therefore Wick theorem is not applicable. The last equation is rather a consequence of a generalized version of Eq. (3.92) for second order minors.

3.2.4.2 Weak-coupling algorithm

The starting point of the so-called weak-coupling CTQMC is, in contrast to the method described in the last section, an expansion in the interaction strength U. The action of the AIM is split up into a quadratic Gaussian part and a non-Gaussian interaction part, $S = S_0 + S_U$. With the following definitions for S_0 and S_U:

$$S_0 = -\sum_\sigma \int_0^\beta \int_0^\beta d\tau d\tau' c_\sigma^\dagger(\tau) G_0^{-1}(\tau-\tau') c_\sigma(\tau') \tag{3.95}$$

$$S_U = +\int_0^\beta d\tau U n_\uparrow(\tau) n_\downarrow(\tau). \tag{3.96}$$

Here $G_0(\tau, \tau')$ is the bare Green's function, i.e., the Green's function of the non-interacting problem. In order to make an expansion in U, the path integral formalism is again used. The partition function reads:

$$Z = \int e^{-S_0} e^{-S_U} \mathcal{D}[cc^*]. \tag{3.97}$$

Performing the Taylor expansion one gets:

$$Z = \int e^{-S_0} \sum_{k=0}^{\infty} \frac{(-1)^k}{k!} U^k \int_0^\beta d\tau_1 \ldots \int_0^\beta d\tau_k \, n_\uparrow(\tau_1) n_\downarrow(\tau_1) \ldots n_\uparrow(\tau_k) n_\downarrow(\tau_k) \tag{3.98}$$

$$Z = Z_0 \sum_{k=0}^{\infty} \frac{(-1)^k}{k!} U^k \int_0^\beta d\tau_1 \ldots \int_0^\beta d\tau_k \, \langle n_\uparrow(\tau_1) n_\downarrow(\tau_1) \ldots n_\uparrow(\tau_k) n_\downarrow(\tau_k) \rangle_0 \tag{3.99}$$

In the last step the definition for the expectation value in the interaction free system has been used:

$$\langle \ldots \rangle_0 = \frac{1}{Z_0} \int \ldots e^{-S_0} \mathcal{D}[cc^*]. \tag{3.100}$$

Taking into account that S_0 is per definition Gaussian, and therefore Wick theorem is applicable here, Eq. (3.99) can be further simplified. The trace over fermionic operators can be expressed as a sum over all possible contractions leading to a fermionic determinant. If special attention is paid to the fact that the occupation number operator can be expressed using the bare Green's function, one ends up with the following formula:

$$Z = Z_0 \sum_{k=0}^{\infty} \frac{(-1)^k}{k!} U^k \int_0^\beta d\tau_1 \ldots \int_0^\beta d\tau_k \prod_\sigma \det G_0^\sigma. \tag{3.101}$$

The last equation is of the same form as Eq. (3.77) in the strong-coupling case. The weight of a configuration consists of a fermionic determinant combined with a term describing the interaction on the impurity. In the preceding section this interaction was given by the expectation value of impurity creation and annihilation operators, here it is just the bare electron-electron interaction U. It is not astonishing that Eq. (3.99) can be expressed in a diagrammatic way as in the last section. Figure 3.11 shows a typical configuration for the case $k = 2$. In contrast to the strong-coupling expansion, there is no segment picture in the weak-coupling case, because the interaction is local in time.

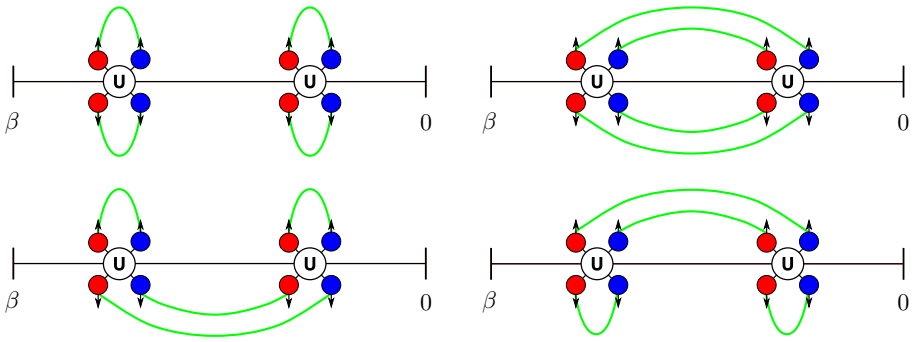

FIGURE 3.11: Diagrammatic representation of a typical weight configuration in the weak-coupling expansion for expansion order $k = 2$. Interaction vertices are placed locally in time and are then connected with the free propagator, which originates from the fermionic determinant. In this figure spin-conservation is assumed.

A typical configuration of order k consists of k interaction vertices placed between 0 and β. The vertices are then connected via the free propagator, the bare Green's function G_0. If the problem is spin diagonal one gets $2 \cdot k!$ diagrams for expansion order k.
In terms of Monte Carlo weights Eq. (3.99) can be expressed as:

$$Z = Z_0 \sum_{k=0}^{\infty} \int_0^\beta d\tau_1 \ldots \int_{\tau_{k-1}}^\beta d\tau_k \, \mathrm{sgn}\,(W_k)|W_k|, \tag{3.102}$$

with

$$W_k = (-1)^k U^k \prod_\sigma G_0^\sigma. \tag{3.103}$$

In the last step the integration boundaries have been rewritten to reach an explicit time ordered representation and to cancel the $1/k!$ factor in front of W_k. In Eq. (3.101) all $k!$ permutations for a given set of times contribute equally to the integral. Therefore it is possible to rewrite the integral in such way that the $k!$ term cancels. An additional sign is not required since all permutations can be transformed into each other by permuting an even number of Grassmann variables. The final equation is in principle of the same form as Eq. (3.42), but has a grave shortcoming: the alternating-sign nature of the Monte Carlo weight makes it numerically impossible to acquire good statistics because of the inherent sign problem. The main contribution of Rubtsov and coworkers [4, 51]

was to find that the theory can be rewritten in such a way that the sign problem is suppressed or even vanishes completely for the one orbital case.

α-parameters The main idea to eliminate the sign problem caused by the definition of Eq. (3.103) is to introduce additional free parameters, which can be chosen in such a way to eliminate the sign problem. This is done by adding a Gaussian term to the action part S_0 and subtracting the same term from the expression for the interaction part S_U. The only requirement to this additional action part is that it is quadratic, so that Wick's theorem is still valid.
This procedure is possible because Monte Carlo is employed to sum up the whole perturbation series. In this case it does not matter if a quadratic action term is shifted from the exactly solvable part S_0 to S_U, as long as the total action stays unchanged. In chapter 5 a similar trick is used to alleviate the non-causality problem of the superperturbation theory at low temperatures, but only a partial series is summed up there. In that case it will also be important that the shifted part is rather small.
In the weak-coupling case the additional free parameter is called α-parameter and is just a c-number and not a Grassmann variable. In principle this number can depend on spin, site and τ, but for the following derivation only the spin dependence is considered. The α-dependent term is introduced as follows:

$$S_0 = -\sum_\sigma \int_0^\beta \int_0^\beta d\tau d\tau' c_\sigma^*(\tau) G_0^{-1}(\tau - \tau') c_\sigma(\tau') - U\alpha_{-\sigma} n_\sigma(\tau) \tag{3.104}$$

$$S_U = \int_0^\beta U[n_\uparrow(\tau) - \alpha_\uparrow][n_\downarrow(\tau) - \alpha_\uparrow]. \tag{3.105}$$

The steps to follow are the same as described above: The Taylor expansion in U is performed and afterwards Wick's theorem is employed. This procedure ends up in an equation very similar to Eq. (3.103).

$$Z = Z_0 \sum_{k=0}^{\infty} \int_0^\beta d\tau_1 \ldots \int_{\tau_{k-1}}^\beta d\tau_k \,\mathrm{sgn}\,(W_k)|W_k| \tag{3.106}$$

$$W_k = (-1)^k U^k \langle (n_\uparrow(\tau_1) - \alpha_\uparrow)(n_\downarrow(\tau_1) - \alpha_\downarrow) \ldots (n_\uparrow(\tau_k) - \alpha_\uparrow)(n_\downarrow(\tau_k) - \alpha_\downarrow)\rangle_0 \tag{3.107}$$

$$=(-1)^k U^k \prod_\sigma \tilde{G}_0^\sigma \tag{3.108}$$

with:

$$\tilde{G}_0^\sigma(\tau_i - \tau_j) = G_0^\sigma(\tau_i - \tau_j) - \alpha \cdot \delta(\tau_i - \tau_j). \tag{3.109}$$

The fact that the α-parameter only occurs on the diagonal of $\tilde{G}_0^\sigma$ is owed to α being a normal c-number and not a Grassmann variable.
To eliminate the sign problem for the single orbital half filled case any choice of α is sufficient, if the following condition between $\alpha_\uparrow$ and $\alpha_\downarrow$ holds.

$$\alpha = \alpha_\downarrow = 1 - \alpha_\uparrow \tag{3.110}$$

Away from half filling a sign problem only occurs if α lies between zero and one. In practice an α-parameter slightly above one is used. The method described here is also applicable to the multi orbital case. But a proper choice of α-parameters to completely alleviate the sign problem in this case has not been found yet.

Monte Carlo sampling The procedure of Monte Carlo sampling is very similar to the case of the strong-coupling expansion. To reach ergodicity one again only needs in principle two updates. One that preserves the expansion order and only rearranges the position of interaction vertices and one that allows to go from one expansion order to another. The latter can be easily reached by an update inserting or removing an interacting vertex. To show that the proposed approach also fulfills the detailed balance condition, one again employs the Metropolis-Hastings [36, 37] algorithm. To do so we define the necessary probabilities. The probability of configuration c_k is given by its weight times a dimensional factor to conserve the units:

$$P(c_k) = |W_k| = U^k \det \tilde{G}_0^\sigma|_k \det \tilde{G}_0^{-\sigma}|_k \tag{3.111}$$

$$P(c_{k+1}) = |W_{k+1}| = U^{k+1} \det \tilde{G}_0^\sigma|_{k+1} \det \tilde{G}_0^{-\sigma}|_{k+1}. \tag{3.112}$$

The probabilities to propose a transition from one expansion order to another can be constructed in the following way: The probability to have a transition from order $k+1$

to k is the probability to pick one of the $k+1$ interaction vertices and remove it. The probability is thus given by

$$\Pi^{\text{prop}}_{k+1\to k} = \frac{1}{k+1}. \tag{3.113}$$

The term for the reverse step is constructed in a similar way. The probability to insert a vertex in the imaginary time domain between zero and β is just:

$$\Pi^{\text{prop}}_{k\to k+1} = \frac{d\tau}{\beta}. \tag{3.114}$$

If the above definitions are inserted in Eq. (3.48) one ends up with the following formula for the acceptance criterion that automatically fulfills the detailed balance condition.

$$\Pi^{\text{acc}}_{k\to k+1} = \min(1, \frac{\beta U}{k+1} \frac{\det \tilde{G}^{\sigma}_0|_{k+1} \det \tilde{G}^{-\sigma}_0|_{k+1}}{\det \tilde{G}^{\sigma}_0|_{k} \det \tilde{G}^{-\sigma}_0|_{k}}) \tag{3.115}$$

Measurement of Green's function The impurity Green's function for a single orbital model with a spin diagonal Hamiltonian is defined as follows:

$$G^{\sigma}(\tau_p - \tau_q) = -\langle T_\tau c_\sigma(\tau_p) c^\dagger(\tau_q)\rangle. \tag{3.116}$$

Starting from this definition a similar expansion to the one described in this chapter is possible. This would correspond to developing a Monte Carlo sampling in terms of the Green's function rather than in terms of the partition function. In the following a different route is described. The sampling is done in terms of the partition function and an estimator for the Green's function is developed. It is not clear if this procedure is efficient, because it assumes that there is a large overlap between the partition function and other observables such as the Green's function. Practical experience shows that a weight formulation in terms of the partition function is very successful. The estimator is described similarly to the one in the strong-coupling case:

$$\langle G^{\sigma}(\tau_p - \tau_q)\rangle_{\text{est}} = \frac{\langle c_\sigma(\tau_p) c^\dagger_\sigma(\tau_q) \prod_{i=1}^{k} (n_\uparrow(\tau_i) - \alpha_\uparrow)(n_\downarrow(\tau_i) - \alpha_\downarrow)\rangle_0}{\langle \prod_{i=1}^{k} (n_\uparrow(\tau_i) - \alpha_\uparrow)(n_\downarrow(\tau_i) - \alpha_\downarrow)\rangle_0}. \tag{3.117}$$

Applying again Wick's theorem, the estimator can be regrouped in the following way:

$$\langle G^\sigma(\tau_p - \tau_q)\rangle_{\text{est}} = \frac{\tilde{G}_0^\sigma|_{(k;G_0^\sigma(\tau_p-\tau_q))}}{\tilde{G}_0^\sigma|_k}, \tag{3.118}$$

where the nominator of Eq. (3.118) has been defined as:

$$\tilde{G}_0^\sigma|_{(k;G_0^\sigma(\tau_p-\tau_q))} = \begin{pmatrix} \tilde{G}_0^\sigma|_k & G_0^\sigma(\tau_i - \tau_q) \\ G_0^\sigma(\tau_p - \tau_j) & G_0^\sigma(\tau_p - \tau_q) \end{pmatrix}. \tag{3.119}$$

The determinant can be calculated using inverse matrix formulas [55].

$$\det \tilde{G}_0^\sigma|_{(k;G_0^\sigma)} = \det \tilde{G}_0^\sigma|_k \Big(G_0^\sigma(\tau_p - \tau_q) - \sum_{ij} G_0^\sigma(\tau_p - \tau_i)(\tilde{G}_0^\sigma|_k)^{-1} G_0^\sigma(\tau_j - \tau_q) \Big) \tag{3.120}$$

With this, the expression for the Green's function estimator reads:

$$\langle G^\sigma(\tau_p - \tau_q)\rangle_{\text{est}} = G_0^\sigma(\tau_p - \tau_q) - \sum_{ij} G_0^\sigma(\tau_p - \tau_i) M_{i,j}^\sigma G_0^\sigma(\tau_j - \tau_q). \tag{3.121}$$

As can be seen from the last equation, the impurity Green's function is measured as a correction to the bare Green' function, which is a direct consequence of the expansion in the interaction. The bare Green's function is so to say the zeroth order approximation in this case. Estimators for higher order correlation functions can also be easily derived. Because S_0 is quadratic Wick's theorem can be applied to express a n-particle Green's function as contractions of the single particle one. For further reading see ref. [56].

Chapter 4

Dual fermion perturbation theory

In the many-body theory of solids, one is often interested in the solution of systems with a large number of interacting degrees of freedom. Even though the conceptual formulation of these models might be simple, the exact solution is quite often beyond the possibilities of modern analytical and numerical approaches.
A prototype of such a system is the class of Hubbard type [57] models. Even tough the model is already known for decades and is often classified as 'a highly oversimplified model' [58], the literature still lacks of a comprehensive solution for these kinds of systems. Due to the complexity of the task, most approaches to solve these systems rely on some kind of approximation. A common scheme is to expand in a small parameter. For the Hubbard model this parameter could be the electron-electron interaction or the inter-site hoping. The problem with this strategy is that in most situations interesting physics is caused by two or more competing phases and therefore no small parameter can be found. A perturbation expansion will lead to poor results in these cases. The main drawback is that the starting point of the perturbation theory is often oversimplified and does not give a proper description of the physical state of the system. In the case of the Hubbard model and small interaction the starting point of the expansion is the non-interacting system. In the case of a small inter-site hopping the system is expanded around the atomic solution.
In this chapter we describe a different kind of perturbation theory. The main innovation

will be that a series expansion is not done around a simple starting point, but around an exactly solvable reference problem, which already contains essential physical information. The key idea is to include as many degrees of freedom in this reference system as possible and to solve it exactly by numerical or analytical techniques. The information not included is then added by a perturbation expansion around this reference system.
This kind of approach was first introduced by Rubtsov [59] in the context of $O(N)$ models. Later the theory was applied to the two-dimensional Hubbard model under the name of dual fermion approach (DF) [60]. The motivation for the work was to find a perturbation expansion around the DMFT solution in order to treat non-local correlations. In this case the reference system was the solution of the DMFT and the full system the whole lattice problem. Meanwhile this approach has been successfully applied to the two-dimensional Hubbard model on a square [60, 61] and triangular lattice [62] and has also been used in the context of superconductivity [63]. In a recent paper it was shown that the underlying perturbation expansion of the dual fermion technique has superior convergence properties over standard diagrammatic approaches [64].
In a later paper we showed that the concept first described in the dual fermion context is general enough to describe also Anderson impurity models. Here an impurity problem with a continuous energy spectrum in the bath is approximated by a finite size effective reference problem with the same interaction [65].
In this chapter we like to give a brief introduction to the underlying perturbation expansion of these approaches. During the derivation we will use the most general formulation of the theory, which will allow us to show that the dual fermion technique and the superperturbation method are special cases of the same theory.
For a more pedagogical introduction to the formal details of the theory we recommend the interested reader reference [56]. Although the superperturbation method on the Keldysh contour is also based on the described approach here, it will be introduced in chapter 7 separately, because it needs the concept of non-equilibrium perturbation theory.

4.1 Derivation of the dual action

As described earlier the aim of this section is to formulate a perturbation expansion of a problem with many degrees of freedom around an easier to solve model. In the following we will entitle the first one as full system and the second one as reference system. The action of the full system can be written in the following way:

$$S^{\mathrm{F}}[c^*, c] = -\frac{T}{N_k} \sum_{\mathbf{k}\omega ab} c^*_{\mathbf{k}\omega a}[(i\omega + \mu)\mathbb{1} - \square(\mathbf{k}, \omega)]_{ab} c_{\mathbf{k}\omega b} + \sum_{\mathbf{i}} S^{\mathrm{NG}}[c^*_{\mathbf{i}}, c_{\mathbf{i}}]. \tag{4.1}$$

Here the notation has been chosen in such a way that the action is able to describe lattice problems as well as Anderson impurity models. The key quantity is $\square(\mathbf{k}, \omega)$. For a lattice model it is jut a placeholder for the dispersion $\epsilon_{\mathbf{k}}$. An Anderson impurity model can be described if a hybridization function $\Delta(i\omega)$ is inserted for $\square(\mathbf{k}, \omega)$. During the derivation we will stay with the most general formulation of the problem. The different flavors of the theory, depending on the actual details of $\square(\mathbf{k}, \omega)$, will be introduced in section 4.3. In equation (4.1) S^{NG} stands for some local non-Gaussian part in the action. In principle the actual form of S^{NG} does not matter, the only requirement for the steps to follow is that this part of the action is local. For a not so exotic model S^{NG} will just be the local Coulomb interaction. The derivation will be done in the multi orbital formulation, so that Latin indices describe orbital and spin degrees of freedom, spatial coordinates are denoted by $\mathbf{i}$ and k vectors by $\mathbf{k}$. T is the temperature and N_k the number of k points. Local problems arise from Eq. (4.1) if N_k is set to one. The following conventions for sums are introduced:

$$\frac{T}{N_k} \sum_{\mathbf{k}} \equiv \sum^{\mathbf{k}} \quad \text{and} \quad T \sum_{\mathbf{i}} \equiv \sum^{\mathbf{i}}. \tag{4.2}$$

With this Eq. (4.1) takes the following form:

$$S^{\mathrm{F}}[c^*, c] = -\sum_{ab}^{\mathbf{k}} c^*_{\mathbf{k}\omega a}[(i\omega + \mu)\mathbb{1} - \square(\mathbf{k}, \omega)]_{ab} c_{\mathbf{k}\omega b} + \sum_{\mathbf{i}} S^{\mathrm{NG}}[c^*_{\mathbf{i}}, c_{\mathbf{i}}]. \tag{4.3}$$

In order to introduce the reference system, the key step is to add and subtract a local frequency dependent function $\triangle(\omega)$. In doing so the full action can be rewritten in the

following way[1]:

$$S^{\mathrm{F}}[c^*, c] = S^{\mathrm{Ref}}[c^*_{\mathbf{i}}, c_{\mathbf{i}}] - \sum_{ab}^{\mathbf{k}} c^*_{\mathbf{k}\omega a}[\triangle(\omega) - \square(\mathbf{k}, \omega)]_{ab} c_{\mathbf{k}\omega b} \tag{4.4}$$

$$S^{\mathrm{Ref}}[c^*_{\mathbf{i}}, c_{\mathbf{i}}] = -\sum_{ab}^{\mathbf{i}} c^*_{\mathbf{i}\omega a}[(i\omega + \mu)\mathbb{1} - \triangle(\omega)]_{ab} c_{\mathbf{i}\omega b} + \sum_{\mathbf{i}} S^{\mathrm{NG}}[c^*_{\mathbf{i}}, c_{\mathbf{i}}]. \tag{4.5}$$

At this point it is important to note the following facts:

1. Eq. (4.4) is an exact reformulation of the initial action in Eq. (4.1).
2. The function $\triangle(\omega)_{ab}$ is not specified at the moment. To stress this fact we have chosen to denote the function with a triangle, rather than a Greek letter.

S^{Ref} is the action of the reference problem. At the moment this part of the action is most general, the only requirement is that the reference problem can be solved exactly. It can already be seen at this early point of the derivation that the reference system described in Eq. (4.5) is far away from being a trivial starting point for a perturbation expansion. S^{Ref} has the same interaction as the full system and the function $\triangle(\omega)$ allows to take care of temporal quantum fluctuations.
The second term in Eq. (4.4) is the difference between the full problem and the reference system. The goal of the following part is to formulate a perturbation theory in this term. Consequently $\triangle(\omega) - \square(\mathbf{k}, \omega)$ will be the small parameter of the theory.
Technically this perturbation expansion is not straightforward. Since S^{Ref} contains a non-Gaussian part it is not possible to expand in $\triangle(\omega) - \square(\mathbf{k}, \omega)$ and to evaluate the expectation values using Wick's theorem. Instead, a different scheme is applied: Via a Hubbard-Stratonovich transformation new auxiliary Grassmann variables are introduced. In the second step one integrates out the old variables and reaches an exact reformulation of the problem in the space of the new variables. In the context of lattice problems these auxiliary quantities have been called dual fermions. In the following we will also use this nomenclature. In the dual space it is then possible to expand in the dual interaction and to construct a Feynman-like perturbation theory for the problem.

[1] In this step, all k-dependent sums over local functions have been Fourier transformed to their spatial counterparts.

Once a partial series has been summed up in the dual space, it is possible to transform back to the old variables, since all transformations have been exact.
The Hubbard-Stratonovich transformation is a standard tool in many body physics [33] and can be written in the following form[2]:

$$e^{c_1^* n_{12} D_{23}^{-1} n_{34} c_4} = \frac{1}{\det D} \int \mathcal{D}[f^*, f] e^{-f_1^* D_{12} f_2 + f_1^* n_{12} c_2 + c_1^* n_{12} f_2}. \tag{4.6}$$

In order to introduce dual variables the choice of the matrices n_{ij} and D_{ij} is not unique. But to end up in a most simple form of the theory, both matrices have been chosen in the following way:

$$\left.\begin{aligned} n &= -g^{-1}(\omega) \\ D &= g^{-1}(\omega)[\triangle(\omega) - \square(\mathbf{k},\omega)]^{-1} g^{-1}(\omega) \end{aligned}\right\} \rightarrow n_{12} D_{23}^{-1} n_{34} = [\triangle(\omega) - \square(\mathbf{k},\omega)]_{14}. \tag{4.7}$$

In this definition $g(\omega)$ is the Green's function of the reference problem. If the transformation is applied to the second term in Eq. (4.4), S^{F} can be brought into a form, which now contains old and new variables:

$$\begin{aligned} S^{\mathrm{F}}[c^*, c, f^*, f] =& S^{\mathrm{Ref}}[c_{\mathbf{i}}^*, c_{\mathbf{i}}] + S^{\mathrm{C}}[f_{\mathbf{i}}^*, f_{\mathbf{i}}, c_{\mathbf{i}}^*, c_{\mathbf{i}}] \\ &+ \sum_{ab}^{\mathbf{k}} f_{\mathbf{k}\omega a}^* [g^{-1}(\omega)[\triangle(\omega) - \square(\mathbf{k},\omega)]^{-1} g^{-1}(\omega)]_{ab} f_{\mathbf{k}\omega b}, \end{aligned} \tag{4.8}$$

with:

$$S^{\mathrm{C}}[f_{\mathbf{i}}^*, f_{\mathbf{i}}, c_{\mathbf{i}}^*, c_{\mathbf{i}}] = \sum_{ab}^{\mathbf{i}} f_{\mathbf{i}\omega a}^* g^{-1}(\omega)_{ab} c_{\mathbf{i}\omega b} + \sum_{ab}^{\mathbf{i}} c_{\mathbf{i}\omega a}^* g^{-1}(\omega)_{ab} f_{\mathbf{i}\omega b}. \tag{4.9}$$

In this form S^{F} consists of the action of the reference problem, a Gaussian term, which only contains dual variables and a part which describes the coupling between the reference system and the dual space, S^{C}. Since the coupling terms only contain local quantities, it is already clear at this point that the coupling of dual fermions to the reference system is purely local. That implies that all quantities necessary to perform the

[2]The reader should be aware that this identity holds regardless of the sign of the matrix n. Therefore some signs in the subsequent derivation might differ from formulations in the literature, but will end in the same results. In this work we have chosen the same convention as in [56].

perturbation expansion can be extracted from the exact solution of the reference problem. This point, which is seen rather easily from Eq. (4.9), is one important condition for the practicability of this theory.

To derive a representation, which only depends on the dual variables, it is necessary to integrate out the old variables. This is done by introducing the following identity:

$$\begin{aligned}\int \exp(-(S^{\mathrm{Ref}}[c^*_{\mathbf{i}}, c_{\mathbf{i}}] + S^{\mathrm{C}}[c^*_{\mathbf{i}}, c_{\mathbf{i}}, f^*_{\mathbf{i}}, f_{\mathbf{i}}]))\mathcal{D}[c^*_{\mathbf{i}}, c_{\mathbf{i}}] \\ \stackrel{!}{=} \mathcal{Z}_{\mathrm{Ref}} \exp(-\sum_{ab}^{\mathbf{i}} f^*_{\mathbf{i}\omega a} g^{-1}(\omega)_{ab} f_{\mathbf{i}\omega b} + \mathcal{V}[f^*_{\mathbf{i}}, f_{\mathbf{i}}]).\end{aligned} \tag{4.10}$$

The last equation has to be understood as a defining equation for an up to now not specified interaction in the dual space $\mathcal{V}$. The old variables are integrated out by choosing this dual potential in such a way that identity (4.10) holds.

Technically this is done by expanding Eq. (4.10) in a Taylor series and comparing the coefficients of both sides with each other. In the following we will briefly summarize the results of this expansion. For shorter expressions and since all indices are local anyway, spatial and orbital degrees of freedom are combined in a number, summation over repeated indices is assumed. For the left-hand side this leads to the following series:

$$\begin{aligned}\int \exp(-(S^{\mathrm{Ref}}[c^*_{\mathbf{i}}, c_{\mathbf{i}}]+S^{\mathrm{C}}[c^*_{\mathbf{i}}, c_{\mathbf{i}}, f^*_{\mathbf{i}}, f_{\mathbf{i}}]))\mathcal{D}[c^*_{\mathbf{i}}, c_{\mathbf{i}}] \\ = \sum_n \langle \frac{1}{n!}(f^*_1 g^{-1}_{12} c_2 + c^*_1 g^{-1}_{12} f_2)^n \rangle_0 \end{aligned} \tag{4.11}$$

$$= 1 - g^{-1}_{12} f^*_1 f_2 + \frac{1}{4}\chi^{(4)}_{2367} g^{-1}_{12} g^{-1}_{34} g^{-1}_{56} g^{-1}_{78} f^*_1 f_4 f^*_5 f_8 \pm \dots . \tag{4.12}$$

Here the exponential of S^{C} has been expanded and the resulting terms have been averaged in the basis of the reference system, denoted by the expectation value symbol $\langle \dots \rangle_0 = \int \dots \exp(-S^{\mathrm{Ref}})\mathcal{D}[c^*, c]$. Consequently, all occurring products of c-variables could be replaced by n-particle Green's functions of the reference problem.

With the following ansatz for the dual potential,

$$\mathcal{V}[f^*_{\mathbf{i}}, f_{\mathbf{i}}] = \sum_i \nu_i[f^*_{\mathbf{i}}, f_{\mathbf{i}}] = k^2_{12} f^*_1 f_2 + k^4_{1234} f^*_1 f_2 f^*_3 f_4 + \dots , \tag{4.13}$$

it is possible to write down the expansion for the right-hand side of Eq. (4.10) [3]:

$$\begin{aligned}\exp\left(-(f_1^* g_{12}^{-1} f_2) + \mathcal{V}[f_{\mathbf{i}}^*, f_{\mathbf{i}}]\right) = 1 - \left(f_1^* g_{12}^{-1} f_2 + k_{12}^2 f_1^* f_2\right. \\ \left. + k_{1234}^4 f_1^* f_2 f_3^* f_4 + \dots\right) + \frac{1}{2!}\left(f_1^* g_{12}^{-1} f_2 f_3^* g_{34}^{-1} f_4 + \dots\right) - \frac{1}{3!}\dots .\end{aligned} \tag{4.14}$$

A comparison of the series expansion of the left-hand and right-hand side yields the final result for the dual interaction potential:

$$\mathcal{V}[f_{\mathbf{i}}^*, f_{\mathbf{i}}] = \sum_i \nu_i[f_{\mathbf{i}}^*, f_{\mathbf{i}}] = -\frac{1}{4}\gamma_{1234}^{(4)} f_1^* f_2 f_3^* f_4 + \frac{1}{36}\gamma_{123456}^{(6)} f_1^* f_2 f_3^* f_4 f_5^* f_6 \mp \dots . \tag{4.15}$$

Subsequently the action in the dual space can be formulated in the following way:

$$S^{\mathrm{d}}[f^*, f] = -\sum_{ab}^{\mathbf{k}} f_{\mathbf{k}\omega a}^* [G_0^{\mathrm{d}}(\omega, \mathbf{k})]_{ab}^{-1} f_{\mathbf{k}\omega b} + \mathcal{V}[f_{\mathbf{i}}^*, f_{\mathbf{i}}], \tag{4.16}$$

with G_0^{d} being the bare dual Green's function:

$$G_0^{\mathrm{d}}(\omega, \mathbf{k}) = -g(\omega)[g(\omega) + [\triangle(\omega) - \square(\mathbf{k}, \omega)]^{-1}]^{-1} g(\omega). \tag{4.17}$$

A back transformation to c-fermions can be also formulated in an exact way, see Appendix A for the non-equilibrium case. In the situation at hand the back transformation has the following form:

$$\begin{aligned}G(\omega, \mathbf{k}) = \big(\triangle(\omega) - \square(\mathbf{k}, \omega)\big)^{-1} + [g(\omega)\big(\triangle(\omega) - \square(\mathbf{k}, \omega)\big)]^{-1} \\ \times G^{\mathrm{d}}(\omega, \mathbf{k})[\big(\triangle(\omega) - \square(\mathbf{k}, \omega)\big) g(\omega)]^{-1}.\end{aligned} \tag{4.18}$$

At this point it is important to note that the final result for the dual action is just a reformulation of the initial action in Eq. (4.1). Up to now no additional approximation has been made and all transformations have been exact.
On the other hand, the latter action exactly describes the physical situation we wanted to achieve: The full problem can be described by an expansion around a reference problem. This is true since the interaction-free dual problem exactly corresponds to a zero

[3] Only terms up to fourth order in f are displayed.

order approximation to the full problem. The bare dual propagator G_0^{d} contains the information of the reference problem as well as the difference of the full and the reference system. Now a series expansion around the reference system can be achieved by performing a diagrammatic expansion in the dual potential. This is possible since Wick's theorem is applicable in Eq. (4.16).

In addition to that this diagrammatic technique promises good convergence properties, since the dual potential has a very advantageous form. The n-particle interaction of the dual fermions is the exact n-particle reducible vertex of the reference problem. This interaction is already frequency dependent and contains screening effects. In comparison to the initial Coulomb interaction, the problem has been rewritten in a formulation, which reduces the interaction. This means that the non-quadratic term in the initial action has been minimized in the dual formulation [61]. In the following we describe briefly why the dual interaction is small.

Although the dual action contains interaction terms up to all orders one can see that higher orders of the dual interaction only play a minor role. On the one hand, higher order terms involve many-particle interactions, which are diminished by phase space arguments [66], on the other hand, their contribution will be small because of the properties of the expansion. In a perturbation expansion in the dual potential two quantities will enter, the dual Green's function and vertices up to all orders. If the interaction is small all vertices are small and the weight of higher order vertices will decrease rapidly: $\gamma^{(4)} \approx U, \gamma^{(6)} \approx U^2, \ldots$. In this case the dual potential can be reduced to a four particle interaction term.

In the opposite case of strong interaction and weak hybridization, i.e. an expansion around the atomic limit, the dual Green's function itself is small. As a consequence all higher order diagrams with many connecting lines will be small. Consequently the perturbation expansion will converge in both limits. In between a good convergence can not be proven analytically but numerical results suggest a good convergence in the intermediate regime [64]. In most cases it is a good approximation to truncate the dual potential after $\gamma^{(4)}$.

In the next section it will be explained how the dual perturbation theory is constructed.

4.2 Construction of the dual diagrammatic technique

The final version of the dual action in Eq. (4.16) allows to formulate a standard Feynman-like perturbation theory in the dual potential. The key concept is to expand the expectation value for the dual Green's function in the non-quadratic part of the action and to employ Wick's theorem to solve the necessary integrals by summing up all possible contractions. This leads to the construction of diagrams for the dual Green's function. Diagrams for the self-energy are then obtained by cutting the external lines of these diagrams, which leads to the possibility to gain an approximation for the dual Green's function by solving Dyson's equation. In the following it will be shown how the two lowest-order diagrams can be constructed.
The expectation value for the dual Green's function can be expressed in the following form:

$$G^{\mathrm{d}}_{12} = -\langle f_1 f^*_2 \rangle = -\frac{Z_f}{Z} \int f_1 f^*_2 e^{-S^{\mathrm{d}}[f,f^*]}\, \mathcal{D}[f^*, f]. \tag{4.19}$$

The dual action is rewritten in the subsequent shorthand notation

$$S^{\mathrm{d}}[f^*, f] = S^{\mathrm{d}}_0[f^*, f] + \mathcal{V}[f^*_{\mathbf{i}}, f_{\mathbf{i}}], \tag{4.20}$$

and is inserted in Eq. (4.19). Afterwards a series expansion in the dual potential is performed:

$$\begin{aligned} G^{\mathrm{d}}_{12} =& -\frac{Z_f}{Z} \int f_1 f^*_2 e^{-\sum_i \nu_i[f^*_{\mathbf{i}}, f_{\mathbf{i}}]}\, e^{-S^{\mathrm{d}}_0}\, \mathcal{D}[f^*, f] && (4.21)\\ =& -\frac{Z_f}{Z} \int f_1 f^*_2 \Big(1 - \sum_l \nu_l[f^*_{\mathbf{l}}, f_{\mathbf{l}}] + \frac{1}{2!} \sum_{lm} \nu_l[f^*_{\mathbf{l}}, f_{\mathbf{l}}] \nu_m[f^*_{\mathbf{m}}, f_{\mathbf{m}}] \\ & - \frac{1}{3!} \sum_{lmn} \nu_l[f^*_{\mathbf{l}}, f_{\mathbf{l}}] \nu_m[f^*_{\mathbf{m}}, f_{\mathbf{m}}] \nu_n[f^*_{\mathbf{n}}, f_{\mathbf{n}}] + \dots \Big) e^{-S^{\mathrm{d}}_0[f^*, f]}\, \mathcal{D}[f^*, f]. && (4.22) \end{aligned}$$

Now the expression for the dual potential is inserted in the Eq. (4.22) and the integrals are solved using Wick's theorem. Since it is the goal to deduce an expression for the two lowest diagrams, only the first term of the dual potential is inserted in Eq. (4.22). A generalization to diagrams containing contributions of higher order terms of the dual potential is straightforward and can be found in [56].

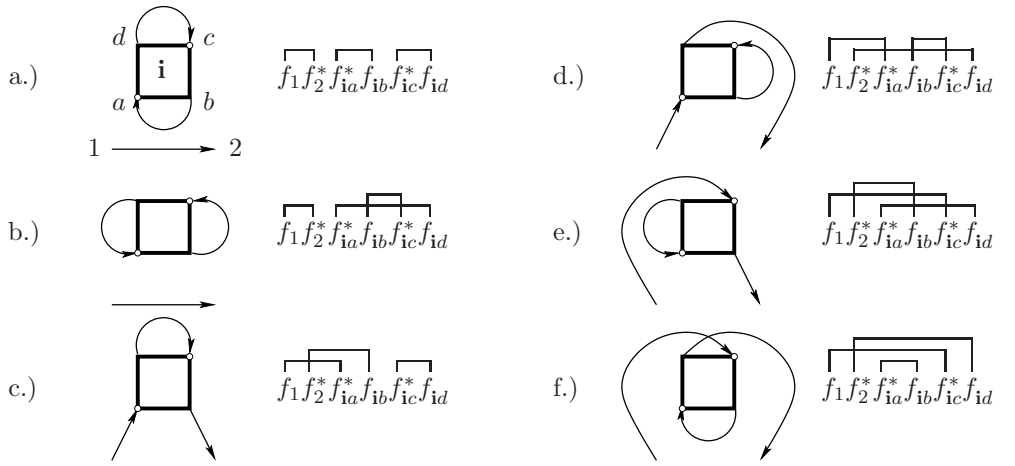

FIGURE 4.1: All possible contractions and the corresponding diagrams of the integral in Eq. (4.24). Diagrams a.) and b.) are disconnected and do not contribute to the dual self-energy. The remaining diagrams are topologically equivalent and can be taken into account by an additional symmetry factor.

The zero-order approximation to the Green's function is the bare dual Green's function, which is defined as the expectation value of two Grassmann numbers using the quadratic part of the dual action:

$$G_0^d|_{12} = -\frac{Z_f}{Z} \int f_1 f_2^* \, e^{-S_0^{\mathrm{d}}} \, \mathcal{D}[f^*, f]. \tag{4.23}$$

An expression for the bare dual Green's function in terms of reference quantities has been already given in Eq. (4.17).

The first-order correction contains the dual potential linearly. Therefore all diagrams derived from this order are purely local. The diagram containing $\gamma^{(4)}$ can be derived from the following integral and its contractions:

$$\frac{-Z_f}{Z} \int f_1 f_2^* \frac{1}{4} \gamma^{(4)}_{\mathbf{i}abcd} f^*_{\mathbf{i}a} f_{\mathbf{i}b} f^*_{\mathbf{i}c} f_{\mathbf{i}d} \, e^{-S_0^{\mathrm{d}}} \mathcal{D}[f^*, f]. \tag{4.24}$$

Fig. 4.1 shows all possible contractions of the 6 Grassmann numbers in the last equation. The first two diagrams do not contribute to the dual self-energy since they are disconnected. The remaining four diagrams are all topologically equivalent. Their contribution to the dual self-energy can be combined in the following expression for the first

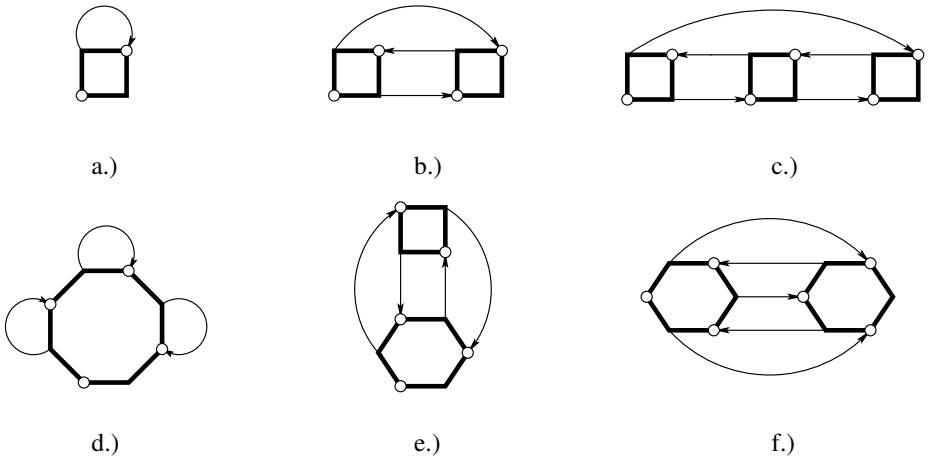

FIGURE 4.2: First few diagrams contributing to the dual self-energy.

local diagram:

$$\Sigma^{\mathrm{d}(a)}_{\mathbf{ii}}|_{ab} = -\gamma^{(4)}_{\mathbf{i}abcd} G^{\mathrm{d}}_{\mathbf{ii}dc}. \tag{4.25}$$

The last equation corresponds to diagram a.) of Fig. 4.2. All higher order diagrams are constructed in the same way. For a certain expansion order of Eq. (4.22), the corresponding integrals are calculated by summing up all non zero contractions. This is done by drawing the diagram of one contraction and then by multiplying this diagram by a weight factor, which corresponds to the number of topologically equivalent diagrams. For the next order in $\gamma^{(4)}$ one has to solve the following integral:

$$\frac{-Z_f}{Z} \int f_1 f_2^* \frac{1}{4} \gamma^{(4)}_{\mathbf{i}abcd} f^*_{\mathbf{i}a} f_{\mathbf{i}b} f^*_{\mathbf{i}c} f_{\mathbf{i}d} \frac{1}{4} \gamma^{(4)}_{\mathbf{j}efgh} f^*_{\mathbf{j}e} f_{\mathbf{j}f} f^*_{\mathbf{j}g} f_{\mathbf{j}h}\, e^{-S^{\mathrm{d}}_0} \mathcal{D}[f^*, f]. \tag{4.26}$$

In this case there are 16 different contractions, which lead to a non zero contribution and which are again topologically equivalent. The total contribution to the dual self-energy is given by:

$$\Sigma^{\mathrm{d}(b)}_{\mathbf{ij}ah} = -\frac{1}{2} \gamma^{(4)}_{\mathbf{i}abcd} \gamma^{(4)}_{\mathbf{j}efgh} G^{\mathrm{d}}_{\mathbf{ij}bg} G^{\mathrm{d}}_{\mathbf{ji}fc} G^{\mathrm{d}}_{\mathbf{ij}de}. \tag{4.27}$$

The corresponding diagram is depicted in Fig. 4.2 b.), for completeness the first higher order diagrams are also shown.

The diagrams discussed so far are the first and simplest contributions to the dual self-energy. But the reader has to be aware that the qualitative contribution to the perturbation theory is different for both diagrams. Since diagram a.) only contains one vertex, the contribution to the dual self-energy will be purely local, even if the full problem is a lattice model. So if the perturbation theory is intended to describe non-local correlation effects, at least diagram b.) has to enter the perturbation series. For a purely local problem cutting the expansion after diagram a.) can be a good approximation, as we will see in chapter 5. Even though the theory is constructed in such a way that the dominant effects of the perturbation series are carried by low order diagrams, it is in some cases necessary to include higher order diagrams or special sub classes of diagrams to describe special physical situations [64].

One of these examples is the description of long ranged spatial correlations, as for example in the case of the 2d Hubbard model in the vicinity of the pseudo-gap formation. Here it is necessary to sum up a ladder of diagrams in order to describe correctly the physical situation. The reason for this is that, as mentioned earlier, the coupling of dual fermions to the reference problem is purely local. As a consequence all spatial correlations are carried by the connecting lines of the diagrams. Since the spatial scope of the dual propagator is limited, one has to include diagrams with many vertices and propagators into the self-energy in order to describe long range spatial correlations.

The construction of a ladder dual fermion approximation (LDFA) was first described in [64], and is similar to the FLEX [67–69] approach, even though the quality of the approximation is totally different in both cases. Whereas the FLEX is an expansion in the bare interaction, the LDFA expands in the reducible vertex of the reference problem. As mentioned earlier, this improved starting point of the expansion promises better convergence properties.

The main idea of the LDFA is to find an approximation to the full vertex of the full problem. This is done by iteration of the Bethe-Salpeter equation, with the full vertex of the reference model being an approximation for the irreducible vertex of the full problem. When an approximation for the full vertex is reached, the Schwinger-Dyson equation is used to obtain the dual self-energy. At the moment the LDFA is the state of the art implementation of the dual fermion perturbation theory.

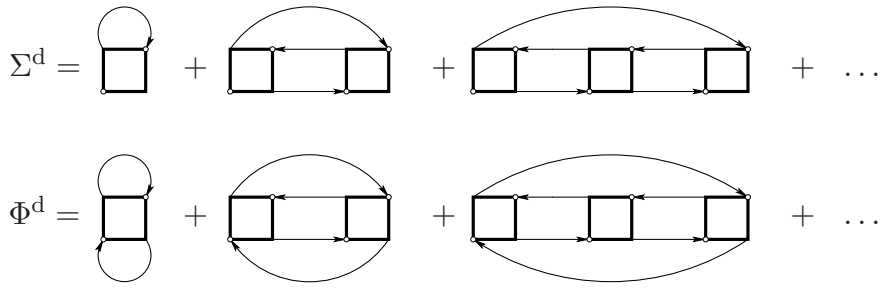

FIGURE 4.3: First diagrams contributing to the ladder dual fermion approximation and the corresponding dual Luttinger-Ward functional.

Another important extension of the theory is the formulation of a conserving approximation in the Baym-Kadanoff sense [70, 71]. Since the transformations to dual variables and back are exact, it is sufficient to obtain a conserving approximation in the dual space. As a consequence, energy, particle number and momentum will be also conserved in terms of real fermions.
Technically such a theory can be constructed in terms of skeleton diagrams, that means, connecting lines have to be understood as fully renormalized propagators. Numerically such a skeleton diagram is computed by calculating an approximation for the dual Green's function and then by inserting this Green's function again into the diagrams until a self-consistency is reached. Mathematically a conserving approximation can be constructed as a functional derivative of a Luttinger-Ward functional. The functional corresponding to the LDFA is depicted in Fig. 4.3.

4.3 Overview of different flavors of the theory

In the following it is shown that the dual fermion perturbation theory is able to describe a great variety of models. We give an overview of systems, that can be treated, and show how approximations to these problems can be constructed by varying the reference system. The main focus will be to show the scope of the approaches and to clarify their differences. For a more complete description of the methods we refer the reader

TABLE 4.1: Overview of different flavors of the dual theory, depending on the actual form of $\square(\mathbf{k},\omega)$ and $\triangle(\omega)$.

$\square(\mathbf{k},\omega)$	$\triangle(\omega)$	Name
$\epsilon_{\mathbf{k}}/\mathbf{h}_{\mathbf{k}}$	$\Delta(\omega)$	Dual Fermion
$\epsilon_{\mathbf{k}}/\mathbf{h}_{\mathbf{k}}$	$\Delta^{\mathrm{N}}(\omega)$	VLA
$\Delta(\omega)$	$\Delta^{\mathrm{N}}(\omega)$	Superperturbation
$\epsilon_{\mathbf{k}}/\mathbf{h}_{\mathbf{k}}$	$\Delta^{\mathrm{N}}(t,t')$	VLA on Keldysh contour
$\Delta(t,t')$	$\Delta^{\mathrm{N}}(t,t')$	Superperturbation on Keldysh contour

to the corresponding chapters. For a quick reference the different methods have been summarized in table 4.1 and diagram 4.4.

4.3.1 Dual fermion

The original dual fermion method has been developed with the intention to include non-local correlations in the description of lattice problems, starting from a local reference system. The main idea was to solve the Anderson-type reference problem efficiently with the help of modern impurity solvers, and to treat all non-local effects perturbatively. This idea is illustrated in Fig. 4.5. To deduce the correct formulation of the theory from the derivation of the last section, $\square(\mathbf{k},\omega)$ has to be replaced by the dispersion relation of the lattice $\epsilon_{\mathbf{k}}$ and $\triangle(\omega)$ by a hybridization function, $\Delta(\omega)$, describing the local problem. Since the local reference system has not been specified so far, the choice of the hybridization function is in principle not fixed and an additional condition is necessary to choose $\Delta(\omega)$ in an optimal way.
Such a constraint can be the elimination of purely local diagrams in the perturbation series. This can be achieved by requiring that the local contribution of the bare dual Green's function is zero. But this condition is exactly equal to the DMFT self-consistency equations for the hybridization function $\Delta(\omega)$. This circumstance leads to a very important connection of the DMFT approach and the dual fermion method: From a dual fermion point of view the DMFT corresponds to the best possible local approximation

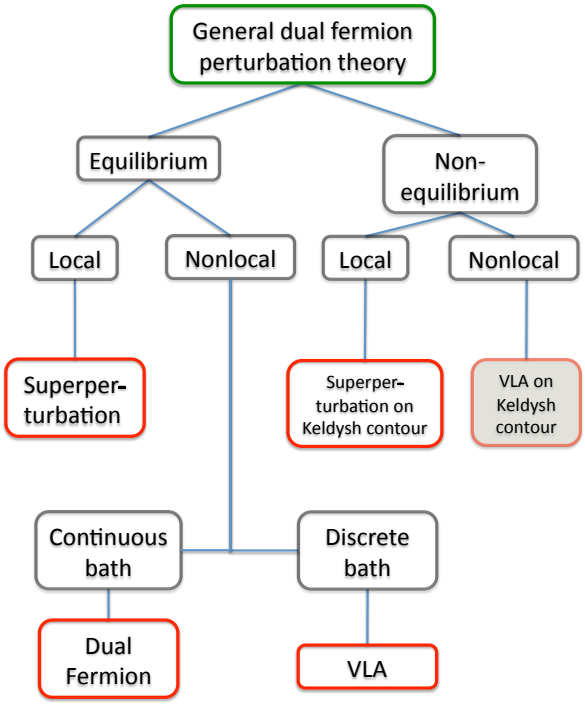

FIGURE 4.4: Overview of the different methods described in this thesis and their relation.

of the full system.

Nevertheless the DMFT hybridization function might not be the optimal choice for the reference problem if non-local diagrams are included. Therefore the DMFT hybridization function is chosen as a starting point for $\Delta(\omega)$ and afterwards an optimal choice for the reference system is determined self-consistently. The reader should be aware, that as soon as $\Delta(\omega)$ differs from the DMFT self-consistency solution, local diagrams contribute again to the series expansion. An introduction to the dual fermion calculation scheme can be found in [72].

4.3.2 Variational lattice approach

The freedom of choice for the local function $\triangle(\omega)$ leads to the development of the variational lattice approach (VLA). The idea behind the VLA is to take a finite number

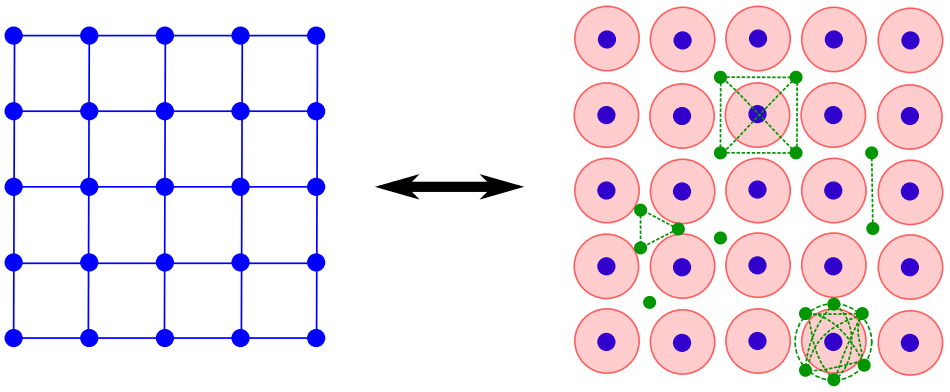

FIGURE 4.5: Illustration of the dual fermion method: The original lattice problem (blue) is replaced by a collection of local Anderson-type reference problems (red circles). All non-local effects enter via the dual perturbation expansion (green particles).

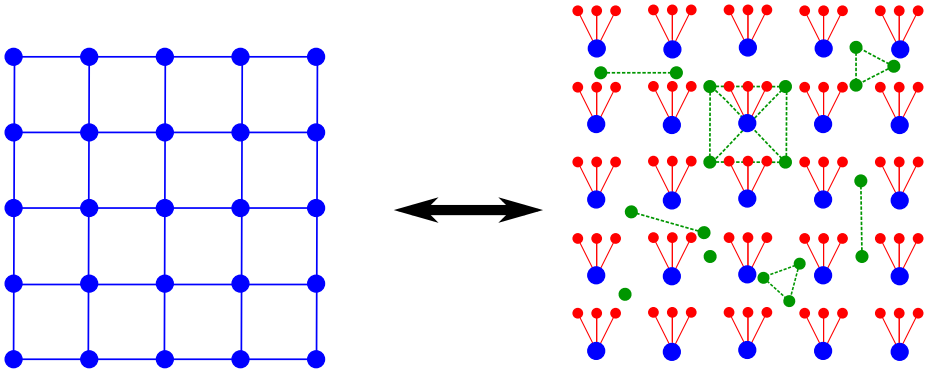

FIGURE 4.6: Illustration of the variational lattice method: The original lattice problem (blue) is replaced by a collection of local Anderson-type reference problems with a finite number of bath sites. All non-local effects enter via the dual perturbation expansion (green particles)

of bath sites coupled to an interacting impurity as a reference system for the full lattice problem. This finite system can be solved using exact diagonalization, which promises a good possibility to do analytic continuation of the final result, because of the numerical precision inherent from the ED solution. In the following the hybridization function for this reference model is denoted by $\Delta^{\mathrm{N}}(\omega)$, where N is the number of bath sites. The conceptual idea of the VLA is depicted in Fig. 4.6. It is important to note that this approach does not necessarily need a convergence in the number of bath sites as for

example the DMFT with ED as solver. The fundamental difference is that in the dual fermion approach the local hybridization function can be arbitrary, which means if all possible diagrams are summed up then every $\triangle(\omega)$ will lead to the solution of the full problem. In the DMFT a convergence in the number of bath sites is needed, because the self-consistency condition can not be fulfilled on the finite subspace of $\Delta^{\mathrm{N}}(\omega)$. This implies that in the VLA a small number of bath sites and diagrams might be sufficient to get a good approximation for the lattice model.
Because of its construction the VLA is somewhat similar to the hybridization expansion technique for lattice models [73–77]. In the latter approach a perturbation around the atomic limit is performed, which corresponds to the VLA, if the hybridization function is zero for all frequencies. So the VLA can be seen as a generalization of the latter approach. In this sense the VLA is variational, because the additional bath parameters allow to optimize the function $\Delta^{\mathrm{N}}(\omega)$. In the hybridization expansion such a variation is not possible because of the missing bath.

4.3.3 Superperturbation

The superperturbation (SPERT) is a solver for Anderson impurity models. The full problem is characterized by a hybridization function $\Delta(\omega)$, which replaces $\square(\mathbf{k}, \omega)$ in the former derivation.
Such a problem can be solved by methods like the CTQMC or the ED. But both methods have their drawbacks: The CTQMC relies on statistical methods such as MAXENT to continue the final data to the real axis because of the statistical error inherent to the method. The ED on the other hand makes it possible to calculate quantities directly on the real axis, but the result is only valid in the limit of an infinite number of bath sites. Consequently one is faced with an exponentially growing Hilbert space when using this method.
The idea of the SPERT is to improve the exact diagonalization result via perturbation expansion. Therefore a system with a small number of bath sites, described by a hybridization function $\triangle(\omega) = \Delta^{\mathrm{N}}(\omega)$, is chosen as a reference system. The expansion is constructed in such a way that it is possible to converge to the exact result using two

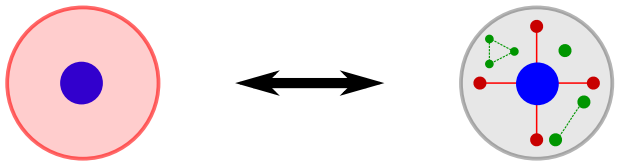

FIGURE 4.7: Concept of the super perturbation solver: The Anderson impurity problem with a hybridization function $\Delta(\omega)$, is described by a reference system with a small number of bath parameters. Then the difference is treated perturbatively by dual fermions (green dots).

opposite ways. First by improving the reference system by including more bath sites, and second by including higher orders into the series. In addition to that the superior possibility of ED to continue data to the real axis is preserved, because the SPERT is based on ED data.
Like the VLA the SPERT can be seen as a generalization of the hybridization expansion solver for impurity problems proposed in [78] to reference system including a bath. The concept of the SPERT is illustrated in Fig. 4.7.

4.3.4 Systems out of equilibrium

The dual perturbation theory is general enough to describe systems out of equilibrium. The concept of the method stays the same, the full problem is described by a smaller reference system and the difference of both problems is treated perturbatively. The only differences are the details of the involved quantities and the underlying theory. In the non-equilibrium case the hybridization function will not depend on one imaginary time frequency, but on two time arguments, $\triangle(t, t') = \Delta(t, t')$. In addition to that the perturbation expansion is constructed with the help of the Keldysh formalism and not on Matsubara frequencies. Besides these changes all equations will be very similar.
It is in principle possible to formulate a general dual fermion technique, a VLA, and a SPERT for the non-equilibrium case. In this thesis the SPERT for a system out of equilibrium is described in Chapter 7 and a formulation of the VLA is planned.

Chapter 5

Superperturbation solver for the Anderson impurity problem

The investigation of modern materials and their compounds is one of the main aspects of modern condensed matter theory. If the material under consideration exhibits strong correlations, most approaches rely in one way or the other on the solution of an Anderson impurity model. The LDA+DMFT approach for example is one of the most common approaches in this case.
As mentioned in Chapter 3, there are several solvers available. Continuous-time quantum Monte Carlo algorithms for instance are today efficient enough to treat 5 or 7 orbital systems in the DMFT approach. Nevertheless, they suffer from some severe drawbacks: All available implementations work on the imaginary time axis and need a complicated continuation to the real axis, which is up to now an ill-posed problem. Additionally, the stochastic nature of quantum Monte Carlo causes a strong fermionic sign problem away from half-filling if complicated interaction terms are involved.
An alternative is the exact diagonalization (ED). Here the continuous bath is discretized by a collection of effective bath sites. This approach has no problems with analytic continuation, since an analytic representation of the Green's function is known and all quantities are numerically exact up to floating point precision. However the disadvantage of the scheme is that the method only converges to the exact result in the limit of infinite

number of bath sites. Even though this convergence is exponentially fast for quantities on the imaginary axis, the limit of a continuous bath is often hard to reach, due to the also exponentially fast growing Hilbert space. At the moment the world record in the total number of sites is of the order of 16. This means that for a 5 orbital model only 2 bath sites for each orbital are available at maximum. This limits the approach to systems with a few orbitals only.

There are also alternative solvers available, which work by perturbation expansion around some trivial limits. These solvers are the IPT [79, 80], the FLEX [67], the NCA [81] and the hybridization expansion solver [78]. All these algorithms are limited to a small parameter window and fail outside this region. The FLEX and the IPT are applicable in the weak-coupling case, the hybridization solver in the strong coupling area.

In the following chapter we will introduce a solver, which combines the strength of all mentioned methods, the superperturbation solver for the Anderson impurity model. The key idea is to apply a dual transformation in order to expand around an exact diagonalization result. This procedure promises good possibilities to do an analytic continuation, because all data will be numerically exact and analytic formulas are known for all quantities and transformations. Additionally, this perturbation expansion will have a non trivial starting point: the exact diagonalization result. This allows to converge to the exact result in two ways: First by improving the ED starting point by including more bath sites and making the perturbation smaller, and second by including more diagrams into the perturbation expansion. Additionally the method at hand has two exact limits, the weak-coupling limit and the strong coupling regime.

The presented results have been obtained in collaboration with Hartmut Hafermann, who provided the general dual fermion code to treat more than one diagram and performed the part of the simulations that compared the Kondo temperature to NRG (Fig. 5.7). Some of the results have been already published in [56, 65].

5.1 Dual formulation of the problem

In the following section we will briefly review the main steps of the dual transformation in the superperturbation case and give a collection of the main formulas. A detailed derivation in its most general form can be found in chapter 4. The model under consideration is the Anderson impurity model with the following Hamiltonian:

$$H = \sum_{k\alpha} \epsilon^b_{k\alpha} b^\dagger_{k\alpha} b_{k\alpha} + \sum_{\alpha} \epsilon^c_\alpha c^\dagger_\alpha c_\alpha + H_{\mathrm{loc}}[c^\dagger, c] + \sum_{k\alpha\beta} \left(V_k^{\alpha\beta} c^\dagger_\alpha b_{k\beta} + V_k^{*\beta\alpha} b^\dagger_{k\alpha} c_\beta \right). \quad (5.1)$$

The definitions concerning indices and abbreviations are the same as in Eq. (2.1) in chapter 2. Greek letters are used as a combined index for orbital and spin degrees of freedom. $b^\dagger$ and b are the bath, $c^\dagger$ and c the impurity creation and annihilation operators. H_{loc} is the local electron-electron interaction, $V_k^{\alpha\beta}$ the transition amplitude for a hopping process from the bath to an impurity orbital. To derive a dual formulation of the problem, the action representation of the AIM is employed:

$$S^{\mathrm{F}}[c^*, c] = -T \sum_{\omega ab} c^*_{\omega a} [(i\omega + \mu)\mathbb{1} - \Delta(\omega)]_{ab} c_{\omega b} + S^{\mathrm{NG}}[c^*, c]. \quad (5.2)$$

Here $\Delta(\omega)$ is the hybridization function of the full system, which has been obtained from Eq. (5.1), by integrating out the bath degrees of freedom. The key idea of the superperturbation is to add and subtract the hybridization function $\Delta^{\mathrm{N}}(\omega)$ of a properly chosen reference system, where N is the number of bath sites used in the reference problem. Properly chosen means in this case that the reference system is already a good approximation to the full system and that some essential physics is already captured. In principle the choice of $\Delta^{\mathrm{N}}(\omega)$ is arbitrary, but since it is the aim to perform a perturbation expansion in $D = \Delta^{\mathrm{N}}(\omega) - \Delta(\omega)$, it is clear that the quality of the approach will depend on the chosen reference problem. The applied procedure of choosing the reference system is discussed in the next section. After this step the action of the full system reads:

$$S^{\mathrm{F}}[c^*, c] = S^{\mathrm{Ref}}[c^*_{\mathbf{i}}, c_{\mathbf{i}}] - T \sum_{ab} c^*_{\omega a} [\Delta^{\mathrm{N}}(\omega) - \Delta(\omega)]_{ab} c_{\omega b} \quad (5.3)$$

$$S^{\mathrm{Ref}}[c^*_{\mathbf{i}}, c_{\mathbf{i}}] = -T \sum_{ab} c^*_{\mathbf{i}\omega a} [(i\omega + \mu)\mathbb{1} - \Delta^{\mathrm{N}}(\omega)]_{ab} c_{\mathbf{i}\omega b} + S^{\mathrm{NG}}[c^*, c]. \quad (5.4)$$

This expression has a very convenient form: It consists of the action of a finite reference system with the same interaction as the full problem and an additional part, which is the difference of both systems: $D = \Delta^{\mathrm{N}}(\omega) - \Delta(\omega)$. To formulate a perturbation expansion in this quantity it is necessary to change to the dual space, since in the c-fermion representation the action contains a non-quadratic part and Wick's theorem is not applicable. The main steps of this transformation have been presented in Chapter 4 and will only be briefly discussed here. In a first step dual variables are introduced using an exact Hubbard-Stratonovitch transformation. The transformation can be written in the following way:

$$e^{c_1^* n_{12} \mathcal{T}_{23}^{-1} n_{34} c_4} = \frac{1}{\det \mathcal{T}} \int \mathcal{D}[f^*, f] e^{-f_1^* \mathcal{T}_{12} f_2 + f_1^* n_{12} c_2 + c_1^* n_{12} f_2}, \tag{5.5}$$

where n and $\mathcal{T}$ have the following form:

$$\left.\begin{aligned} n &= -g^{-1}(\omega) \\ \mathcal{T} &= g^{-1}(\omega)[\Delta^{\mathrm{N}}(\omega) - \Delta(\omega)]^{-1} g^{-1}(\omega) \end{aligned}\right\} \rightarrow n_{12} \mathcal{T}_{23}^{-1} n_{34} = [\Delta^{\mathrm{N}}(\omega) - \Delta(\omega)]_{14} = D. \tag{5.6}$$

After the transformation, the resulting action is a mixed representation of c- and f-fermions:

$$\begin{aligned} S^{\mathrm{F}}[c^*, c, f^*, f] =& S^{\mathrm{Ref}}[c^*, c] + S^{\mathrm{C}}[f^*, f, c^*, c] \\ &+ T \sum_{ab} f_{\omega a}^* [g^{-1}(\omega)[\Delta^{\mathrm{N}}(\omega) - \Delta(\omega)]^{-1} g^{-1}(\omega)]_{ab} f_{\omega b}, \end{aligned} \tag{5.7}$$

with:

$$S^{\mathrm{C}}[f^*, f, c^*, c] = T \sum_{ab} f_{\omega a}^* g^{-1}(\omega)_{ab} c_{\omega b} + T \sum_{ab} c_{\omega a}^* g^{-1}(\omega)_{ab} f_{\omega b}. \tag{5.8}$$

The remaining c-fermions are integrated out by introducing a dual interaction potential, which is chosen in such a way, that the following identity holds:

$$\begin{aligned} \int \exp(-(S^{\mathrm{Ref}}[c^*, c] + S^{\mathrm{C}}[c^*, c, f^*, f])) \mathcal{D}[c^*, c] \\ \stackrel{!}{=} \mathcal{Z}_{\mathrm{Ref}} \exp(-T \sum_{ab} f_{\omega a}^* g^{-1}(\omega)_{ab} f_{\omega b} + \mathcal{V}[f^*, f]). \end{aligned} \tag{5.9}$$

After expanding both sides in powers of f and comparing the coefficients, the final dual action has the following form:

$$S^{\mathrm{d}}[f^*, f] = -T \sum_{ab} f^*_{\omega a} [G^{\mathrm{d}}_0(\omega)]^{-1}_{ab} f_{\omega b} + \mathcal{V}[f^*, f], \tag{5.10}$$

with G^{d}_0 being the bare dual Green's function

$$G^{\mathrm{d}}_0(\omega) = -g(\omega)[g(\omega) + [\Delta^{\mathrm{N}}(\omega) - \Delta(\omega)]^{-1}]^{-1} g(\omega) \tag{5.11}$$

and $\mathcal{V}[f^*, f]$ the dual potential:

$$\mathcal{V}[f^*_{\mathbf{i}}, f_{\mathbf{i}}] = \sum_i \nu_i[f^*_{\mathbf{i}}, f_{\mathbf{i}}] = -\frac{1}{4}\gamma^{(4)}_{1234} f^*_1 f_2 f^*_3 f_4 + \frac{1}{36}\gamma^{(6)}_{123456} f^*_1 f_2 f^*_3 f_4 f^*_5 f_6 \mp \dots . \tag{5.12}$$

The dual perturbation theory is then formulated in a standard way by expansion in the dual potential and application of Wick's theorem. The diagrams are the same as already discussed in chapter 4, see Fig. 4.2. After summing up a sub-class of diagrams the dual Green's function can be transformed back by the following exact relation:

$$G(\omega) = \big(\Delta^{\mathrm{N}}(\omega) - \Delta(\omega)\big)^{-1} + [g(\omega)\big(\Delta^{\mathrm{N}}(\omega) - \Delta(\omega)\big)]^{-1} \times G^{\mathrm{d}}(\omega)[\big(\Delta^{\mathrm{N}}(\omega) - \Delta(\omega)\big) g(\omega)]^{-1}, \tag{5.13}$$

where $G(\omega)$ is the Green's function of the full system and $g(\omega)$ the Green's function of the reference system.

5.1.1 The first diagram

In the following a special representation of the first diagram is presented, which does not require the explicit calculation of the vertex. The formulation in this section was introduced by X. Dai [78] in the case of the hybridization expansion solver for the Anderson impurity problem, which has a similar form as the superperturbation solver. As a start we split the calculation of the first diagram into two parts: One containing the

two particle Green's function and the other containing the trivial contribution only:

$$\Sigma_{12}^{\mathrm{d}(a)} = -\gamma_{1234} G_{43}^{\mathrm{d}} \tag{5.14}$$
$$= g_{11'}^{-1} g_{33'}^{-1} (\chi_{1'2'3'4'} - g_{1'2'} g_{3'4'} + g_{1'4'} g_{3'2'}) g_{2'2}^{-1} g_{4'4}^{-1} G_{43}^{\mathrm{d}} \tag{5.15}$$
$$= g_{11'}^{-1} g_{33'}^{-1} (\chi_{1'2'3'4'}) g_{2'2}^{-1} g_{4'4}^{-1} G_{43}^{\mathrm{d}} + g_{11'}^{-1} g_{33'}^{-1} (-g_{1'2'} g_{3'4'} + g_{1'4'} g_{3'2'}) g_{2'2}^{-1} g_{4'4}^{-1} G_{43}^{\mathrm{d}} \tag{5.16}$$
$$= \Sigma_{12}^{\mathrm{d}0} + \Sigma_{12}^{\mathrm{d}1} \tag{5.17}$$

Both terms can be significantly simplified if one performs the multiplication of the Green's functions with their inverse. For $\Sigma_{12}^{\mathrm{d}0}$ this leads to the following result:

$$\Sigma_{12}^{\mathrm{d}0} = g_{11'}^{-1} g_{33'}^{-1} (\chi_{1'2'3'4'}) g_{2'2}^{-1} g_{4'4}^{-1} G_{43}^{\mathrm{d}} \tag{5.18}$$
$$= - g_{11'}^{-1} g_{33'}^{-1} (\chi_{1'2'3'4'}) g_{2'2}^{-1} g_{4'4}^{-1} g_{45} \Delta_{56}^{\mathrm{d}} g_{63} \tag{5.19}$$
$$= - g_{11'}^{-1} (\chi_{1'2'65}) g_{2'2}^{-1} \Delta_{56}^{\mathrm{d}} \tag{5.20}$$
$$= - g_{11'}^{-1} (\chi_{1'2'3'4'}) g_{2'2}^{-1} \Delta_{4'3'}^{\mathrm{d}}. \tag{5.21}$$

In this expression the important quantity Δ^{d} has been introduced. It has the following definition:

$$\Delta_{12}^{\mathrm{d}}(\omega) = [g(\omega) + (\Delta^{\mathrm{N}}(\omega) - \Delta(\omega))^{-1}]_{12}^{-1} \tag{5.22}$$

and is connected to the bare dual Green's function by the subsequent relation:

$$G_0^{\mathrm{d}} = -g \Delta^{\mathrm{d}} g. \tag{5.23}$$

The expression for the second part of the first diagram can also be strongly reduced by explicitly writing out all contributing terms:

$$\Sigma_{12}^{\mathrm{d}1} = g_{11'}^{-1} g_{33'}^{-1} \beta (-g_{1'2'} g_{3'4'} + g_{1'4'} g_{3'2'}) g_{2'2}^{-1} g_{4'4}^{-1} G_{43}^{\mathrm{d}} \tag{5.24}$$
$$= - g_{11'}^{-1} g_{33'}^{-1} \beta (-g_{1'2'} g_{3'4'} + g_{1'4'} g_{3'2'}) g_{2'2}^{-1} g_{4'4}^{-1} g_{45} \Delta_{56}^{\mathrm{d}} g_{63} \tag{5.25}$$
$$= - g_{12}^{-1} \beta \,\mathrm{Tr}(\Delta^{\mathrm{d}} g) + \Delta_{12}^{\mathrm{d}}. \tag{5.26}$$

The expression for the total self-energy contribution of the first diagram reads:

$$\Sigma_{12}^{\mathrm{d}(a)} = -g_{12}^{-1} \beta \,\mathrm{Tr}(\Delta^{\mathrm{d}} g) + \Delta_{12}^{\mathrm{d}} - g_{11'}^{-1} (\chi_{1'2'3'4'}) g_{2'2}^{-1} \Delta_{4'3'}^{\mathrm{d}}. \tag{5.27}$$

The main finding of X. Dai was that the spectral representation of the second part in Matsubara frequencies can be written in a very advantageous form:

$$
\begin{aligned}
\Sigma_{12}^{\mathrm{d}(0)}(i\omega) = \frac{1}{\beta}\sum_{i\omega_{n'}} \chi_{1234}(i\omega, i\omega, i\omega', i\omega')\Delta_{43}^{\mathrm{d}} = \sum_{34}\sum_{ijkl} \times \\
+\langle c_1 c_3^* c_4 c_2^* \rangle_{ijkl} \big[\frac{\mathcal{R}_{34}(E_j, E_k)}{E_{jl}(i\omega - E_{ji})} + \frac{\mathcal{R}_{34}(E_l, E_k)}{E_{lj}(i\omega - E_{li})} + \frac{\mathcal{Q}_{34}(i\omega, E_i, E_k)}{(i\omega - E_{li})(i\omega - E_{ji})} \big] \\
+\langle c_1 c_4 c_3^* c_2^* \rangle_{ijkl} \big[\frac{\mathcal{R}_{34}(E_k, E_j)}{E_{jl}(i\omega - E_{ji})} + \frac{\mathcal{R}_{34}(E_k, E_l)}{E_{lj}(i\omega - E_{li})} - \frac{\mathcal{Q}_{34}(-i\omega, E_k, E_i)}{(i\omega - E_{li})(i\omega - E_{ji})} \big] \\
+\langle c_3^* c_4 c_1 c_2^* \rangle_{ijkl} \big[\frac{\mathcal{R}_{34}(E_k, E_j)}{E_{ki}(i\omega - E_{lk})} + \frac{\mathcal{R}_{34}(E_i, E_j)}{E_{ik}(i\omega - E_{li})} - \frac{\mathcal{Q}_{34}(-i\omega, E_l, E_j)}{(i\omega - E_{li})(i\omega - E_{lk})} \big] \\
+\langle c_4 c_3^* c_1 c_2^* \rangle_{ijkl} \big[\frac{\mathcal{R}_{34}(E_j, E_k)}{E_{ki}(i\omega - E_{lk})} + \frac{\mathcal{R}_{34}(E_j, E_i)}{E_{ik}(i\omega - E_{li})} + \frac{\mathcal{Q}_{34}(i\omega, E_j, E_l)}{(i\omega - E_{li})(i\omega - E_{lk})} \big] \\
+\langle c_4 c_1 c_3^* c_2^* \rangle_{ijkl} \frac{1}{(i\omega - E_{kj})(i\omega - E_{li})} \times \\
\big[\mathcal{R}_{34}(E_k, E_l) - \mathcal{R}_{34}(E_j, E_i) + \mathcal{Q}_{34}(i\omega, E_j, E_l) - \mathcal{Q}_{34}(-i\omega, E_k, E_i) \big] \\
+\langle c_3^* c_1 c_4 c_2^* \rangle_{ijkl} \frac{1}{(i\omega - E_{kj})(i\omega - E_{li})} \times \\
\big[\mathcal{R}_{34}(E_l, E_k) - \mathcal{R}_{34}(E_i, E_j) + \mathcal{Q}_{34}(i\omega, E_i, E_k) - \mathcal{Q}_{34}(-i\omega, E_l, E_j) \big],
\end{aligned}
\tag{5.28}
$$

with the following definitions for the matrix elements:

$$
\langle \mathcal{O}_a \mathcal{O}_b \mathcal{O}_c \mathcal{O}_d \rangle_{ijkl} = \langle i|\mathcal{O}_a|j\rangle \langle j|\mathcal{O}_b|k\rangle \langle k|\mathcal{O}_c|l\rangle \langle l|\mathcal{O}_d|i\rangle. \tag{5.29}
$$

The functions $\mathcal{R}$ and $\mathcal{Q}$ are direct consequence of the Fourier transform and have the following definition:

$$
\mathcal{R}_{12}(E_i, E_j) = \frac{1}{Z}(e^{-\beta E_i} + e^{-\beta E_j}) \frac{1}{\beta} \sum_{i\omega'} \frac{\Delta_{12}^{\mathrm{d}}(i\omega')}{i\omega - E_{ij}}, \tag{5.30}
$$

$$
\mathcal{Q}_{12}(i\omega, E_i, E_j) = \begin{cases} -\frac{\beta}{Z} e^{-\beta E_2} \Delta_{12}^{\mathrm{d}}(i\omega) & \text{for } E_i = E_j \\ \frac{1}{Z}(e^{-\beta E_i} - e^{-\beta E_j}) \frac{1}{\beta} \sum_{i\omega'} \frac{\Delta_{12}^{\mathrm{d}}(i\omega')}{i\omega' - i\omega - E_{ij}} & \text{else.} \end{cases} \tag{5.31}
$$

Special attention has to be given to the divergences in the first 4 lines of Eq. (5.28). They can be lifted by application of L'Hosptial's rule, which results in the following formulae:

$$\text{first line: } E_{lj} \to 0: \ \frac{\mathcal{R}^{(1)}_{34}(E_j, E_k)}{i\omega - E_{ji}} + \frac{\mathcal{R}_{34}(E_j, E_k)}{(i\omega - E_{ji})^2} \tag{5.32}$$

$$\text{second line: } E_{lj} \to 0: \ \frac{\mathcal{R}^{(2)}_{34}(E_k, E_j)}{i\omega - E_{ji}} + \frac{\mathcal{R}_{34}(E_k, E_j)}{(i\omega - E_{ji})^2} \tag{5.33}$$

$$\text{third line: } E_{ik} \to 0: \ \frac{\mathcal{R}^{(1)}_{34}(E_k, E_j)}{i\omega - E_{lk}} - \frac{\mathcal{R}_{34}(E_k, E_j)}{(i\omega - E_{lk})^2} \tag{5.34}$$

$$\text{fourth line: } E_{ik} \to 0: \ \frac{\mathcal{R}^{(2)}_{34}(E_j, E_k)}{i\omega - E_{lk}} - \frac{\mathcal{R}_{34}(E_j, E_k)}{(i\omega - E_{lk})^2}. \tag{5.35}$$

Here the notation $\mathcal{R}^{(1)}_{12}(E_i, E_j) = \partial\mathcal{R}_{12}(E_i, E_j)/\partial E_i$ and $\mathcal{R}^{(2)}_{12}(E_i, E_j) = \partial\mathcal{R}_{12}(E_i, E_j)/\partial E_j$ have been used. These derivatives evaluate to:

$$\mathcal{R}^{(1)}_{12}(E_i, E_j) = \frac{1}{Z\beta}(e^{-\beta E_i} + e^{-\beta E_j}) \sum_{i\omega'} \frac{\Delta^{\mathrm{d}}(i\omega')}{(i\omega' - E_{ij})^2} - \frac{e^{-\beta E_i}}{Z} \sum_{i\omega'} \frac{\Delta^{\mathrm{d}}(i\omega')}{i\omega' - E_{ij}} \tag{5.36}$$

$$\mathcal{R}^{(2)}_{12}(E_i, E_j) = -\frac{1}{Z\beta}(e^{-\beta E_i} + e^{-\beta E_j}) \sum_{i\omega'} \frac{\Delta^{\mathrm{d}}(i\omega')}{(i\omega' - E_{ij})^2} - \frac{e^{-\beta E_j}}{Z} \sum_{i\omega'} \frac{\Delta^{\mathrm{d}}(i\omega')}{i\omega' - E_{ij}}. \tag{5.37}$$

The advantages of the formulation at hand can be summarized in the following two points:

Computational speed up: The main numerical effort in calculating the first diagram stems from its frequency dependence. In the present formulation the major contribution originates from the loop over Matsubara frequencies in the functions $\mathcal{R}$ and $\mathcal{Q}$. Since both functions only depend on energy differences, they can be precalculated and stored in memory. The additional utilization of degeneracies can decrease the numerical effort even further. In comparison to the 'standard' computation of the vertex the speed gain is two orders of magnitude.

Analytic continuation: In this formulation it will be possible to do an exact analytic continuation of the first diagram without the usage of any additional method like Padé or MAXENT. The continuation requires the transition from $i\omega \to E + i\delta$.

Special care has to be taken concerning the functions $\mathcal{R}$ and $\mathcal{Q}$, this will be done in section 5.6.

5.2 Exact limits of the theory

In this section it will be shown that the superperturbation impurity solver naturally incorporates three exact limiting cases, the weak- and strong-coupling regimes and the limit of an infinite number of bath sites. In order to discuss the first two cases we assume that the perturbation expansion is done around the atomic limit, which means $D = -\Delta$.

5.2.1 Weak-coupling limit

The first exact limit of the theory is the limit of weak interaction and large hybridization. For this problem it is possible to write down an analytic representation of the vertex in the single band atomic limit:

$$\begin{aligned}\gamma^{\uparrow\downarrow}(\omega_1,\omega_2,\omega_3,\omega_4) =& -U + \frac{U^3}{8}\frac{\omega_1^2+\omega_2^2+\omega_3^2+\omega_4^2}{\omega_1\omega_2\omega_3\omega_4} + \frac{3U^5}{16\omega_1\omega_2\omega_3\omega_4} \\ &+ \beta\frac{U^2}{4}\frac{1}{1+e^{\beta U/2}}\frac{2\delta_{\omega_2,-\omega_3}+\delta_{\omega_1,\omega_2}}{\omega_2^2\omega_3^2}\left(\omega_2^2+\frac{U^2}{4}\right)\left(\omega_3^2+\frac{U^2}{4}\right) \\ &- \beta\frac{U^2}{4}\frac{1}{1+e^{-\beta U/2}}\frac{2\delta_{\omega_2,\omega_3}+\delta_{\omega_1,\omega_2}}{\omega_1^2\omega_3^2}\left(\omega_1^2+\frac{U^2}{4}\right)\left(\omega_3^2+\frac{U^2}{4}\right),\end{aligned} \tag{5.38}$$

$$\gamma^{\uparrow\uparrow}(\omega_1,\omega_2,\omega_3,\omega_4) = \beta\frac{U^2}{4}\frac{\delta_{\omega_1,\omega_2}-\delta_{\omega_2,\omega_3}}{\omega_1^2\omega_3^2}\left(\omega_1^2+\frac{U^2}{4}\right)\left(\omega_3^2+\frac{U^2}{4}\right). \tag{5.39}$$

For small U the leading order of $\gamma^{\uparrow\downarrow}$ is $-U$ and the limit of the bare dual Green's function is:

$$\lim_{\Delta\to\infty} G_0^{\mathrm{d}} = -\lim_{\Delta\to\infty} g(g-\Delta^{-1})^{-1}g \tag{5.40}$$

$$= -g, \tag{5.41}$$

where g is the atomic Green's function. For weak interaction g can be approximated by the bare Green's function, since the self-energy is almost zero. Consequently the

superperturbation expansion is totally equivalent to the standard expansion in U in the case of weak interaction and strong hybridization. This naturally implies that the theory is exact for $U = 0$.

5.2.2 Strong-coupling limit

In the following it is shown that for the weak hybridization limit the results of X. Dai in [78] are recovered. Starting from the atomic limit the following approximation for the dual Green's function is used:

$$G^{\mathrm{d}} = G_0^{\mathrm{d}} + G_0^{\mathrm{d}} \Sigma_0^{\mathrm{d}(a)} G_0^{\mathrm{d}}. \tag{5.42}$$

Here $\Sigma_0^{\mathrm{d}(a)}$ is the already known expression for the first diagram:

$$\Sigma_0^{\mathrm{d}(a)}|_{12} = -\gamma_{1234} G_0^{\mathrm{d}}|_{43}. \tag{5.43}$$

Approximation (5.42) can be simplified further by inserting the explicit definition of the bare dual Green's function and exploiting that $g\Delta^{\mathrm{d}} = [1 + (gD)^{-1}]^{-1}$ holds:

$$G^{\mathrm{d}} = G_0^{\mathrm{d}} + [1 + (gD)^{-1}]^{-1} \Big(\big(\chi - \chi_0\big) \Delta^{\mathrm{d}} \Big) [(Dg)^{-1} + 1]^{-1}. \tag{5.44}$$

In order to derive an approximation for the c-Green's function, Eq. (5.44) is inserted into the expression for the back transformation (5.13):

$$G = A + B, \tag{5.45}$$

with

$$A = D^{-1} + (gD)^{-1} G_0^{\mathrm{d}} (Dg)^{-1} \tag{5.46}$$

$$B = (gD)^{-1} [1 + (gD)^{-1}]^{-1} \Big(\big(\chi - \chi_0\big) \Delta^{\mathrm{d}} \Big) [(Dg)^{-1} + 1]^{-1} (Dg)^{-1}. \tag{5.47}$$

Both terms can be simplified further:

$$A = D^{-1} + (gD)^{-1} G_0^{\mathrm{d}} (Dg)^{-1} \tag{5.48}$$

$$=D^{-1} - D^{-1}\Delta^{\mathrm{d}}D^{-1} \tag{5.49}$$
$$=D^{-1} - \big[DgD + D\big]^{-1} \tag{5.50}$$
$$=g(Dg+1)^{-1}. \tag{5.51}$$

B can be brought into a more convenient form if one simplifies the coefficients on the left and right:

$$(gD)^{-1}[1+(gD)^{-1}]^{-1} = \big[Dg+1\big]^{-1} \tag{5.52}$$
$$[1+(Dg)^{-1}]^{-1}(Dg)^{-1} = \big[gD+1\big]^{-1}. \tag{5.53}$$

The final result for the c-Green's function reads:

$$G = g(Dg+1)^{-1} + \big[1+gD\big]^{-1}\Big(\big(\chi-\chi_0\big)\Delta^{\mathrm{d}}\Big)\big[Dg+1\big]^{-1}. \tag{5.54}$$

In order to recover the strong-coupling limit, we expand to first order in $D = -\Delta \to 0$, which gives the following result:

$$G_{12} =g_{12} - [gDg]_{12} + \big(\chi_{1234} - \chi^0_{1234}\big)D_{43} \tag{5.55}$$
$$=g_{12} - [gDg]_{12} + \chi_{1234}D_{43} - g_{12}\,\mathrm{Tr}(Dg) + [gDg]_{12} \tag{5.56}$$
$$=g_{12} + \chi_{1234}D_{43} - g_{12}\,\mathrm{Tr}(Dg) \tag{5.57}$$
$$=g_{12} - \chi_{1234}\Delta_{43} + g_{12}\,\mathrm{Tr}(\Delta g). \tag{5.58}$$

The last expression corresponds exactly to the results obtained by X. Dai in [78] for the strong-coupling impurity solver. The different sign in front of χ is due to a different definition for the two particle Green's function in [78].

5.2.3 Large number of bath sites

As we have seen, the present solver is exact in two very opposite limits, the weak- and strong-coupling regime. This unique situation promises also a good convergence in the intermediate region.

The situation can be further improved by changing the starting point of the perturbation

expansion. On the one hand it is possible to alter the frequency dependence of the reference system by changing the weight function or on the other hand it is possible to increase the number of bath sites in order to make the perturbation smaller. This is possible because the theory is naturally exact in the limit of an infinite number of bath sites, when the reference system coincides with the full system. This statement sounds trivial but is actually a very unique situation. The present solver is exact in two opposite limits and in the intermediate regime a convergence of the theory can be achieved by including more bath sites. This implies that one is able to adjust the reference system to the needs of the actual problem. Such a procedure is not possible in the 'standard' perturbation theory, where one is in most cases limited to an easy starting point.

Choice of the reference system In principle the effective parameters of the reference system can be determined as described in section 3.1, by the minimization of a predefined weight function:

$$d = \frac{1}{N_\omega} \sum_{\omega_n}^{N_\omega} \omega_n^{-s} |\Delta^n(i\omega_n) - \Delta(i\omega_n)|^2. \tag{5.59}$$

By fixing the parameters N_ω and s it is possible to fix the region where the difference of both hybridization functions receives a higher weight. In this chapter we use a different strategy. Since all calculations were performed at half-filling, a N-bath site reference system has N free parameters to choose. These parameters were determined in such a way that both hybridization functions coincide exactly on the first N frequencies. This procedure naturally improves the result of the perturbation expansion at low frequencies and is advantageous if one is interested in the physics at the Fermi level.

5.3 A first test

To test the presented approach, various approximation schemes of the superperturbation were benchmarked against CTQMC calculations. As a first test a single impurity Anderson model with Hubbard interaction $H_{\text{Int}} = Un^\uparrow n^\downarrow$ and a semicircular density of

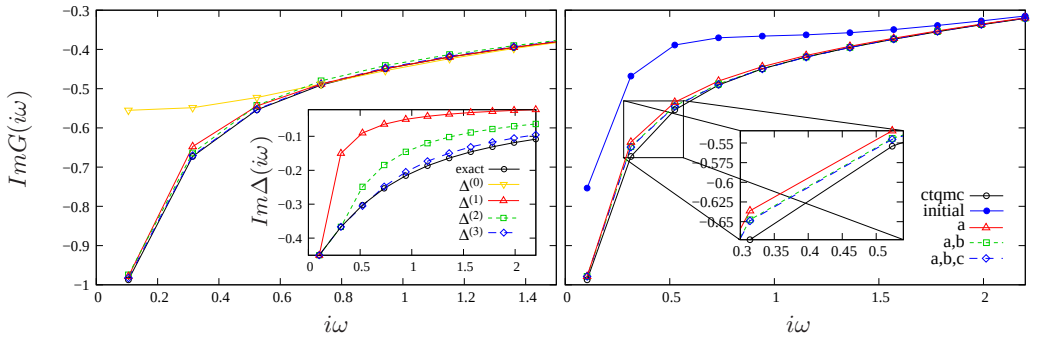

FIGURE 5.1: Results for a superperturbation calculation with Hubbard interaction and a semicircular density of states. The parameters are: $\beta = 30$ and $U/(2t) = 3$. *Left:* Dependence of the superperturbation result on the number of bath sites used. The calculations have been performed including the first two box diagrams. Already one bath site gives a good approximation, even though the difference between the hybridization function of the full system and the reference system is quite high, as shown in the inset. *Right:* Dependence on the number of diagrams used. Calculations were performed for one bath site. An increase in the number of diagrams leads to fast convergence of the perturbation series. The curves for two and three diagrams are nearly indistinguishable, the curve including three diagrams is closer to the exact result. The most prominent effect is carried by the first diagram, which gives by far the largest correction.

states with bandwidth $W = 4t$ was considered:

$$\Delta(i\omega) = \frac{2t^2}{i\omega + i\sqrt{4t^2 - (i\omega^2)}}. \tag{5.60}$$

First the dependence on the total number of bath sites in the reference system was investigated. Therefore, several simulations with a varying bath cluster size from 0 to 3 were performed for a fixed number of diagrams. The effective parameters of the reference system were chosen in such a way that the hybridization function of the full system coincides with the one of the reference system on the first N Matsubara frequencies. The left part of figure 5.1 shows the results of calculations performed for $\beta = 30$ and $U/(2t) = 3$ at half-filling. The dual self-energy was approximated by the first two boxed-type diagrams (diagrams a.) and b.) in figure 4.2) and was computed in a self-consistent manner, leading to a conserving approximation in the Baym-Kadanoff sense.
The convergence towards the exact CTQMC result (black line) is exponentially fast as one expects since the method is based on exact diagonalization. Already one bath site

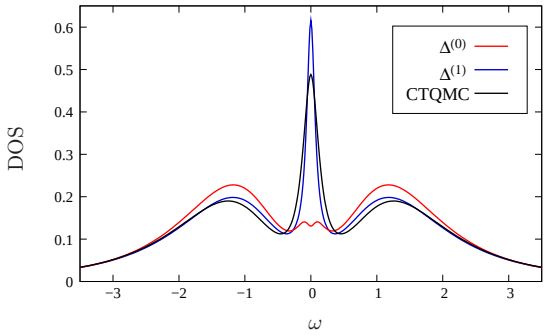

FIGURE 5.2: Maximum entropy density of states for CTQMC data and superperturbation calculations including no ($\Delta^{(0)}$) and one ($\Delta^{(1)}$) bath site. Whereas the perturbation around the atomic solution shows no resonance at the Fermi level, the one bath solution exhibits a clear Kondo resonance.

gives a good approximation to the exact solution, even though the difference in the hybridization functions is quite high, as shown in the inset. The improvement of the ED result can be visualized, if one compares the red curve of the left figure (SPERT solution) to the blue curve of the right plot, which shows the ED result for one bath site. The dual correction is quite large.

In order to investigate the convergence properties of the dual perturbation series, the amount of bath sites was fixed to one and the simulations were repeated for different number of diagrams. The right plot of Figure 5.1 shows the results. The most prominent correction is carried by the first diagram. The inclusion of higher orders gives only little improvement, as one sees in the inset. From both investigations one can conclude that for the applied parameters, an approximation including only one bath site and the first dual diagram gives an already good approximation to the problem, even though the difference between the solution of the reference system and the full system is quite large.

In the investigation of the Anderson impurity model, one is often not interested in the Green's function on Matsubara frequencies, but in its analytic continuation to the real axis, the density of states. In order to compare the density of states calculated in the superperturbation framework to CTQMC data, we employ the maximum entropy method. For CTQMC the application of this method is necessary, because the data sets contain statistical noise. In the superperturbation case this procedure is in principle not necessary, because the data is numerically exact, but in order to treat both methods on

the same footing MAXENT has been used in both cases. Results for a direct analytic continuation or a continuation via Padé will be discussed in section 5.6.
The left plot of figure 5.2 shows the maximum entropy density of states of CTQMC data and superperturbation results for zero bath sites ($\Delta^{(0)}$) and for one bath site ($\Delta^{(1)}$). The parameters and the approximation of the dual self-energy are the same as in figure 5.1. In accordance with reference [78] we were not able to find a quasiparticle peak at the Fermi level, when starting from the atomic reference system, but the solution including one bath site already exhibits a Kondo resonance and is in good agreement with the CTQMC result.

5.4 Application in the DMFT framework

In the last section it was shown that the superperturbation solver gives good approximation to the Anderson impurity model, even if the number of bath sites is small and only a few diagrams are taken into account. In the following it will be shown that the superperturbation gives also reliable results when the method is applied in self-consistent DMFT calculations. It is not a priori clear that the results of the superperturbation remain stable in an iterative procedure like DMFT. Systematic errors could increase from iteration to iteration and lead to a break down of the approximation. We therefore benchmark the superperturbation against CTQMC in a DMFT calculation. In the following a two-dimensional Hubbard model with nearest neighbor hopping is considered and the point of the Mott insulator transition is investigated. From CTQMC calculations it is known that in the DMFT framework the transition takes place at a critical U of $U_c = 9.35$ and a temperature of $T/t = 0.1$.
Several simulations for different U were performed and compared to the CTQMC result. In the superperturbation calculations the implementation of section 5.1.1 has been used, i.e., only the first box type diagram without any self-consistency in the dual diagrammatic technique has been considered.

The four plots in figure 5.3 show the results for different number of bath sites. The upper row corresponds to calculations performed with one bath site, the lower row to

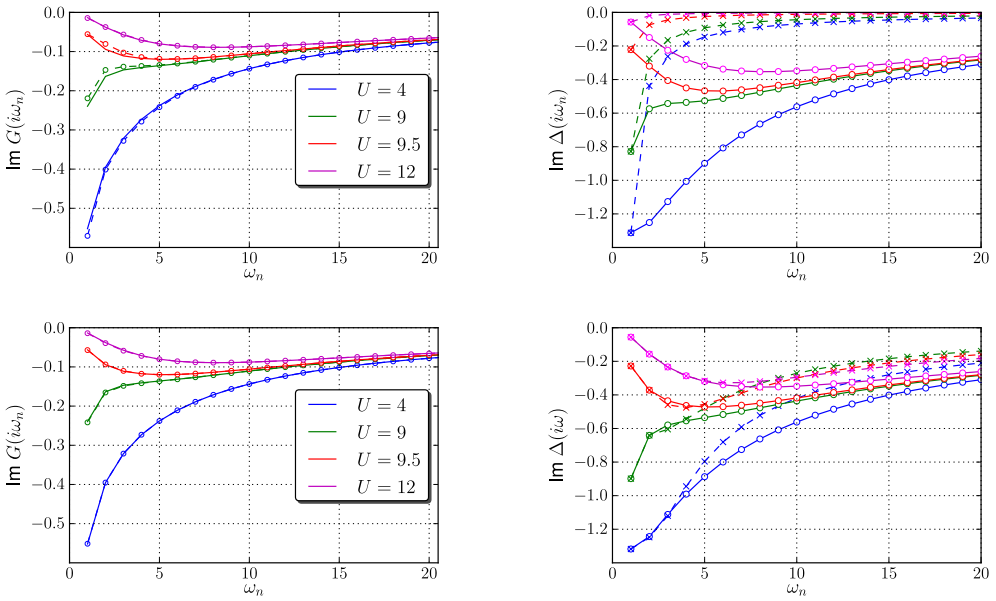

FIGURE 5.3: DMFT analysis of the Mott metal insulator transition in the 2D-Hubbard model. The left column shows results for the self-consistent local Green's functions. Solid lines correspond to exact CTQMC data, dashed lines to SPERT results. The right column shows the corresponding hybridization functions. In the upper row results including 1 bath site are illustrated. Here some small deviations in the local Green's function in the vicinity of the transition are visible. In the lower row results including three bath sites are depicted, they completely coincide with the CTQMC results.

calculations including three bath sites. From the upper left plot it is clear that, as in the last section, a calculation including only one bath site is also a good approximation for the DMFT. Solid lines correspond to the exact CTQMC result, whereas the superperturbation results are depicted using doted lines. As one can see, the results are in a very good agreement. From both calculations it is clear that a transition occurs between $U = 9$ and $U = 9.5$, which can be deduced from the different bending at low frequencies. The discrepancy between the SPERT and the exact result increases near the transition. This is understandable, because the number of iterations to converge the DMFT self-consistency equations increases exponentially at the transition. Nevertheless the SPERT is very stable in the DMFT process, even though the difference in the hybridization functions is quite large, as shown in the plot on the right side. The same

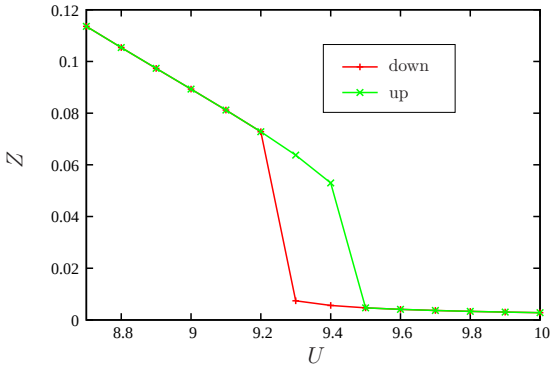

FIGURE 5.4: Hysteresis in the quasiparticle weight for the 2D-Hubbard model at $\beta = 20$, calculated in the superperturbation scheme. Two different curves are clearly visible in the coexistence region.

calculations have been performed including 3 bath sites. Here (lower row) no difference between the SPERT and the CTQMC is visible.

In order to demonstrate that the SPERT is also capable to investigate the phase boundary of the Mott metal insulator transition a hysteresis in the quasiparticle weight was calculated. In the underlying half-filled case, Z is inversely proportional to the effective electron mass:

$$Z = \frac{m_e}{m^*}. \tag{5.61}$$

The quasiparticle weight is defined as a derivative of the self-energy on the real axis, but can be obtained approximately on the imaginary axis using Cauchy-Riemann conditions and an approximation for the first derivative:

$$Z = \left[1 - \frac{\mathrm{dRe}\ \Sigma(\omega)}{\mathrm{d}\omega}\right]^{-1}_{\omega=0} \approx \left[1 - \frac{\mathrm{Im}\ \Sigma(i\omega_0)}{\omega_0}\right]^{-1}. \tag{5.62}$$

Figure 5.4 shows the results for $\beta = 20$. A hysteresis is clearly visible, which proves the coexistence of two different phases. The width of the hysteresis and its position are in good agreement with the phase diagram in reference [82].

5.5 The superperturbation solver and Kondo physics

Although it is known in the literature [2] that the Kondo problem is non-perturbative, a quasiparticle peak was observed in superperturbation calculations including one or more bath sites (see section 5.3). Because the SPERT itself is a perturbation expansion, the natural question arises to what extent Kondo physics is included in superperturbation results. To answer this question, this section is dedicated to the magnetic properties of the SIAM. We investigate the impurity susceptibility using SPERT and compare again to CTQMC. From these calculations the Kondo temperature is extracted and compared to NRG results.

The magnetic susceptibility is defined as the derivative of the magnetization with respect to the field:

$$\chi = \frac{\partial M}{\partial h}\Big|_{h=0}. \tag{5.63}$$

Since data sets obtained from SPERT are numerically very precise the magnetization can be easily calculated by a direct discretization of the last equation:

$$\chi = \frac{M(h_0) - M(0)}{h_0}. \tag{5.64}$$

In numerical calculations the discretization in the magnetic filed was fixed to $h_0/D = 10^{-5}$. The magnetization is perfectly linear in this regime, so that the susceptibility can be computed nearly without any discretization error. Figure 5.5 shows the results of these investigations for different U. Before the SPERT results are discussed, we would like to comment on the CTQMC data. For high temperature the CTQMC results (dashed lines) fall off like $1/T$, which indicates that the thermodynamics is governed by a local moment, which has formed on the impurity. For very low temperature the susceptibility saturates to a constant value. This behavior is typical for the formation of a singlet and indicates that the impurity electron is screened by the bath, which is the essential mechanism behind the Kondo effect.

The SPERT curves (solid lines upper row) mimic this behavior, but fail to follow the exact result for very low temperature. Here a clear deviation is visible. Again the results can be improved by including an additional bath site (upper right plot), but the 2 bath

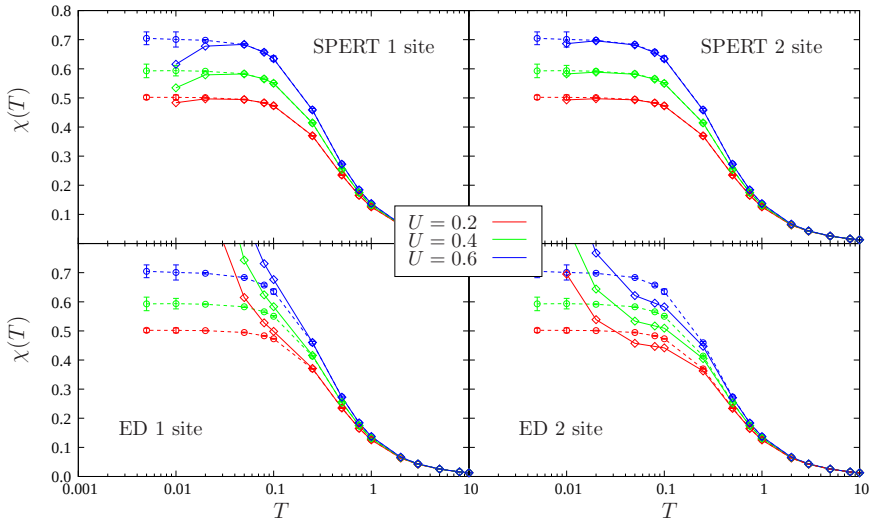

FIGURE 5.5: Magnetic susceptibility of the SIAM calculated with ED (lower row) and SPERT (upper row) in comparison to CTQMC data (dashed lines) for different values of U. The SPERT approximation breaks down for very low temperature. The reason for this behavior is the formation of a local moment in the reference system, because the hopping $v(T)$ tends to zero for low temperatures and the impurity gets decoupled from the bath. Including one more bath site (right column) improves the result, but cannot recover the formation of a singlet.

site solution also breaks down at low temperature. The reason for this becomes clear, if one looks at the solution of the reference system. The ED curves in the lower row diverge as $1/T$ as the temperature tends to zero. This divergence is again owed to the formation of a local moment on the impurity, which is connected with the choice of the effective parameters for the reference system. For a semicircular density of states and one bath site, the temperature dependence of the hopping amplitude can be written down explicitly, if one requires that the hybridization function of the reference system and the full system are equal on the first Matsubara frequency:

$$v(T) = t \sqrt{\frac{2}{1 + \sqrt{1 + \left(\frac{2t}{\pi T}\right)^2}}}. \tag{5.65}$$

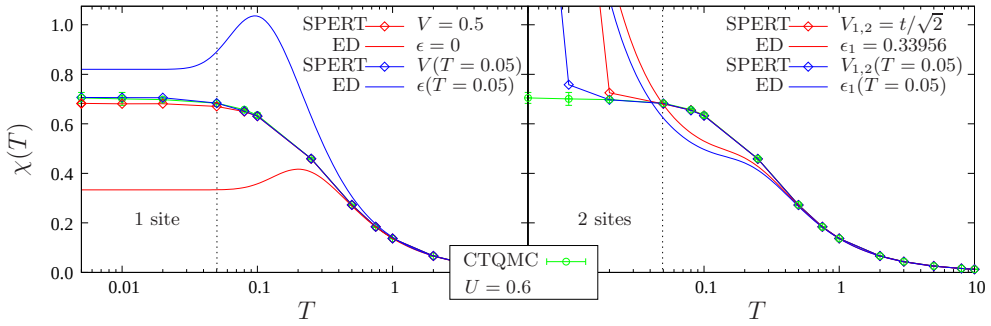

FIGURE 5.6: Susceptibility of the SIAM, calculated in SPERT for a fixed v in comparison to ED. For one bath site the results are drastically improved in comparison to a temperature dependent $v(T)$, because the ground state of the reference system itself is a singlet. The inclusion of an additional bath site gives no improvement because the ground state is a free moment.

Apparently the limit $v(T)$ is zero for very low temperature:

$$\lim_{T\to 0} v(T) = 0. \tag{5.66}$$

This implies that the impurity gets decoupled from the bath in the $T = 0$ limit. Consequently, the susceptibility of the reference system behaves like a free moment in this limit and the SPERT breaks down, because the perturbation series cannot recover the formation of a singlet. For two bath sites the same effect occurs, but the decoupling from the bath in the low temperature regime is slower than for one bath sites. This leads to a slower breakdown of the perturbation theory.

The superperturbation results can be improved drastically, if one starts the perturbation expansion from a reference system, which has singlet ground state. This situation can be reached for a system with an odd number of bath sites, if the hopping is fixed to a temperature independent value. Figure 5.6 compares the results for one and two bath sites. For one bath site (left curve) the ED results again falls off like $1/T$ for high temperatures, but are constant in the low temperature regime. The corresponding SPERT curves nicely follow this trend and no breakdown is visible in the $T \to 0$ limit. Only a small difference in the height of the plateau is noticeable for the $v = 0.5$ curve. If the hopping is fixed to another value ($v = v(T = 0.05)$) an agreement within the CTQMC

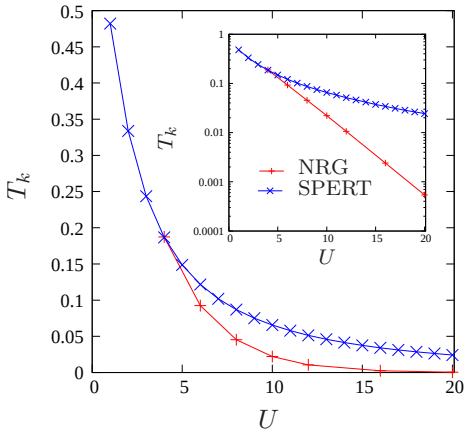

FIGURE 5.7: Scaling of the Kondo temperature for a wide band model calculated with SPERT and compared to NRG [1] results. The NRG nicely follows an exponential trend, as can be seen on the logarithmic inset, while the SPERT deviates from the NRG. The reason for this difference is the finite number of diagrams used in the SPERT.

error bars can be reached. Unfortunately, no recipe for the optimal choice of the hopping parameter for a given U was found.

If the bath is extended by an additional site the results are not improved, but again breakdown at low temperatures (right plot). The reason for this behavior is obvious: The ground state of the reference system is not a singlet, but a free moment.

Consequently, the choice of the reference system is extremely important. The superperturbation gives the best results, if the main physics is already included in the reference system. In the case of the SIAM and the investigation of the magnetic susceptibility this means to start from a reference system with an odd number of bath sites, which leads to a singlet ground state.

The temperature at which the formation of the singlet starts is called Kondo temperature T_k. This point is usually defined as the temperature, at which the susceptibility reaches 70% of its maximum value, but can also be defined as the full with at half maximum (FWHM) of the Kondo resonance. The characteristic feature of the Kondo problem is that T_k scales exponentially with the effective coupling $J = t^2/U$:

$$T_k = D \exp 1/g \qquad \text{with: } g = N(0)/J. \tag{5.67}$$

[1] The NRG results have been gratefully provided by Prof. Frithjof Anders, University of Dortmund.

This formula is valid for a wide band density of states, where D is the width of the band, $N(0)$ the density of states at the Fermi level and J the coupling constant. In order to see if the superperturbation can recover this exponential scaling, the Kondo temperature has been determined in susceptibility calculations. The results in comparison to NRG are depicted in figure 5.7. From the inset, which shows the same data with a logarithmic scale, one can see that the NRG scales perfectly exponentially with U. The superperturbation, on the other hand, does not follow this exponential trend, but clearly deviates from the NRG. It follows that the SPERT does not incorporate the correct scaling. The reason for this is the fact that only the first diagram has been used in the SPERT calculations. It is nearly impossible to recover the exponential trend in the interaction by summing up a finite number of diagrams. A better approach would be to sum up an infinite series like in the ladder dual fermion or like in a dual Parquet approach. Unfortunately, none of this schemes has been implemented yet.
An alternative way to solve the scaling problem would be to choose the hopping parameter $v(U)$ of the reference system in such a way that a part of the exponential scaling is already included in the reference system. But this approach also needs some further analysis of the reference system properties, which has not been done at the moment.

5.6 Analytic continuation to the real axis

So far the superperturbation scheme has been formulated on the imaginary axis using Matsubara frequencies, but the actual quantity of interest, the density of states (DOS), requires information on the real axis . Today, there are several methods available to extract this information from the imaginary time data via an analytic continuation. One of those is the already mentioned maximum entropy method or the Padé approach. Since analytic continuation is in general an ill posed problem, both methods suffer from serious drawbacks. The MAXENT is designed for data containing statistical noise and has therefore a bad resolution on the real axis. Very fine structures, like multiplets for example, are very hard to resolve using this method. The Padé has a higher resolution on the real axis but requires very accurate input data, because the solution of a badly conditioned linear system of equations is needed to perform the continuation.

Since the SPERT is based on the exact diagonalization of a reference system, the best way to access real axis information is to directly compute on the real axis. In ED this is easily done by directly performing the transition $i\omega \to E + i\delta$, where δ is a small broadening parameter. For the one particle Green's function this leads to the following formula:

$$g(E+i\delta)_{\alpha\beta} = \frac{1}{Z}\sum_{n,m}\frac{\langle n|c_\alpha|m\rangle\langle m|c_\beta^\dagger|n\rangle}{E+i\delta+E_n-E_m}\left(e^{-\beta E_n}+e^{-\beta E_m}\right). \tag{5.68}$$

From latter expression the DOS can be obtained as the negative imaginary part:

$$DOS(E) = -\frac{1}{\pi}\mathrm{Im}\, g(E+i\delta). \tag{5.69}$$

Since all dual transformations can be written down analytically, such a transition is also possible in the SPERT case. Special attention has to be paid to the calculation of diagrams, since these computations involve summations over fermionic loops, where the continuation is more involved.

In the following the analytic continuation of the first diagram (diagram a.) of Fig. 4.2) is discussed. We use the formulation of section 5.1.1 for this purpose.

Here the analytic continuation reduces to the continuation of the function $\mathcal{Q}(i\omega, E_i, E_j)$. Since $\mathcal{R}(E_i, E_j)$ does not depend on $i\omega$ the function can be in principle calculated using definition (5.30). In order to treat both function evaluations on the same footing, we discuss in the following how $\mathcal{R}$ and $\mathcal{Q}$ can be calculated via an integral along the real axis.

The general idea is very simple and can be found in nearly every textbook about quantum field theory. If one wants to find an analytic continuation of a Matsubara sum, the problem can be rewritten as a sum over residues of the function itself times the Fermi function, which has poles of first order at the Matsubara frequencies:

$$\frac{1}{\beta}\sum_{i\omega}F(i\omega) = -\frac{1}{2\pi i}\oint_C \frac{F(E)}{e^{\beta E}+1}dE. \tag{5.70}$$

Such a situation is depicted in Fig. 5.8. The contour which is used for the integral corresponds to the first picture. If the function is analytic in the rest of the complex plane, one can deform the contour as long a no other singularity is crossed. This makes

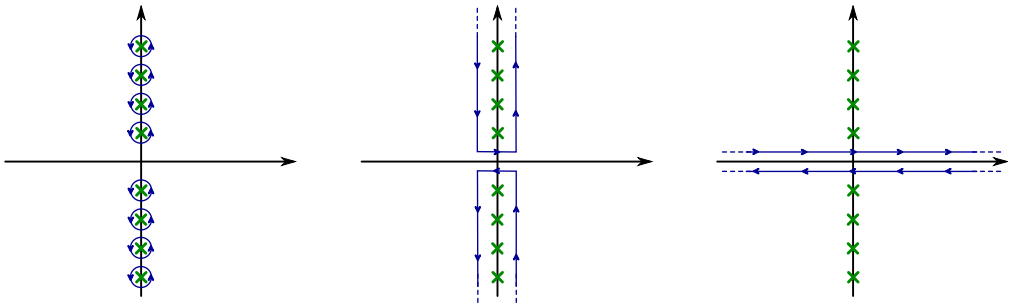

FIGURE 5.8: Illustration of the conversion of a Matsubara sum into a contour integral. In a first step the sum is replaced by an integral over the function itself times the Fermi function, which has poles at Matsubara frequencies. In the second and third step the contour is deformed to two line integrals along the real axis. The illustrated contour deformation can be applied in the calculation of $\mathcal{R}$.

it possible to replace the first contour by a contour along the imaginary axis and in the second step to deform the contour to a path along the real axis (last picture). Consequently, the summation over Matsubara frequencies has been replaced by two line integrals: One integral from minus infinity to plus infinity above the real axis, and one line integral backwards below the real axis. This leads to the following expression for $\mathcal{R}$:

$$\mathcal{R}(E_1, E_2) = -\frac{X_1 + X_2}{2\pi i}\Big[\int_{-\infty}^{\infty} \frac{\Delta^{\mathrm{d}}(z^+) f(z^+)}{z^+ - E_{12}} - \int_{-\infty}^{\infty} \frac{\Delta^{\mathrm{d}}(z^-) f(z^-)}{z^- - E_{12}}\Big] dz, \tag{5.71}$$

where $z^{\pm} = z \pm i\epsilon$, with $\epsilon < \pi/\beta$, and $X_i = \exp(-\beta E_i)/Z$. For $\mathcal{Q}$ the situation is similar, but one has to take into account an additional pole in the imaginary plane at $z = i\omega + E_{12}$:

$$\begin{aligned}\mathcal{Q}(i\omega, E_1, E_2) = (X_1 - X2)\Bigg[&- \frac{1}{2\pi i}\Bigg(\int_{-\infty}^{\infty} \frac{\Delta^{\mathrm{d}}(z^+) f(z^+)}{z^+ - i\omega - E_{12}} \\ &- \int_{-\infty}^{\infty} \frac{\Delta^{\mathrm{d}}(z^-) f(z^-)}{z^- - i\omega - E_{12}}\Bigg) - \mathrm{Res}(i\omega + E_{12})\Bigg].\end{aligned} \tag{5.72}$$

The minus sign in front of the residue arises form the clockwise orientation of the contour. Now the crucial point is to calculate the residue before doing the analytic continuation.

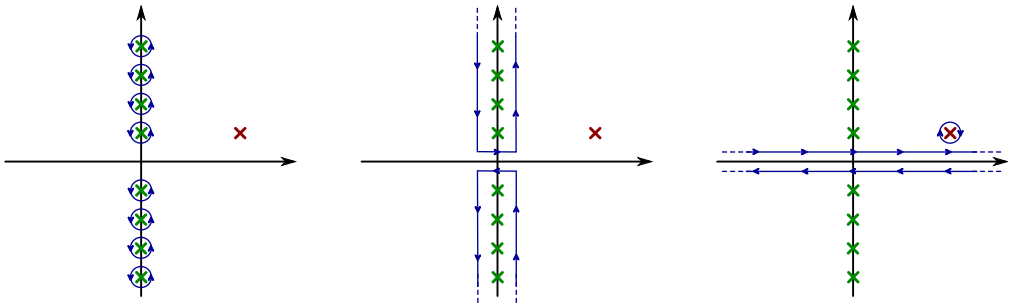

FIGURE 5.9: Construction of the contour integral to calculate $\mathcal{Q}$. In comparison to Fig. 5.8 one has to take into account an additional pole at $\tilde{z} = i\omega + E_{12}$.

For the residue one gets the following expression:

$$\begin{aligned}\mathrm{Res}(i\omega + E_{12}) =& f(i\omega + E_{12})\Delta^{\mathrm{d}}(i\omega + E_{12}) && (5.73)\\ =& \frac{1}{e^{\beta(i\omega+E_{12})}+1}\Delta^{\mathrm{d}}(i\omega + E_{12}) && (5.74)\\ =& \frac{1}{1-e^{\beta E_{12}}}\Delta^{\mathrm{d}}(i\omega + E_{12}). && (5.75)\end{aligned}$$

The final result for $\mathcal{Q}(i\omega, E_1, E_2)$ reads:

$$\begin{aligned}\mathcal{Q}(i\omega, E_1, E_2) = (X_1 - X_2)\Bigg[-\frac{1}{2\pi i}\Bigg(\int_{-\infty}^{\infty}\frac{\Delta^{\mathrm{d}}(z^+)f(z^+)}{z^+ - i\omega - E_{12}}\\ - \int_{-\infty}^{\infty}\frac{\Delta^{\mathrm{d}}(z^-)f(z^-)}{z^- - i\omega - E_{12}}\Bigg) - \frac{1}{1-e^{\beta E_{12}}}\Delta^{\mathrm{d}}(i\omega + E_{12})\Bigg]. \quad (5.76)\end{aligned}$$

Now the analytic continuation can be performed by replacing $i\omega$ with $E + i\delta$:

$$\begin{aligned}\mathcal{Q}(\tilde{z}, E_1, E_2) = (X_1 - X_2)\Bigg[-\frac{1}{2\pi i}\Bigg(\int_{-\infty}^{\infty}\frac{\Delta^{\mathrm{d}}(z^+)f(z^+)}{z^+ - \tilde{z} - E_{12}}\\ - \int_{-\infty}^{\infty}\frac{\Delta^{\mathrm{d}}(z^-)f(z^-)}{z^- - \tilde{z} - E_{12}}\Bigg) - \frac{1}{1-e^{\beta E_{12}}}\Delta^{\mathrm{d}}(\tilde{z} + E_{12})\Bigg], \quad (5.77)\end{aligned}$$

with $\tilde{z} = E + i\delta$ and $z^{\pm} = z \pm i\epsilon$. The last expression completes the analytic continuation. $\mathcal{R}$ and $\mathcal{Q}$ have been rewritten as a contour integral along the real axis and all

other quantities can be calculated by a substitution of $i\omega$ with $E + i\delta$.
Nevertheless a few remarks are necessary. First of all the reader should not mix the two quantities ϵ and δ. The first one is the distance of the integration contour to the real axis, the latter one the broadening of the final solution. In any case, δ should be greater than ϵ, because the residue was supposed to lie outside the contour.
Numerically the evaluation of the real axis integrals is not very difficult and a simple quadrature rule (Simpson for example) is sufficient to solve the integrals. For low temperatures one should be aware of the fact that Δ^{d} itself has a second order pole at zero. This makes it hard to compute the integrals numerically on a fixed grid. In this case the contour integrals were solved by an adaptive Gauss-Kronrod rule taken from the GNU scientific library [15].

Figure 5.10 shows some illustrative results. In the upper left plot the calculation on the real axis (CORA) is compared to an analytic continuation using Padé and the initial solution of the reference system. The ED curve has a clear splitting at the Fermi level, whereas the CORA curve exhibits a Kondo peak. The CORA is in a good agreement with Padé. The lower left plot shows an additional example with an applied magnetic field. Here the splitting of the peaks is clearly visible and the CORA is again in good agreement with Padé. For completeness the data on Matsubara frequencies have been added on the right.

5.7 The non-causality problem

From reference [78] it is known, that the strong-coupling solver for the Anderson impurity model exhibits a non-causality problem for certain parameters. This non-causality is an artifact of the perturbation expansion around the atomic limit and manifests itself as a negative density of states, which is caused by a pole on the upper complex plane of the Green's function. Since the SPERT is closely related to the strong-coupling solver (see section 5.2.2), non-causal behavior can also occur in the superperturbation.

Figure 5.11 shows the result of SPERT calculations with a one-bath-site reference system for different β. The interaction was $U/D = 3$ and the broadening δ was fixed to $\delta/D = 0.3$. Blue curves show simulations with a fixed hoping amplitude in the reference

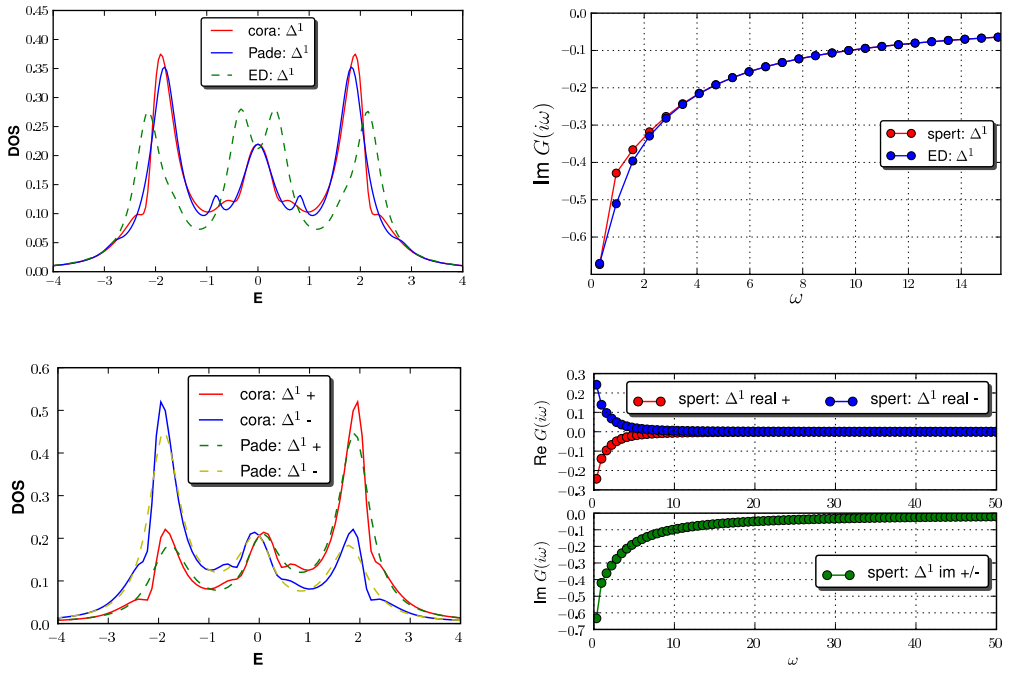

FIGURE 5.10: SPERT calculations on the real axis (CORA). The upper row shows an example for $\beta = 10$ and $U/D = 3$. Here the agreement between CORA and Padé is good, but the CORA shows a more detailed resolution on the real axis. The lower row shows the same system with an applied magnet field: $B/D = 0.05$.

system ($v/D = 0.5$) and red curves correspond to data sets with a temperature dependent hopping parameter as discussed in section 5.2.3. Both procedures develop sharp kinks in the low temperature regime and the red curves are non-causal above $\beta = 50$. For the blue curves all data sets seem to be causal, but it should be clear that a smaller parameter δ would have produced a negative density of states even for the blue data sets.

The non-causality problem can be best understood, if one analyzes the effective action of the superperturbation expansion. For low temperatures the DOS of the reference system is given by a collection of delta peaks. Now the superperturbation tries to shift and broaden these peaks in such a way that they recover the solution of the full system. But the shift of an infinitesimally sharp delta peak to a new position is nearly impossible

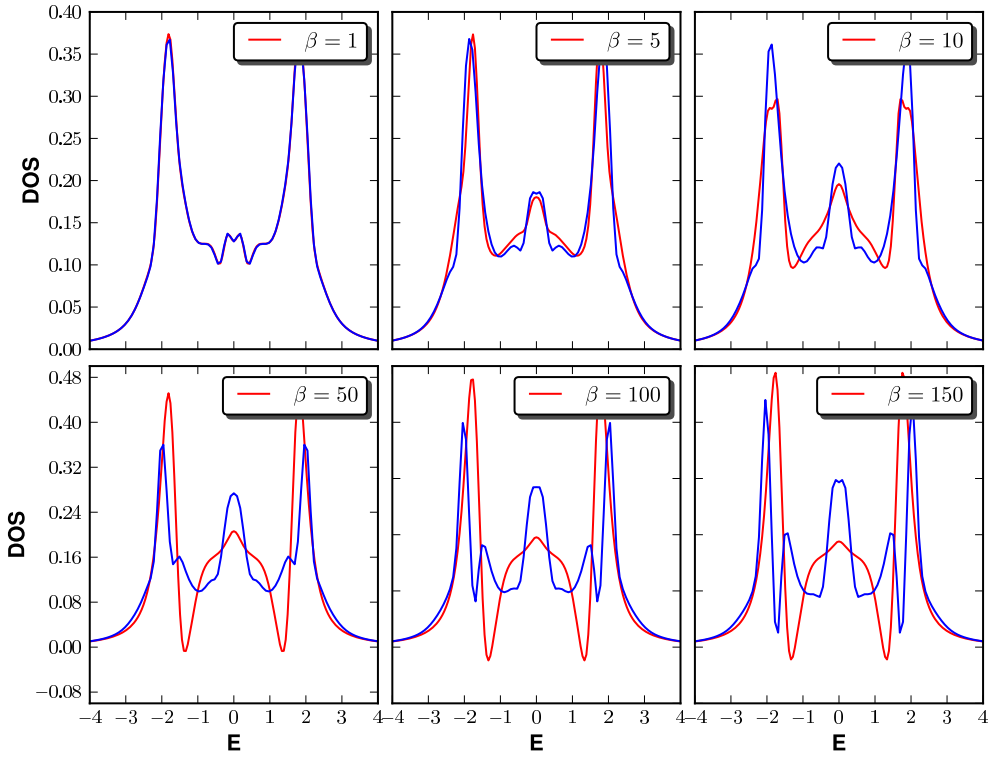

FIGURE 5.11: Temperature dependence of SPERT calculations for a reference system including one bath site. The interaction was $U/D = 3$ and the broadening δ was fixed to $\delta/D = 0.3$. Blue curves show data with a fixed hopping, red curves with a temperature dependent one. *parameters:* $U/D = 3$ and $\delta/D = 0.3$.

for a finite order perturbation theory. Therefore the superperturbation gets more and more problems in the DOS at low temperatures. We would like to mention that even if it is complicated to obtain a causal DOS at low temperatures, the thermodynamic properties, which can be accessed using imaginary time data, are in most cases very reliable and in good agreement with other methods. From Padé one knows that a slight change of the Green's function on Matsubara frequencies can cause a totally different DOS on the real axis, even though the change was very small and the thermodynamics did not change.

To elucidate the problem in a little more detail, we discuss in the following the expansion around a half filled atomic reference system for $T = 0$, which was first discussed in [83]. In this case the atomic Green's function has only two poles at $\pm U/2$ and is totally analytic

in the rest of the complex plane. This also applies for the hybridization function, which is analytic by construction. Consequently, the only place were non-causal behavior can arise is the dual perturbation expansion. We therefore analyze the pole structure of the dual Green's function. In this case the bare dual Green's function can be written in the following form:

$$G_0^{\mathrm{d}} = -g\left[g - \Delta^{-1}\right]^{-1} g \tag{5.78}$$

$$= -\frac{\Delta}{g^{-1}(g^{-1} - \Delta)} \tag{5.79}$$

$$\approx -\frac{\Delta}{(\epsilon - U/2 + i0^+)(\epsilon - U/2 + i0^+ - \Delta(U/2))} \tag{5.80}$$

Since we are only interested in the pole structure of the bare dual Green's function and the problem is half filled only contributions for a positive ϵ have been taken into account. The hybridization function has been approximated by its value at the atomic pole, since here the contribution of Δ is the largest. From the last equation one can deduce that the bare dual Green's function is still analytic and has two close poles, one at $U/2$ and an additional singularity at $U/2 + \Delta(U/2)$. Consequently, a non-causality has to enter via the dual self-energy. We therefore analyze the dual Dyson equation:

$$G^{\mathrm{d}} = \frac{1}{(G_0^{\mathrm{d}})^{-1} - \Sigma^{\mathrm{d}}} \tag{5.81}$$

$$= \frac{\Delta}{g^{-1}(g^{-1} - \Delta) - \Sigma^{\mathrm{d}}\Delta} \tag{5.82}$$

$$\approx \frac{\Delta}{(\epsilon - U/2 + i0^+)(\epsilon - U/2 + i0^+ - \Delta(U/2)) - \Sigma^{\mathrm{d}}\Delta(U/2)}. \tag{5.83}$$

The poles of this expression are given by the following solution of a quadratic equation:

$$\epsilon_{\mathrm{pole}} = \frac{U - \Delta(U/2)}{2} \pm \sqrt{\left(\frac{U - \Delta(U/2)}{2}\right)^2 + \Sigma^{\mathrm{d}}\Delta(U/2) - \frac{U}{2}\left(\frac{U}{2} + \Delta(U/2)\right)}. \tag{5.84}$$

It is clear that ϵ_{pole} can develop an imaginary part if the discriminant is negative. This is the case for

$$\Sigma^{\mathrm{d}} < -\frac{\Delta(U/2)}{4}. \tag{5.85}$$

So the dual self-energy can bring the already very close poles of the bare dual Green's function even closer together, until they form an imaginary part and become complex. From this analysis we can conclude that the non-causality behavior has its origin in the shifting of atomic poles. This result suggest a very simple solution to the problem: One should require that the dual self-energy is zero at the poles of the reference system. A possible way to fulfill this additional condition is discussed in the following section.

5.8 Renormalization of the superperturbation theory

In the last section it has become clear that the non-causality problem is connected to the shifting of poles in the reference system due to the dual self-energy. In this section we show how this problem can be solved by the additional requirement that the dual self-energy vanishes at the poles of the reference system. The key idea is to introduce an additional parameter by adding and subtracting a quadratic term to the action. The free parameter is then chosen in such a way that the dual correction vanishes at the atomic poles. This idea was first introduced in [83] for the $T = 0$ case for an expansion around the atomic problem. In this section the scheme is generalized to finite temperatures. We start by writing down the action of the full problem:

$$S = -\frac{1}{\beta}\Big(\sum_{n\sigma} c_\sigma^*[i\omega_n - \mu - \Delta(i\omega)]c_\sigma - U(n^\uparrow - \frac{1}{2})(n^\downarrow - \frac{1}{2})\Big). \tag{5.86}$$

Here $\mu = 0$ corresponds to the half filled case, which is considered in the following. Now the Gaussian part $\pm\lambda \cdot i\omega$ is added and subtracted. Afterwards the action is split up into an atomic part and a part which will be treated by the perturbation expansion:

$$S = S_\lambda = \underbrace{-\frac{1}{\beta}\Big(\sum_{n\sigma} c_\sigma^*[i\omega_n - \mu]c_\sigma - U(n^\uparrow - \frac{1}{2})(n^\downarrow - \frac{1}{2})\Big) - \lambda \cdot i\omega c_\sigma^* c_\sigma}_{S_\lambda^{\mathrm{at}}} \tag{5.87}$$

$$\underbrace{+\frac{1}{\beta}\Big(\sum_{n\sigma} c_\sigma^*\Delta(i\omega)c_\sigma\Big) + \lambda \cdot i\omega c_\sigma^* c_\sigma}_{S_\lambda^{\Delta}}\,. \tag{5.88}$$

Both terms can be simplified further:

$$S_\lambda^{\mathrm{at}} = -\frac{1}{\beta}\Big(\sum_{n\sigma} c_\sigma^*[(1-\lambda)i\omega_n - \mu]c_\sigma - U(n^\uparrow - \frac{1}{2})(n^\downarrow - \frac{1}{2})\Big) \tag{5.89}$$

$$S_\lambda^{\Delta} = \frac{1}{\beta}\sum_{n\sigma} c_\sigma^* \tilde{\Delta}(i\omega) c_\sigma, \tag{5.90}$$

with $\tilde{\Delta}(i\omega) = \Delta(i\omega) + \lambda i\omega$. With a few redefinitions the ladder formulation of the problem can be evaluated using the existing code. The easiest term to handle is S^{Δ}: By replacing Δ with $\tilde{\Delta}$ this part of the action is identical to the representation without λ. The computation of S_λ^{at} via exact diagonalization is a bit more involved. In order to find a Hamilton representation, one has to rescale S_λ^{at} in such a way that the λ parameter vanishes. This is done by rescaling the creation and annihilation operators, which leads to a redefinition of the physical parameters.

$$S_\lambda^{\mathrm{at}} = \tilde{S}^{\mathrm{at}} = -\frac{1}{\beta}\Big(\sum_{n\sigma} \tilde{c}_\sigma^*[i\omega_n - \tilde{\mu}]\tilde{c}_\sigma - \tilde{U}(\tilde{n}^\uparrow - \frac{1}{2})(\tilde{n}^\downarrow - \frac{1}{2})\Big), \tag{5.91}$$

where the following rescaling of operators has been done:

$$c_\sigma^* = \frac{1}{\sqrt{1-\lambda}}\tilde{c}_\sigma^* = \mathcal{R}\tilde{c}_\sigma^* \tag{5.92}$$

$$c_\sigma = \frac{1}{\sqrt{1-\lambda}}\tilde{c}_\sigma = \mathcal{R}\tilde{c}_\sigma. \tag{5.93}$$

The new parameters are given by:

$$\tilde{\mu} = \mathcal{R}\mu\mathcal{R} = \frac{1}{1-\lambda}\mu \tag{5.94}$$

$$\tilde{U} = \mathcal{R}\mathcal{R}U\mathcal{R}\mathcal{R} = \frac{1}{(1-\lambda)^2}U. \tag{5.95}$$

The expression in Eq. 5.89 can thus be calculated by diagonalization of a Hamiltonian using rescaled parameters. Additionally, one has to take care about the rescaling of the one particle and two particle Green's function, which is caused by the rescaling of operators. In the diagonalization process c-Green's functions are calculated, but $\tilde{c}$-Green's functions are required. Therefore, one has to multiply every creation and

annihilation matrix obtained from ED with a factor $\mathcal{R}^{-1}$. For the one and two particle Green's function one gets:

$$\tilde{g} = \langle \tilde{c}\tilde{c}^* e^{-\tilde{S}^{\mathrm{at}}} \rangle = \langle \mathcal{R}^{-1} c c^* \mathcal{R}^{-1} e^{-S^{\mathrm{at}}_\lambda} \rangle = (1-\lambda) g_\lambda, \tag{5.96}$$

$$\tilde{\chi} = \langle \tilde{c}\tilde{c}^* \tilde{c}\tilde{c}^* e^{-\tilde{S}^{\mathrm{at}}} \rangle = \langle \mathcal{R}^{-1}\mathcal{R}^{-1} c c^* c c^* \mathcal{R}^{-1}\mathcal{R}^{-1} e^{-S^{\mathrm{at}}_\lambda} \rangle = (1-\lambda)^2 \chi_\lambda, \tag{5.97}$$

where g_λ and χ_λ are the results from exact diagonalization and $\tilde{g}$ and $\tilde{\chi}$ the quantities needed in the perturbation expansion.

Now we are able to perform a superperturbation calculation for a given λ. The parameter U has to be rescaled, while Δ is replaced by $\tilde{\Delta}$ and every fermionic operator is multiplied by $\mathcal{R}^{-1}$. All these changes can be implemented in a few lines of code. In order to settle the non-causality problem, it is necessary to choose the parameter λ in such a way that the real part of the dual self-energy vanishes at the poles of the atomic reference problem:

$$\mathrm{Re}\,\Sigma^{\mathrm{d}}(\epsilon_{\mathrm{pole}}) = 0. \tag{5.98}$$

Technically, this is done by a standard steepest descent minimization of the absolute value of $\mathrm{Re}\,\Sigma^{\mathrm{d}}(\epsilon_{\mathrm{pole}})$. The computational effort for this procedure is low, since the dimension of the Hilbert space is only 4 in this case.

Figure 5.12 shows the result of such a renormalization in dependence of λ. For $\beta = 20$ and an unscaled U of $U = 3$, the solution of the rescaled problem is shown. Grey curves correspond to a solution with a negative density of states, yellow curves to a result, which is entirely positive, and the red curve corresponds to $\lambda \approx 0.12$, which fulfills condition (5.98). The fulfillment of this condition leads to a positive spectral weight and all sharp kinks have vanished from the solution. Figure 5.13 shows the real part of the corresponding dual self-energies on the real axis. The data has been obtained via Padé, since a direct calculation on the real axis leads to problems caused by the changed analytic properties of $\tilde{\Delta}$. The curves are very flat in the region of the atomic pole ($U/2$), but in the zoom it is clearly visible that the fulfillment of Eq. (5.98) is reached for $\lambda \approx 0.12$.

The dependence of the scaling parameter λ on the interaction strength is illustrated in figure 5.14. For low temperatures and a small interaction, λ is largest. If the temperature

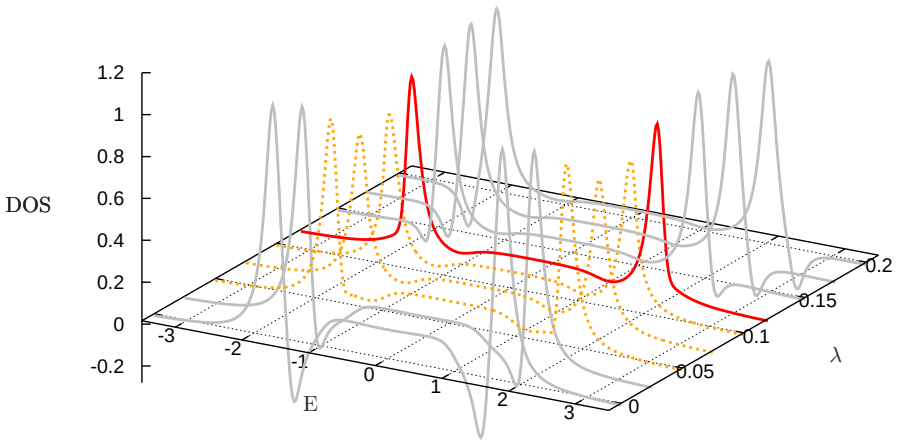

FIGURE 5.12: Results of the rescaled impurity problem for $\beta = 20$, $U = 3$ and $\delta = \pi/beta \approx 0.15$. Grey curves correspond to negative DOS, orange curves to a positive DOS. The red curve corresponds to $\lambda \approx 0.12$ and fulfills condition (5.98).

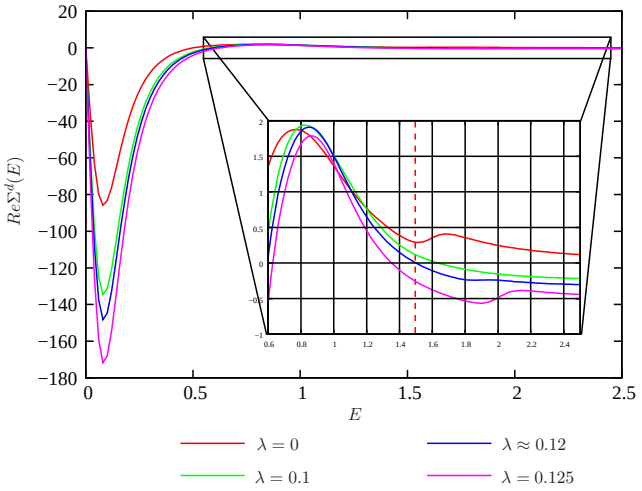

FIGURE 5.13: Real part of the dual self-energy. Parameters correspond to figure 5.12. In the inset it is shown how the fulfillment of condition (5.98) is reached for $\lambda \approx 0.12$.

gets higher, the average λ drops, because the non-causal behavior itself is reduced. For very small interactions the minimization procedure was not able to find a valid solution for λ. The values in the plot have been set to zero in this case. The reason for this behavior is that the real part of the dual selfenergy does not cross the real axis in this

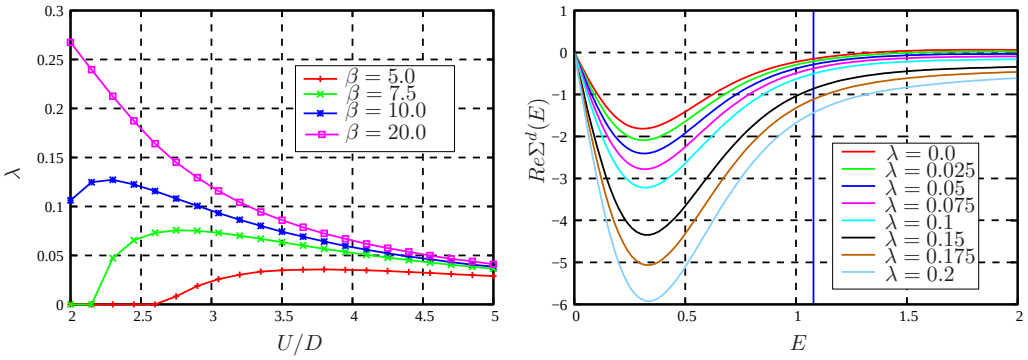

FIGURE 5.14: *left:* dependence of the renormalization parameter λ on the interaction strength. For small U and large temperatures no λ could be found, because of the analytic features of $\Sigma^d(E)$. *right:* $\Sigma^d(E)$ for $U = 2.3$ and $\beta = 5$. For these parameters the atomic pole falls into the dipped region and condition (5.98) can not be fulfilled any more.

parameter regime, as one can see in the right plot of figure 5.14. In this case the condition (5.98) can only be fulfilled by a very large negative λ, which is unphysical, because the non-causality is small here.

In this section it has been shown, that by renormalization the superperturbation theory can be turned into a causal approach. Nevertheless, this procedure does not apply to a reference system with an arbitrary number of bath sites. The reason for this is, that for every pole in the reference system an additional scaling parameter is required. The question is, if by including an additional bath site the number of possible free parameters grows faster than the number of poles in the reference system. Since an additional bath site contributes only two extra parameters, the hopping to the bath and the chemical potential on the bath, the dimensional limit of rescalable problems might be very low. Consequently a deep analysis of the reference system's pole structure is necessary.

We like to stress, that even though the presented scheme might be only a solution for the expansion around the atomic problem, it is also the solution for the non-causality problem of the strong-coupling solver presented by Dai and coworkers [78]. The same rescaling should apply here.

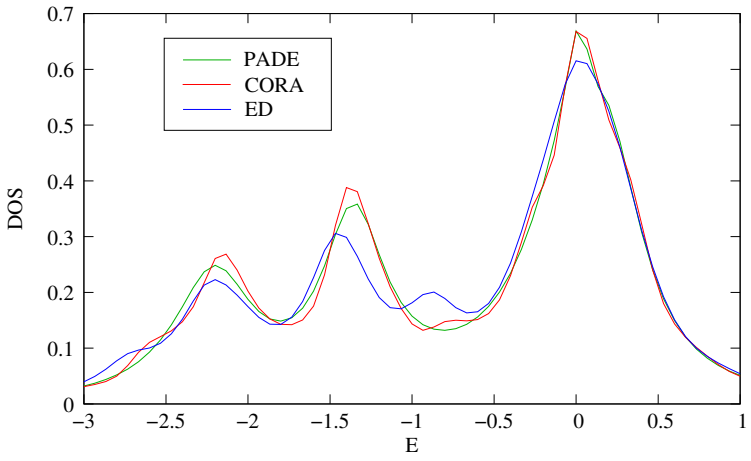

FIGURE 5.15: Example of a CORA calculation for a multi-orbital case. A three orbital impurity with $U = 1.5$, $U' = 0.7$, $J = 0.4$, $\mu = 3.02$ and $\beta = 15$ is embedded in a bath with a constant density of states in the energy window $|\epsilon| < D = 2$. The coupling to the bath was given by $v = 0.1$. The hybridization was approximated by one bath site. In the CORA data set the evolution of small features in the density of states is clearly visible. In the Padé curve these small features have vanished.

5.9 Application to multi-orbital systems

In the following we briefly discuss the applicability of the superperturbation scheme as a solver for multi-orbital Anderson impurity problems. The generalization of the theory to these kind of models is straight forward and can be done without any fundamental problem.

Nevertheless the maximum number of sites in the presented full diagonalization implementation of the SPERT lies in the range of $6 - 7$ sites in total. This implies that the number of bath sites per impurity orbital is strongly restricted.

There are two possible ways out of this dilemma. First one can extend the number of bath sites drastically by employing a Lanczos type of solver for the ED part. This kind of 'Krylov superpertubation' requires a reformulation of the theory in terms of a continuous imaginary time τ, because the direct calculation of the vertex on Matsubara frequencies is not possible using this framework. The reformulation is straight forward, but comes with the price of a discretization error, when numerically treating the imaginary time.

Another approach would be to approximate the bath by a few sites only. An extreme

example would be to replace the whole bath by one single site. This procedure is possible, but the drawback is that the reference system might not contain the symmetry of the full system and it is a priori not clear if the SPERT is strong enough to overcome this difficulty.
Since the Krylov implementation of the SPERT is still a future project, we present an example for a multi-orbital SPERT calculation based on full diagonalization. Figure 5.15 shows the results. A three orbital impurity has been embedded in a bath, which corresponds to a flat density of states in the energy window $|\epsilon| < D$. The coupling to the bath was moderate and has been approximated by a single bath site, which was equally connected to all impurity orbitals. In this parameter regime non-causal behavior did not occur. In comparison to the solution of the reference system a clear shift of nearly all peaks in the CORA is visible. The Padé solution is in good agreement with the CORA data, but fails to reproduce very small features. The reason for this is that analytic continuation using Padé gets more complicated if the function on the real axis has rich structure. This is exactly the case in multi orbital systems.

5.10 Conclusions

It was demonstrated that the superperturbation scheme is an efficient approximate solver for quantum impurity problems. The theory is exact in the strong- and weak-coupling case and gives also reliable results in the intermediate interaction regime at low temperatures. Additionally, the order of approximation can be controlled by the size of the bath. It was shown that the theory can be applied in a self-consistent DMFT scheme and gives nearly the same results as CTQMC on the imaginary axis. Using the example of Kondo screening, the role of the reference system was investigated in detail. It was shown, that the best results are obtained, if the reference system incorporates the symmetries of the full system.
A direct formulation of the superperturbation on the real axis including the first diagram was introduced and compared to existing methods like Padé. At low temperatures it became visible, that the method exhibits non-causal behavior, which arises in the vicinity

of the atomic poles. This problem could be solved in the case of an expansion around the atomic problem by a renormalization of the theory. The applicability of the method to multi-orbital problems was discussed in the last section.

As mentioned in the previous section, future efforts will concentrate on generalizing the theory to the multi-orbital case and to change from a full diagonalization scheme to a Krylov type of solver in the ED part. Additionally, it would be interesting to extend the perturbation expansion from a few diagrams to the summation of an infinite series like in the FLEX or parquet, in order to investigate the Kondo scaling in some more detail.

Chapter 6

The variational lattice approach

Understanding strongly correlated electron physics is one of the major challenges of condensed matter theory. Quantum lattice models are a prototype of such correlated systems, where the interplay of Coulomb repulsion and free electron motion can lead to totally new and unexpected phenomena. One successful approach to address interacting lattice fermions is the dynamical mean field theory (DMFT) [6, 84]. The key idea of the DMFT is to replace the lattice by an interacting impurity in an effective, self-consistent, frequency dependent bath. Consequently, the DMFT fully takes into account local quantum fluctuations, whereas spatial correlations are frozen out. The DMFT has been successfully used to describe the Mott-Hubbard transition [6, 84] and is nowadays a widely used tool in realistic electronic structure calculations [7, 85, 86].
However there are may cases where the **k**-dependence of the problem plays a crucial role. Such problems are: The formation of the Luttinger liquid in low dimensions [87, 88], the physics of systems near quantum critical points [89] or the formation of d-wave superconductivity [90]. In all these examples *non-local* correlations are essential. By construction the DMFT is not a proper tool to describe these problems.
If the spatial correlations are only short ranged, there has been some effort to go beyond the DMFT via various cluster extensions, such as the dynamical cluster approximation (DCA) [11], real space periodic [91] and free cluster approaches [92], as well as the

cellular-DMFT [93] (CDMFT) and the variational cluster approach [94]. These techniques were able to introduce short range correlations into the DMFT scheme, but also lack the description of long range correlations.

A way to overcome the limitation of short range correlations in the DMFT is to perform a diagrammatic expansion around the DMFT solution. This approach was utilized in the so called dynamical vertex approximation [95] and similar methods [96].

In this chapter we introduce a new and efficient strategy to treat non-local correlations, the variational lattice approach (VLA). The VLA is a combination of the dual fermion approach for $\mathbf{k}$-dependent problems and the exact diagonalization technique. The key idea is to take a reference system with a finite number of bath sites and to perform a perturbation expansion in $\Delta^{\mathrm{N}} - \epsilon_{\mathbf{k}}$, where Δ^{N} is the hybridization function of the finite reference system and $\epsilon_{\mathbf{k}}$ the dispersion of the lattice. Since the hybridization function is not specified in the derivation of the dual theory, any hybridization function will lead to the exact result if all diagrams are summed up.

The VLA can be seen as an extension of previous work by Pairault and coworkers [73, 74], who proposed a hybridization expansion around the atomic limit. Like in the SPERT, it can be shown that the VLA is equivalent to this scheme in the limit of weak hybridization. In comparison to an expansion around the atomic solution, the VLA has the advantage that by including a discrete bath, the reference system can be adjusted to the physical problem at hand and is therefore in a sense variational. Additionally the VLA is much faster than standard dual fermion approach using CTQMC as solver. Therefore, the VLA is a good opportunity to calculate the phase diagram of the Mott-Hubbard transition.

This chapter is organized as follows: First the dual formalism is briefly summarized for the VLA, then a small benchmark model is discussed. Afterwards the phase diagram for the MIT transition is discussed in the VLA approximation.

Parts of the simulations for the MIT phase diagram (determination of the crossover line and data points at very low temperatures) have been performed in collaboration with Aljoscha Wilhelm.

6.1 Formalism

In this section we briefly review the dual fermion derivation in the context of **k**-dependent problems and highlight the differences between the VLA and the DF using CTQMC as a solver. For a more detailed derivation with many useful remarks we recommend reading chapter 4. The action of the interacting lattice can be written down as follows:

$$S^{\mathrm{F}}[c^*,c] = -\frac{T}{N_k}\sum_{\mathbf{k}\omega ab} c^*_{\mathbf{k}\omega a}[(i\omega+\mu)\mathbb{1}-\epsilon_{\mathbf{k}}]_{ab}c_{\mathbf{k}\omega b} + \sum_{\mathbf{i}} S^{\mathrm{NG}}[c^*_{\mathbf{i}},c_{\mathbf{i}}]. \tag{6.1}$$

Here $\epsilon_{\mathbf{k}}$ denotes the free dispersion of the lattice and $S^{\mathrm{NG}}[c^*_{\mathbf{i}},c_{\mathbf{i}}]$ is the local Coulomb interaction. Latin letters are a combined indices for orbital and spin degrees of freedom. The key strategy of the approach, like in the DMFT, is to introduce a frequency dependent hybridization function $\Delta^{\mathrm{N}}(\omega)$. This function is just added and subtracted to Eq. (6.1). In the case of the VLA this hybridization function is given by a few bath sites, which are coupled to the impurity. The hybridization function is determined by the hopping amplitudes and the energy levels of the bath:

$$\Delta^{\mathrm{N}}(\omega)_{ab} = \sum_{i}^{\mathrm{N}} \frac{V_{ai}V^*_{ib}}{i\omega-\epsilon_i}. \tag{6.2}$$

After adding and subtracting $\Delta^{\mathrm{N}}(\omega)$ the action reads:

$$S^{\mathrm{F}}[c^*,c] = S^{\mathrm{Ref}}[c^*_{\mathbf{i}},c_{\mathbf{i}}] - \sum_{ab}^{\mathbf{k}} c^*_{\mathbf{k}\omega a}[\Delta^{\mathrm{N}}(\omega)-\epsilon_{\mathbf{k}}]_{ab}c_{\mathbf{k}\omega b} \tag{6.3}$$

$$S^{\mathrm{Ref}}[c^*_{\mathbf{i}},c_{\mathbf{i}}] = -\sum_{ab}^{\mathbf{i}} c^*_{\mathbf{i}\omega a}[(i\omega+\mu)\mathbb{1}-\Delta^{\mathrm{N}}(\omega)]_{ab}c_{\mathbf{i}\omega b} + \sum_{\mathbf{i}} S^{\mathrm{NG}}[c^*_{\mathbf{i}},c_{\mathbf{i}}]. \tag{6.4}$$

In this equation the same conventions for the sums as in chapter 4 (see Eq. (4.2)) have been used. Now the key idea is to solve the reference problem exactly and to formulate a perturbation expansion around this exact solution, which formally means to expand in $\Delta^{\mathrm{N}}(\omega)-\epsilon_{\mathbf{k}}$. The fact that S^{Ref} has non-Gaussian components makes a standard diagrammatic expansion not applicable, since Wick theorem does not apply. To

circumvent this problem, new fermionic variables are introduced via an exact Hubbard-Stratonovich transformation. After integrating out the old c-variables a perturbation expansion in the dual space will be possible. This expansion will exactly correspond with a perturbation series around the reference system in terms of $\Delta^{\mathrm{N}}(\omega) - \epsilon_{\mathbf{k}}$. In the case of the VLA the Hubbard-Stratonovich transformation takes the following form:

$$e^{c_1^* n_{12} D_{23}^{-1} n_{34} c_4} = \frac{1}{\det D} \int \mathcal{D}[f^*, f] e^{-f_1^* D_{12} f_2 + f_1^* n_{12} c_2 + c_1^* n_{12} f_2}, \tag{6.5}$$

with

$$\left.\begin{aligned} n &= -g^{-1}(\omega) \\ D &= g^{-1}(\omega)[\Delta^{\mathrm{N}}(\omega) - \epsilon_{\mathbf{k}}]^{-1} g^{-1}(\omega) \end{aligned}\right\} \rightarrow n_{12} D_{23}^{-1} n_{34} = [\Delta^{\mathrm{N}}(\omega) - \epsilon_{\mathbf{k}}]_{14}. \tag{6.6}$$

Here $g(i\omega)$ represents the impurity Green's function of the reference system. For a shorter notation we have changed from Latin characters for the indices to numbers. After the transformation the action reads:

$$\begin{aligned} S^{\mathrm{F}}[c^*, c, f^*, f] =& S^{\mathrm{Ref}}[c_{\mathbf{i}}^*, c_{\mathbf{i}}] + S^{\mathrm{C}}[f_{\mathbf{i}}^*, f_{\mathbf{i}}, c_{\mathbf{i}}^*, c_{\mathbf{i}}] \\ &+ \sum_{ab}^{\mathbf{k}} f_{\mathbf{k}\omega a}^* [g^{-1}(\omega)[\Delta^{\mathrm{N}}(\omega) - \epsilon_{\mathbf{k}}]^{-1} g^{-1}(\omega)]_{ab} f_{\mathbf{k}\omega b}, \end{aligned} \tag{6.7}$$

with:

$$S^{\mathrm{C}}[f_{\mathbf{i}}^*, f_{\mathbf{i}}, c_{\mathbf{i}}^*, c_{\mathbf{i}}] = \sum_{ab}^{\mathbf{i}} f_{\mathbf{i}\omega a}^* g^{-1}(\omega)_{ab} c_{\mathbf{i}\omega b} + \sum_{ab}^{\mathbf{i}} c_{\mathbf{i}\omega a}^* g^{-1}(\omega)_{ab} f_{\mathbf{i}\omega b}. \tag{6.8}$$

Note that because of the local character of the impurity Green's function, the $\mathbf{k}$-summation in (6.8) could be replaced by an equivalent summation over sites. Hence the coupling of the auxiliary fermions is purely local and S^{C} decomposes in a sum over local terms. With this in mind the change of variables can be completed by integrating out the old variables. This is done by introducing the following identity:

$$\begin{aligned} \int \exp(-(S^{\mathrm{Ref}}[c_{\mathbf{i}}^*, c_{\mathbf{i}}] + S^{\mathrm{C}}[c_{\mathbf{i}}^*, c_{\mathbf{i}}, f_{\mathbf{i}}^*, f_{\mathbf{i}}])) \mathcal{D}[c_{\mathbf{i}}^*, c_{\mathbf{i}}] \\ \stackrel{!}{=} \mathcal{Z}_{\mathrm{Ref}} \exp(-\sum_{ab}^{\mathbf{i}} f_{\mathbf{i}\omega a}^* g^{-1}(\omega)_{ab} f_{\mathbf{i}\omega b} + \mathcal{V}[f_{\mathbf{i}}^*, f_{\mathbf{i}}]). \end{aligned} \tag{6.9}$$

The last equation has to be understood as a defining equation for the dual potential $\mathcal{V}$, which is chosen in such a way that the last identity holds. This is done by expanding both sides in terms of dual variables and integrating out the c-part. Then both sides are compared order by order, which results in a definition of $\mathcal{V}$ in terms of a series:

$$\mathcal{V}[f^*_{\mathbf{i}}, f_{\mathbf{i}}] = \sum_i \nu_i[f^*_{\mathbf{i}}, f_{\mathbf{i}}] = -\frac{1}{4}\gamma^{(4)}_{1234} f^*_1 f_2 f^*_3 f_4 + \frac{1}{36}\gamma^{(6)}_{123456} f^*_1 f_2 f^*_3 f_4 f^*_5 f_6 \mp \dots . \quad (6.10)$$

In this equation γ^4 and γ^6 are the exact irreducible vertices of the impurity problem, which have been already defined in previous chapters. With the final definition of the dual potential, the expression for the dual action reads:

$$S^{\mathrm{d}}[f^*, f] = -\sum_{ab}^{\mathbf{k}} f^*_{\mathbf{k}\omega a}[G^{\mathrm{d}}_0(\omega, \mathbf{k})]^{-1}_{ab} f_{\mathbf{k}\omega b} + \mathcal{V}[f^*_{\mathbf{i}}, f_{\mathbf{i}}], \quad (6.11)$$

with G^{d}_0 being the bare dual Green's function:

$$G^{\mathrm{d}}_0(\omega, \mathbf{k}) = -g(\omega)[g(\omega) + [\Delta^{\mathrm{N}}(\omega) - \epsilon_{\mathbf{k}}]^{-1}]^{-1} g(\omega). \quad (6.12)$$

Up to now Eq. (6.11) is just an exact reformulation of Eq. (6.1), in terms of dual variables. The great advantage of the latter formulation in comparison to the initial one is that now the Wick theorem is applicable and a perturbation expansion in the dual potential is possible. This expansion exactly corresponds to an expansion around the reference problem in terms of $\Delta^{\mathrm{N}}(\omega) - \epsilon_{\mathbf{k}}$ and can be done by applying the diagrammatic rules explained in chapter 4. This leads to the same diagrams as for the standard dual fermion approach. After summing up a subclass of diagrams the dual Green's function can be transformed back using the following identity:

$$G(\omega) = (\Delta^{\mathrm{N}}(\omega) - \epsilon_{\mathbf{k}})^{-1} + [g(\omega)(\Delta^{\mathrm{N}}(\omega) - \epsilon_{\mathbf{k}})]^{-1} \times G^{\mathrm{d}}(\omega)[(\Delta^{\mathrm{N}}(\omega) - \epsilon_{\mathbf{k}})g(\omega)]^{-1}. \quad (6.13)$$

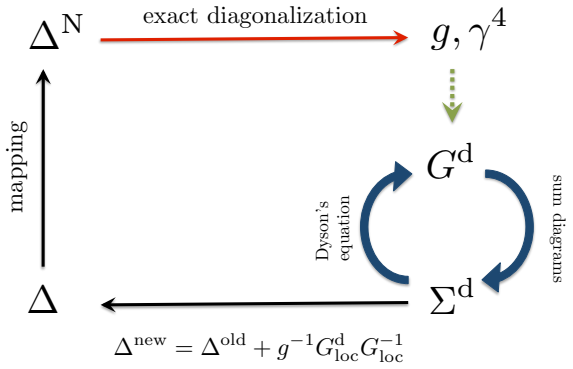

FIGURE 6.1: Calculation procedure of the VLA: The scheme includes an outer loop, which updates the hybridization function until a self-convergence in the effective bath parameters is reached. The inner loop corresponds to the calculation of dual skeleton diagrams, which lead to a conserving approximation.

6.1.1 The meaning of $\Delta^{\mathrm{N}}(\omega)$ and the calculation procedure

Up to now the hybridization function of the reference system has not been specified and enters therefore as an arbitrary quantity. This essentially means that Eq. (6.11) is an exact reformulation of the initial action in Eq. (6.1) for any function $\Delta^{\mathrm{N}}(\omega)$. Therefore, the VLA is totally different from approaches as for example DMFT employing exact diagonalization as a solver. In the latter case the DMFT self-consistency can be reached only in a subspace, which is spanned by the finite number of bath sites. Such a restriction is a priori not given in the VLA.

Nevertheless, it should be clear that as soon as any approximation is applied to the approach the actual configuration of the reference system plays a crucial role and one should expect differences for a varying number of bath sites. Consequently, the choice of the bath parameters gets very important, if only a subclass of diagrams is calculated. In order to optimize these parameters, a self-consistent calculation procedure is applied, which is depicted in figure 6.1. To begin the iteration, a starting guess for the hybridization function is constructed using the interaction-free solution:

$$\Delta_{\mathrm{init}}(i\omega) = (i\omega + \mu) - G^{-1}_{0\mathrm{loc}}(i\omega). \tag{6.14}$$

The same starting guess can be applied in the DMFT case, as already discussed in paragraph 2.2. Afterwards Δ_{init} is mapped onto the exact diagonalization impurity problem. This is done in the same way as described in chapter 4: we require that Δ_{init} coincides with Δ^{N} on the first N frequencies, where N is the number of bath sites:

$$\Delta_{\text{init}}(i\omega_n) \stackrel{!}{=} \Delta^{\text{N}}(i\omega_n) \qquad \text{for } 1 \leq n \leq \text{N}. \tag{6.15}$$

The defined impurity problem is solved via exact diagonalization and the impurity Green's function g and the vertex γ are calculated. These quantities then enter the dual perturbation series. First, the initial dual Green's function is constructed and a subclass of diagrams is summed up. Afterwards, a new dual Green's function is calculated using Dyson's equation and the dual diagrams are again computed. This process is iterated until convergence, which means that $\sum_n^{n_c} |G^{\text{d}}_{i+1}(i\omega_n) - G^{\text{d}}_i(i\omega_n)| < \epsilon$. Here i is the iteration number, n_c a cutoff for the Matsubara sum and ϵ a predefined convergence parameter. The described inner loop is necessary to calculate dual skeleton diagrams and leads to a conserving approximation. From the converged dual Green's function it is possible to construct a hybridization function using the following formula from ref. [56]:

$$\Delta^{\text{new}} = \Delta^{\text{old}} + g^{-1} G^{\text{d}}_{\text{loc}} G^{-1}_{\text{loc}}. \tag{6.16}$$

Here g is the Green's function of the reference system, $G^{\text{d}}_{\text{loc}}$ the local part of the dual Green's function and G_{loc} the local average of the lattice Green's function. The new Δ is then again mapped onto impurity parameters and the loop starts again.
The self-consistent iteration is stopped, when a convergence in the effective parameters of the bath is reached. Since the hybridization function is an arbitrary quantity in the dual theory, condition (6.16) is not unique. This update formula rather corresponds to the condition that the local part of the dual Green's function is zero:

$$G^{\text{dual}}_{\omega, r=0} = 0. \tag{6.17}$$

This requirement corresponds to the minimization of purely local diagrams, which are automatically taken into account by this condition. For the VLA it should be clear that Eq. (6.16) can only be fulfilled approximately, because we are working with a finite

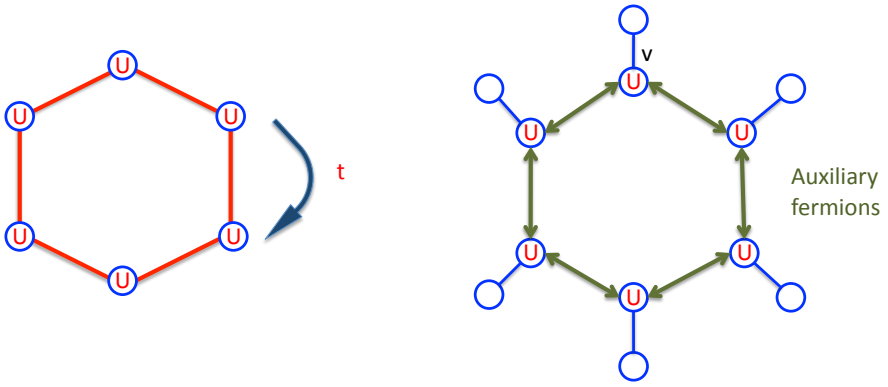

FIGURE 6.2: Illustration of the benchmark model (*left*) and the basic idea of the VLA approximation in this case (*right*). The model is given by a six site ring with onsite Coulomb interaction and nearest neighbor hopping. The basic idea of the VLA is to solve the reference system (blue cluster: impurity + one bath site) exactly and to treat the non-local correlations perturbatively (green arrows).

number of bath sites. Therefore, all diagrams contribute to the dual self-energy, even though the result has been already converged.
In the following a benchmark calculation is discussed.

6.2 A first test

To test the method, an exactly solvable problem was calculated in the VLA approximation and the results were compared to the exact data sets. As a benchmark a one dimensional six site ring with onsite Coulomb interaction and nearest neighbor hopping was chosen. The local density of states was calculated in three different ways: First by exact diagonalization of the Hamiltonian, which yields in the exact result, second by DMFT using a three bath site reference system, and by the VLA using a one bath site reference system.

It should be clear that this kind of benchmark is one of the hardest tests one can choose to analyze the method. The DMFT is exact in infinite dimensions and will with no doubt fail to describe a one dimensional system if the interaction is strong enough. Since the VLA is in some sense a perturbation expansion around the DMFT result, it will be very

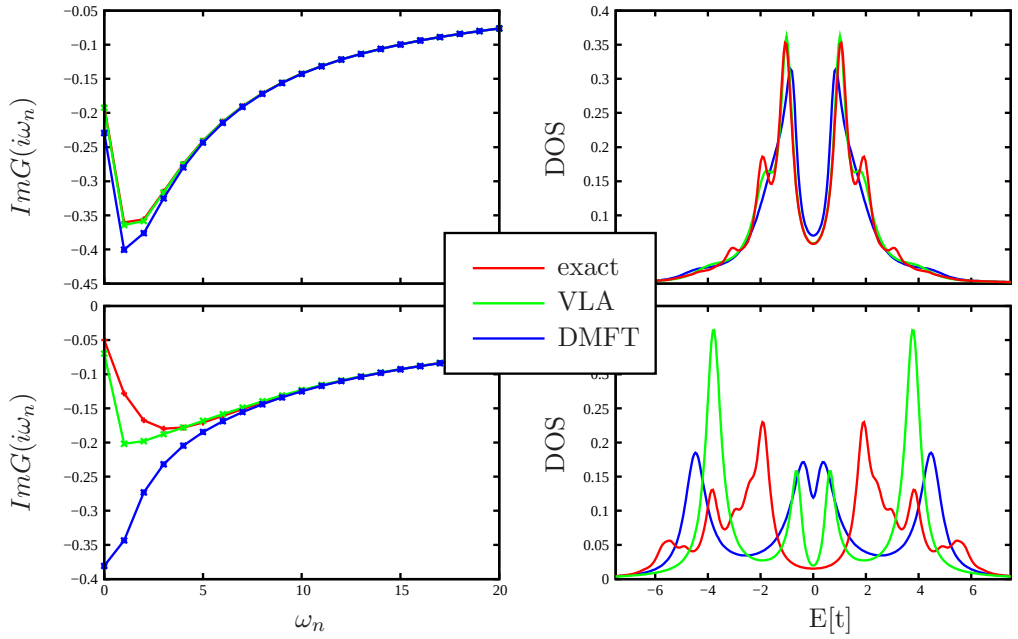

FIGURE 6.3: Results for a half-filled six-site ring with $\beta = 10$ and a bandwidth of $W = 4$. The upper row shows the results for $U = 4$, the lower one for $U = 6$. In the weak interacting case the DMFT as well as the VLA are in good agreement with the exact result. If the interacting is larger the DMFT breaks down, but VLA manages to capture the essential insulating physics. For the calculations a dual ladder of 9 vertices was summed up. The analytic continuation has been done via Padé.

hard for the method to correct the DMFT behavior. An illustration of the basic idea of the VLA is illustrated in figure 6.2 using the benchmark model as an example.

The results of the benchmark simulation are depicted in figure 6.3. For a bandwidth of $W = 4t = 4$ and $\beta = 10$ the model has been solved for two values for U. The upper row shows the results for $U/t = 2$, the lower one for $U/t = 6$. In the left column the local Green's function is shown, in the right one the corresponding density of states.

In the weakly interacting case both methods, the DMFT and the VLA, are in good agreement with the exact result. However, the VLA is closer to the exact solution than the DMFT curve. The imaginary parts of the local Green's function almost lie on top of each other. Also the density of states obtained from the VLA reproduces the gap better than the DMFT.

In the strong interacting case, the difference between the DMFT and the VLA is more

pronounced. The DMFT solution breaks down and indicates a metallic solution, whereas the VLA gives an insulating result. Although the VLA fails to reproduce the correct band gap, it succeeds in reproducing the depth of the gap and improves the width in comparison to the DMFT. Therefore the lower right plot is a very illustrative result. The VLA is in a sense a perturbation around the DMFT and has therefore nearly the same band gap, but succeeds in recovering the essential insulating physics, which is a consequence of the dual perturbation series. To obtain this result, a dual ladder with a maximum of 9 vertices was summed up. The ladder dual fermion approach was not applicable here, because the eigenvalue of the Bethe-Salpeter equation was larger than one.

6.3 The Mott transition in the VLA-Framework

Interaction driven metal insulator transitions (MIT) are a fundamental problem in condensed matter theory. If the local Coulomb repulsion is of the same order as the kinetic energy, the interplay of wave-like characteristics and an increasing localization of the conduction electrons leads to rich and unexpected physics. Inspired by previous works [56, 82], this section is therefore dedicated to the Mott insulator transition in the 2D Hubbard model.

In a recent CDMFT study on a 4 site plaquette, Park and coworkers [82] found strong corrections to the paramagnetic DMFT phase diagram. Induced by short ranged antiferromagnetic correlations the critical U_C of the Mott transition was reduced form $U_C^{\mathrm{DMFT}} = 9.35t$ to $U_C^{\mathrm{CDMFT}} = 6.05t$. While the transition stayed first order, the shape of the transition lines was dramatically changed: A metallic ground state is preferred over a paramagnetic insulator in single site DMFT at low temperatures, whereas the insulator dominates in the CDMFT solution, because the entropy is reduced by formation of singlets.

Motivated by these findings Hafermann approached this problem in an intensive dual fermion study [56]. But because of the highly demanding numerical costs it was only possible to give a rough estimate for the transition lines, since most of the calculations were not converged.

In this section we solve the problem in the VLA framework using the first two dual diagrams (diagrams a.) and b.) in Fig. 4.2) and a reference system including one bath site. In this case the numerical effort for solving the impurity problem is strongly reduced in comparison to a CTQMC study and becomes only considerable at very low temperatures. During the simulation several methods to determine the phase boundary were tested and will be introduced in the following.

At low temperatures the Mott transition can be visualized by a hysteresis in some system quantity, which indicates the coexistence of two possible solutions. For the position of the transition line it does not matter which quantity is taken into account to investigate the hysteresis, but parameters of the reference system are calculated most easily. The double occupancy of the reference system $\langle nn \rangle_{\mathrm{Ref}}$, or the effective hopping parameter to the bath v are such parameters. Figure 6.4 compares several of these system quantities in dependence of U for $\beta = 12.5$. The upper right plot shows the double occupancy of the reference system. The graph clearly shows two separate solutions in the coexistence region. To obtain these data points, two independent calculations were started, one beginning with a small U and the other with a large one. When the simulation has been converged for a fixed value of U, the converged hybridization has been used to start the calculation for the next value. The red curves correspond to simulations where U was increased from a small value of U to a large one. The green curves show the reverse process: U is decreased from a large value. The position of the transition has been defined as the point between the last metallic solution and the next insulating result. The error of this value is given by the distance between these two points. The plot to the left illustrates the behavior of the imaginary part of the local Green's function for points marked in the right figure. The green and magenta curves indicate an insulating solution because the graph tends towards zero for low frequencies. The red and blue curves correspond to a metallic solution. The lower right figure shows the hysteresis in the hopping parameter v. The position of the phase transition is the same. In this case the metal insulator transition can be interpreted as reduction of the hopping amplitude of the reference system.

A more mathematical definition of the coexistence region can be formulated in terms of a stability analysis of the VLA parameter space. If the VLA self-consistency loop is interpreted as the repeated application of a function F on the effective parameters of

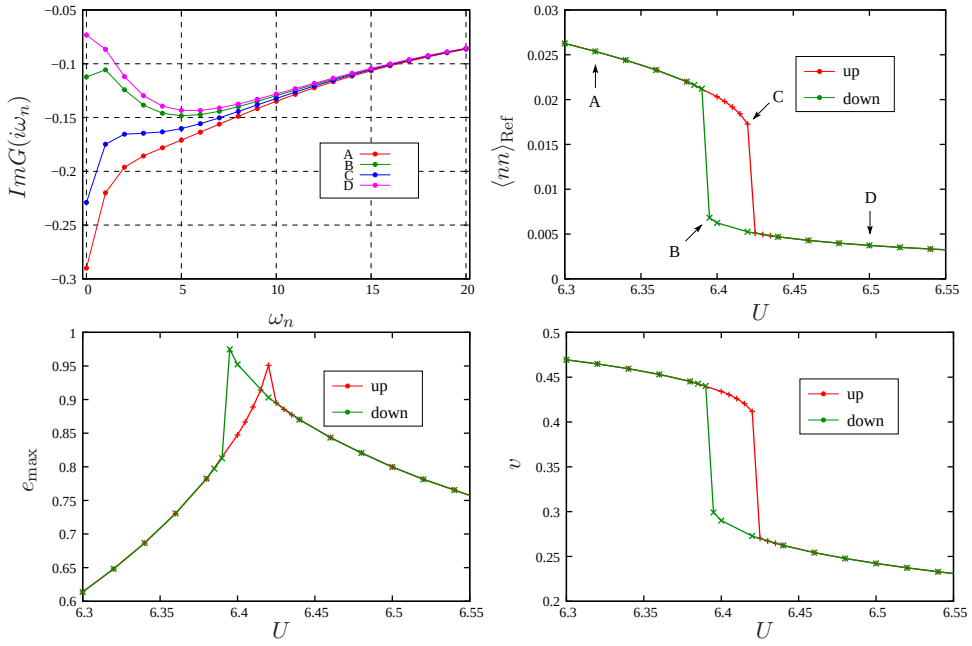

FIGURE 6.4: Hysteresis in references system quantities for $\beta = 12.5$: *Upper right:* double occupancy of the reference system. *Lower right:* hopping parameter of the reference system. *Lower left:* maximum eigenvalue of the Jacobi matrix of the self-consistency loop. In all plots a clear coexistence of two solutions is visible, and all transition points coincide. All the calculations have been converged separately. *Upper left:* Examples for the imaginary part of the local Green's function for the U values marked in the right figure. The calculations have been done including the first two dual diagrams (diagrams a.) and b.) of Fig. 4.2)

.

the bath $\overline{x}$, a stability analysis known form classical chaos theory is possible. In this language the self-consistency loop has to be interpreted as an iterated function, which is comparable to the logistic map:

$$\overline{x}_{i+1} = F(\overline{x}_i). \tag{6.18}$$

In this case $\overline{x}$ represents the effective bath parameters of the reference system and F is a full VLA loop as depicted in figure 6.1. The fixpoint condition of this iteration is: $F(x^*) = x^*$. A fixpoint becomes unstable and a second one arises, if the largest eigenvalue of the Jacobian matrix of F is larger than one. For the present case this

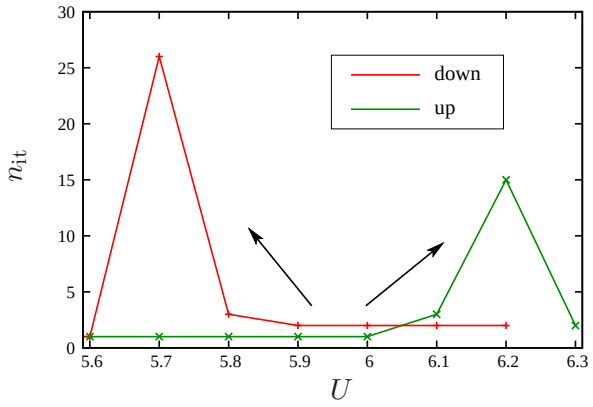

FIGURE 6.5: Number of iterations to reach a predefined convergence criteria in dependence of U for $\beta = 20$. The exponential increase indicates the phase transition.

means a solution becomes unstable, if the derivative with respect to the hopping is greater than one:

$$\frac{F(v + \Delta v) - F(v)}{\Delta v} > 1 \rightarrow \text{ unstable.} \tag{6.19}$$

The results of such an analysis are depicted in the lower left plot of figure 6.4. At the boundary of the coexistence region the eigenvalues of the up and down curve tend to one indicating the coexistence region. Both curves do not reach one, because of the finite step size used. This kind of investigation has been first presented by Hugo Strand[1] in the DMFT context at the Les Houches summer school on "Modern theories of correlated electron systems" (2009), but the scheme has not been published so far.

At very low temperatures the full convergence of a hysteresis near the transition point is numerically very expensive, because the number of iterations needed to converge grows exponentially. Therefore, a different scheme has been applied in this case, which takes advantage of this exponential divergence. Before the simulation starts, a convergence criteria is defined and the number of iterations to fulfill this criteria is plotted against U. An exponential increase of the iteration number indicates the transition point. Such an analysis is depicted in figure 6.5. In comparison to a full convergence the amount of iterations needed to find the transition is drastically reduced. In the present scheme the maximum number of iterations was 26, a full convergence often took more than 90

[1]Department of physics, University of Gothenburg

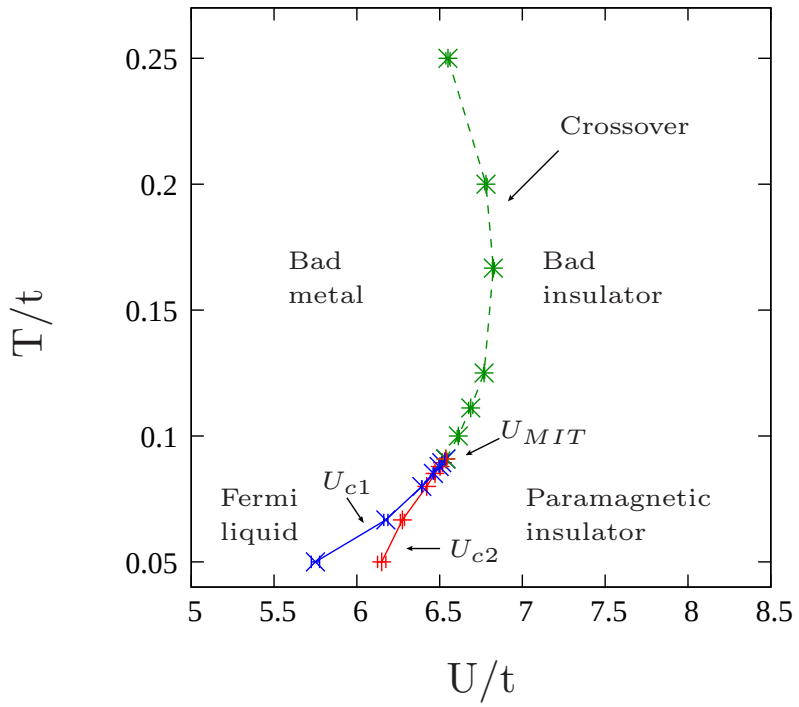

FIGURE 6.6: Paramagnetic U-T phase diagram of the Mott metal insulator transition in the 2D Hubbard model calculated in the VLA framework with one bath site in the reference system and the first two dual diagrams (diagrams a.) and b.) in figure 4.2). The critical U is $U_C^{\mathrm{VLA}} = 6.4 \pm 0.1$

iterations.

At high temperatures the transition from a metallic to an insulation state is given by a smooth crossover. The position of this line has been determined as the maximum slope of the effective hopping parameter in dependence of U.

The final phase-diagram is depicted in figure 6.6 and shows similar characteristics as the CDMFT study by Park et al. [82]. The critical U is reduced in comparison to single site DMFT from $U_C^{\mathrm{DMFT}} = 9.35t$ to $U_C^{\mathrm{VLA}} = 6.4 \pm 0.1$. In comparison to reference [82] the value is slightly above the result of the CDMFT study. The reason for this is the magnitude of antiferromagnetic correlations taken into account. The CDMFT analysis was performed using a 4 by 4 plaquette, which implies that a perfect singlet formation is favored at low temperatures and consequently leads to a very low critical U. The VLA approximation is not limited to these nearest neighbor correlations, which means that

spatial correlations enter the approach, which reduces the formation of a perfect singlet. Consequently the critical U is lifted and lies above the CDMFT value.
In accordance to the work by Park the transition stays first order and the form of the transition lines is very similar to the CDMFT results. The metal is favored over the insulator at higher temperatures below the critical point. For low temperatures above the critical U insulating behavior dominates the phase diagram, because of a lower entropy induced by rising antiferomagnetic order.

6.4 Pseudogap Formation

One characteristic feature of a rising antiferromagnetic order is the formation of a pseudogap in the local density of states in the bad metal regime. This feature has been obtained in the ladder dual fermion approach (LDFA) by Hafermann and coworkers [64]. Until now the pseudogap formation was only discussed in the **k**-averaged density of states. A **k**-resolved investigation of the problem is still missing, because the analytic continuation of CTQMC data is a complicated problem. The reason for this is the poor resolution of the applied MAXENT method on the real axis. In comparison to that the VLA framework offers the great opportunity to use the Padé analytic continuation instead of the MAXENT, because the method provides numerical exact data. This approach offers a good resolution on the real axis.
In this section we present the results of calculation performed at $\beta = 5$ for $U = 4$. The lattice problem was solved using a three bath site reference system and summing up the fully renormalized dual ladder. The basic concepts of the ladder diagrammatic technique are discussed in [56]. In this parameter regime a fully self-consistent VLA iteration is not crucial, therefore the results have been obtained in a single shot calculation, using the non-interacting hybridization function as an input.

The right plot of figure 6.7 shows the **k**-averaged local density of states. The DOS clearly exhibits a gap at the Fermi level of the order $J = 2t^2/U = 0.5$. To analyze the opening of the pseudogap in **k**-space, the spectral function was calculated on high

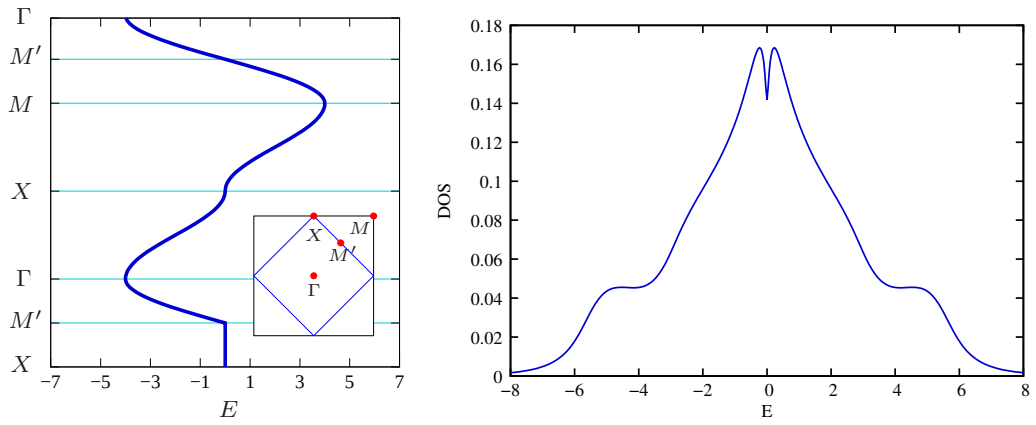

FIGURE 6.7: *Left:* Non-interacting band along the high symmetry line $X \to M' \to \Gamma \to X \to M \to M' \to \Gamma$. The high symmetry points are marked in the inset. *Right:* **k**-averaged density of states for $\beta = 5$ and $U = 4$. The DOS clearly exhibits a pseudogap at the Fermi level.

symmetry lines in the Brillouin-Zone:

$$X \to M' \to \Gamma \to X \to M \to M' \to \Gamma. \tag{6.20}$$

The left plot of figure 6.7 shows the non-interacting band and the symmetry points marked in the Brillouin-Zone (inset).

Figure 6.8 shows the result of the VLA calculation. The band is broadened by the interaction and a pseudogap is visible whenever the Fermi level is crossed. This is the case from $X \to M'$ and at the X and M' point. An additional many body effect is visible at the band edge in the vicinity of the Γ and M point. Here the noninteracting density of state has been washed out and is broadened. This effect leads also to a broadening of the local density of states and is visible as pronounced shoulders at $E = \pm 5$. The reason for this effect is not clear at the moment and deserves further detailed analysis.

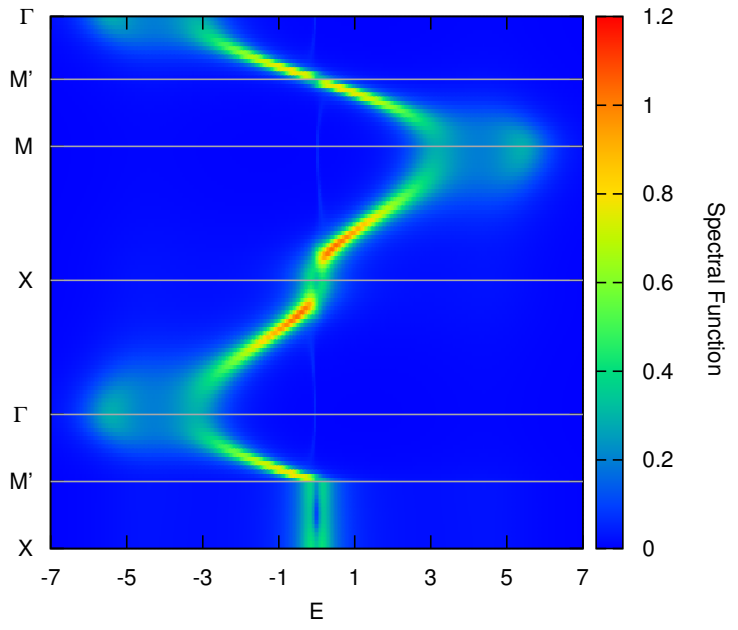

FIGURE 6.8: **k**-resolved spectral function on the high symmetry line $X \to M' \to \Gamma \to X \to M \to M' \to \Gamma$.. The pseudogap is clearly visible whenever the Fermi-level is crossed. The parameters are the same as in figure 6.7.

6.5 Conclusions

In this section we presented a very efficient numerical scheme to treat spatial correlations in fermionic lattice models, the variational lattice approach (VLA). The VLA can be seen as a generalization of the hybridization expansion around the atomic solution by Pairault and coworkers [73, 74] to a perturbation expansion around a finite size impurity model, which can be solved by exact diagonalization. In comparison to the hybridization expansion the VLA is not only exact in the strong-coupling regime, but also in the opposite case, the weak-coupling limit. The restriction to impurity problems with a small Hilbert space makes the VLA numerically more efficient than previous implementations for arbitrary impurity models, which had to be solved by CTQMC. In addition to that the usage of ED generates numerical exact data, which are very easy to map to the real axis via Padé.

Using theses advantages the VLA resolved several open questions in the analysis of the

2D Hubbard model within the dual fermion approach. The paramagnetic phase diagram of the Mott metal insulator transition was calculated. It was found that the critical U_C is $U_C^{\mathrm{VLA}} = 6.05t$, which is slightly above the result of a recent CDMFT study by Park and coworkers [82].

In addition to that the formation of the pseudogap could be resolved in **k**-space, which had not been possible in the original CTQMC based dual approach, because of the bad real axis resolution of MAXENT.

Chapter 7

Superperturbation method on the Keldysh contour

The description of time dependent phenomena plays a key role in the theory of strongly correlated systems, especially in the field of condensed matter physics. Experimental advances in the last decade allow us to access system information at very short time scales as well as at very short distances. This combination of temporal and spatial precision permits the exploration of the very quantum nature of many-body problems in its full complexity.

Prominent examples for these developments are the non-equilibrium transport through nano-devices [97] or matter exposed to strong periodic time dependent fields. In both situations one is interested in the steady state behavior of the system in order to estimate the applicability of these systems for future technologies.

Direct access to the real-time evolution of a system can be gained in pump-probe experiments [98] such as FLASH or SLAC, or by new spectroscopy methods in cold atom experiments [99]. These measurements give direct access to the time evolution on very short time scales and allow to explore fundamental questions in modern condensed matter theory.

Unfortunately, the theoretical description of these experiments is quite a challenging

task. Even though many schemes of equilibrium physics have been generalized to non-equilibrium problems, they often suffer from serious problems arising from the time-dependent nature of the set-up. One example we will deal with is the time-dependent Anderson impurity problem. In the equilibrium case this model is in principle well understood, because there are many efficient solvers available, see chapter 3. In the non-equilibrium situation most of them are not adequate. The exact diagonalization scheme can only describe closed systems and fails to be a good starting point for the investigation of open systems.

As in the equilibrium case, there are diagrammatic Monte Carlo methods available, but they suffer from a dynamical phase problem, which arises due to the sampling of a complex time evolution operator $\exp[-itH]$. This problem is present even if the inherent fermionic sign problem is absent. Since the average sign of a simulation drops exponentially with the perturbation order, these methods are limited to very short times. Consequently, only situations with a very low perturbation order such as the weakly interacting or the strong-coupling case can be treated by these stochastic approaches.

In this chapter we present a new solver for the time-dependent Anderson impurity model, which is based on the earlier described dual transformation. The key idea is, like in the equilibrium case, to solve a reference system with exact diagonalization and to perform a perturbation expansion in the difference between the hybridization function of the finite system and the full system. This solver will be exact in both limits, the weak- and the strong-coupling regime. Therefore, this scheme can be a good candidate to address the intermediate interaction regime, where other solvers are inappropriate.

This chapter is organized as follows: At the beginning the concept of a closed time contour will be briefly reviewed. It will be explained, how this contour can be properly discretized in order to numerically treat objects, which depend on a continuous time argument. For this purpose we will deduce a discretized action representation and discuss the Green's function for some examples. After that the dual perturbation theory is generalized to the non-equilibrium case and the calculation of the Green's function and the two-particle Green's function in the exact diagonalization scheme is discussed. In the last part of the chapter some results will be presented.

7.1 The concept of a closed time contour

In quantum statistical mechanics every observable O is associated with a hermitian operator $\hat{O}$. Its expectation value is given by $\langle \hat{O} \rangle = \mathrm{Tr}\{\, \hat{O}\rho_0 \,\}$, where ρ_0 is the density matrix of the system governed by a Hamiltonian H_0. As long as ρ_0 commutes with the Hamiltonian $[\rho_0, H_0] = 0$, the expectation value of $\hat{O}$ will not have any time dependence. In the following we would like to consider a situation, in which the system is in equilibrium for times smaller than t_0 and is then perturbed by a sudden switch of some not specified internal parameter[1].
In this case the expectation value of $\hat{O}$ is given by the average of $\hat{O}$ in the Heisenberg picture traced over the initial density matrix ρ_0.

$$O(t) = \langle \hat{O}_H(t) \rangle = \mathrm{Tr}\{\, \hat{O}_H(t)\rho_0 \,\} = \mathrm{Tr}\{\, \hat{U}(t_0, t)\hat{O}\hat{U}(t, t_0)\rho_0 \,\} \tag{7.1}$$

$\hat{U}(t, t')$ is the evolution operator of the system. It obeys the following differential equations:

$$i\frac{d}{dt}\hat{U}(t, t') = \hat{H}(t)\hat{U}(t, t'), \tag{7.2}$$

$$i\frac{d}{dt'}\hat{U}(t, t') = -\hat{U}(t, t')\hat{H}(t') \tag{7.3}$$

with the boundary condition: $\hat{U}(t, t) = \mathbb{1}$. $\hat{H}$ is the fully time dependent Hamiltonian of the system. The formal solution of theses equations reads:

$$\hat{U}(t, t') = \begin{cases} \hat{T}\exp\Big(-i\int_{t'}^{t} d\bar{t}\hat{H}(\bar{t})\Big) & t > t' \\ \hat{\bar{T}}\exp\Big(-i\int_{t'}^{t} d\bar{t}\hat{H}(\bar{t})\Big) & t < t'. \end{cases} \tag{7.4}$$

Where $\hat{T}$ is the time ordering operator which reshuffles the operators to a chronological order with earlier times to the right. $\hat{\bar{T}}$ is the anti-chronological time ordering operator, which rearranges later times to the right.
Reading the time arguments of Eq. (7.1) from left to right, one sees that the time

[1] The theory at hand is in principle able to treat any kind of time dependence, but a most general perturbation requires much more complicated numerical framework.

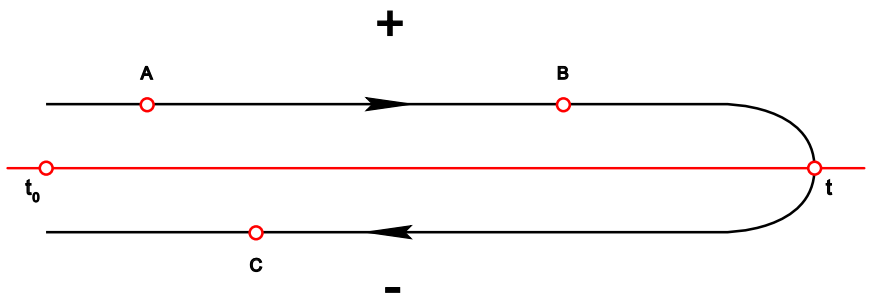

FIGURE 7.1: Illustration of the Keldysh contour: the contour starts and ends at t_0. Times are ordered in such a way that points on the lower branch (-) are always later than points on the upper branch (+), even if they are closer to t_0. In the depicted case the points $A\,B\,C$ are ordered in the following way: $A < B < C$.

evolution of the observable can be defined along a time contour which starts at t_0, propagates to t, and goes back again to t_0. Such a contour is depicted in Fig. 7.1 and is generally called Keldysh contour. On this contour the time evolution operator can be defined with the help of a time-ordering operator along the contour $\hat{T}_C$, which arranges operators according to the position on the contour. For further details see the caption of Fig. 7.1. With this the time-evolution operator can be written in the following form:

$$\hat{U}(t,t') = \hat{T}_C \exp\Big(-i \int_{t'}^{t} d\bar{t}\hat{H}(\bar{t})\Big). \tag{7.5}$$

The whole time evolution of the system can be viewed as an initial value problem. At time t_0 the system is prepared by an initial density matrix ρ_0 and then evolution is governed by Eq. (7.5). The drawback of this formulation is that in order to use it, the initial density matrix ρ_0 must be known for the complete system. In terms of the AIM this means that ρ_0 must be given for the impurity and the bath as well. In cases where the system is correlated before time t_0 and already coupled to a bath it is nearly impossible to obtain the exact expression for ρ_0. In those cases it is necessary to extend the contour in Fig. 7.1 to imaginary times as described in [100].
In the following section it will be shown how the path integral theory can be formulated along a discretized Keldysh contour.

7.2 The coherent state path integral in the Keldysh formalism

In the following an expression for the discretized action on the Keldysh contour will be deduced. The derivation will follow the formulation used in reference [101]. The partition function of a system out of equilibrium can be written in the following way:

$$Z = \mathrm{Tr}\{\,\rho_0 \hat{U}_C\,\} = \int \prod_\alpha d(c_\alpha^*, c_\alpha)\, e^{-\sum_\alpha c_\alpha^* c_\alpha} \langle -c|\rho_0 \hat{U}_C|c\rangle. \tag{7.6}$$

Here $\hat{U}_C$ is the time evolution operator along the whole contour and ρ_0 the initial density matrix. The trace over both quantities has been written in terms of coherent states, where α labels states in the occupancy number basis. The additional minus sign in front of the bra vector is a direct consequence of the anti periodicity of the fermionic operators. To end up with a discretized version of the path integral, the time evolution on the contour is split up in small time intervals Δt. This is done by inserting coherent state identity matrices at each time point on the discrete grid. The identity matrix in a coherent state representation reads

$$\mathbb{1}_k = \int \prod_\alpha d(c_{\alpha k}^*, c_{\alpha k})\, e^{-\sum_\alpha c_{\alpha k}^* c_{\alpha k}} |c_k\rangle\langle c_k|, \tag{7.7}$$

where k labels the time of the insertion. In the following the Keldysh contour is discretized using M time points. The index i labels the turning point of the tip and $\hat{U}_{\pm\Delta t}$ is an abbreviation for the time evolution operator on the time interval. For the discretized version of the partition function one gets:

$$\begin{aligned} Z = \lim_{M\to\infty} \int \prod_{k=1}^{M} \prod_\alpha d(c_{\alpha k}^*, c_{\alpha k}) e^{-\sum_\alpha c_{\alpha k}^* c_{\alpha k}} \langle -c_1|\rho_0|c_M\rangle \ldots \langle c_{i+1}|\hat{U}_{-\Delta t}|c_i\rangle \\ \times \langle c_i|\hat{U}_{+\Delta t}|c_{i-1}\rangle \ldots \langle c_2|\hat{U}_{+\Delta t}|c_1\rangle \end{aligned} \tag{7.8}$$

$$\begin{aligned} = \lim_{M\to\infty} \int \prod_{k=1}^{M} \prod_\alpha d(c_{\alpha k}^*, c_{\alpha k}) e^{-\sum_\alpha c_{\alpha k}^* c_{\alpha k}} e^{-c_1^* c_M \hat{\rho}_0} \times \cdots \times e^{c_{i+1}^* c_i + i\Delta t H(c_{i+1}^* c_i)} \\ \times e^{c_i^* c_{i-1} - i\Delta t H(c_i^* c_{i-1})} \ldots e^{c_2^* c_1 - i\Delta t H(c_2^* c_1)} \end{aligned} \tag{7.9}$$

$$iG^{-1}_{jj'} = \begin{pmatrix} -1 & & & & -\rho_0 \\ h_+ & -1 & & & \\ & h_+ & -1 & & \\ & & h_- & -1 & \\ & & & h_- & -1 \end{pmatrix}$$

EXAMPLE 7.1: Discrete version of $G^{-1}(t,t')$ on the Keldysh contour for a single non-interacting site. $h_\pm = +1 \mp iH\Delta t$

$$= \lim_{M\to\infty} \int \prod_{k=1}^{M} \prod_{\alpha} d(c^*_{\alpha k}, c_{\alpha k}) e^{i\sum_{jj'} c^*_j G^{-1}_{jj'} c_{j'}} \qquad \text{with: } j \equiv \alpha k \tag{7.10}$$

$$= \lim_{M\to\infty} \int \prod_{k=1}^{M} \prod_{\alpha} d(c^*_{\alpha k}, c_{\alpha k}) e^{iS(c^*,c)}, \tag{7.11}$$

with the following expression for iS:

$$\begin{aligned} iS(c^*,c) = &+ \Delta t \sum_{k=i+1}^{M} \Big[\sum_{\alpha} -c^*_{\alpha k} \big(\frac{c_{\alpha k} - c_{\alpha k-1}}{\Delta t} \big) + iH(c^*_{\alpha k}, c_{\alpha k-1}) \Big] \\ &+ \Delta t \sum_{k=2}^{i} \Big[\sum_{\alpha} -c^*_{\alpha k} \big(\frac{c_{\alpha k} - c_{\alpha k-1}}{\Delta t} \big) - iH(c^*_{\alpha k}, c_{\alpha k-1}) \Big] \\ &- \sum_{\alpha} c^*_{\alpha 1} \rho_0 c_{\alpha M}. \end{aligned} \tag{7.12}$$

The expression for S consists of three major parts: the first one describes the discrete time evolution backward in time along the lower branch of the contour, the second one the evolution forward, and the third one represents the boundary condition of the fermionic states. Taking the limit Δt to zero the action can be written in its continuous form:

$$\begin{aligned} Z &= \int D[c^*,c] \exp(iS[c^*,c]) \\ &= \int D[c^*,c] \exp\left(i \int_C dt \int_C dt' \Big[c^*(t) i\partial_{t'} \delta(t-t') c(t) - H\big(c^*(t), c(t')\big) \Big] \right). \end{aligned} \tag{7.13}$$

$$iG^{-1}_{jj'} = \begin{pmatrix} G^{-1}_{\text{imp}} & \hat{V} \\ \hat{V} & G^{-1}_{\text{bath}} \end{pmatrix} = \left(\begin{array}{ccc|ccc} -1 & 0 & -\rho_0^{i} & 0 & 0 & -\rho_0^{ib} \\ h_+ & -1 & 0 & v_+ & 0 & 0 \\ 0 & h_- & -1 & 0 & v_- & 0 \\ \hline 0 & 0 & -\rho_0^{bi} & -1 & 0 & -\rho_0^{b} \\ v_+ & 0 & 0 & h_+ & -1 & 0 \\ 0 & v_- & 0 & 0 & h_- & -1 \end{array}\right)$$

EXAMPLE 7.2: Example of an interaction-free two site model. The Hamiltonian is given by $H = \epsilon_i c^\dagger c + \epsilon_b b^\dagger b + (V c^\dagger b + \text{h.c.})$. In this special case the discretized action can be represented as a matrix, which is diagonal in time but non-diagonal in orbital indices. Terms in the right upper edges (red) are a direct consequence of the anti-periodic bounding conditions on the time contour. The following abbreviations have been used: $v_\pm = \mp iV\Delta\tau$, $h_\pm = +1 \mp iH\Delta t$.

Here the last equation has just a symbolical meaning. All the signs depend on the direction on the contour and the term which corresponds to the boundary condition has vanished in the continuous representation. It is important to note that the discrete formulation of Eq. (7.12) is the natural way to define the matrices when doing numerics. If we had started from the continuous action, the very important boundary term would have been missing.

In the following we will discuss the example of a non-interacting two site problem. The expression for $G^{-1}(t, t')$ is given in example 7.2. The inverse Green's function decouples into four blocks: the upper left part is the inverse Green's function of the impurity site, the lower right one the inverse Green's function of the bath site. Because the problem is totally decoupled in the inverse representation, the structure of both matrices is the same as for the single non-interacting fermionic site in example 7.1. Both blocks are then coupled via an off-diagonal block, which consists of the time dependent coherent state matrix element of the hopping amplitude.

The key quantity to perform a dual series expansion is the hybridization function $\Delta(t, t')$. To construct this quantity one has to change from a path integral representation, which

involves all bath indices, to a formulation which only involves impurity quantum numbers. This is done by integrating out the non-interacting degrees of freedom:

$$Z = \lim_{M\to\infty} \int \prod_{k=1}^{M} \prod_{\alpha} d(c_j^*, c_{j'}) e^{i \sum_{jj'} c_j^* G^{-1}_{jj'} c_{j'}} \qquad |jj' \in \text{bath and imp. indices.} \tag{7.14}$$

$$= \lim_{M\to\infty} \int \prod_{k=1}^{M} \prod_{\alpha} d(c_j^*, c_{j'}) e^{i \sum_{jj'} c_j^* [G^{-1}_{\text{imp}} - \Delta]_{jj'} c_{j'}} \qquad |jj' \in \text{imp. indices.}, \tag{7.15}$$

with the following definition for the hybridization function:

$$\Delta(t, t') = \hat{V} \hat{G}_{\text{bath}} \hat{V}^{\dagger}. \tag{7.16}$$

This formula is already known from the equilibrium case in chapter 2, but the quantities $\hat{V}$ and $\hat{G}_{\text{bath}}$ have a totally different meaning. Whereas $\hat{V}$ was a scalar in the equilibrium context, it is a fully off-diagonal time-dependent matrix in the non-equilibrium case. Consequently, example 7.2 can be understood as a recipe to calculate the hybridization function of a finite reference system: all formulas of the equilibrium case can be applied, but all involved quantities have to be replaced by their non-equilibrium counterparts, which essentially means to replace a scalar hopping parameter by a matrix with time indices. The structure of this matrix will be as described in example 7.2.
Furthermore, one can deduce some important side remarks for numerical calculation from Eq. (7.16) and example 7.2. The first one involves the structure of the time grid. In most works the grid is chosen in such a way that all points are equidistant and the number of points on the upper and lower contour is equal. This approach leads to the time step between the last point on the upper contour and the next one on the lower contour being zero. This causes a vanishing matrix element in $\hat{V}$ and leads to a singular matrix for $\Delta(t, t')$. This fact can lead to a break down of the dual theory, because an inversion of $\Delta(t, t')$ is unavoidable in some cases. This problem can be cured if an additional point at the tip of the contour is introduced, which neither belongs to the upper nor the lower contour. This additional point has no other consequences and can be treated without any further problems. An illustration of the discrete Keldysh contour is given in Fig. 7.2, the structure of a general time matrix, which depends on orbital and spin indices, is explained in Fig. 7.3.

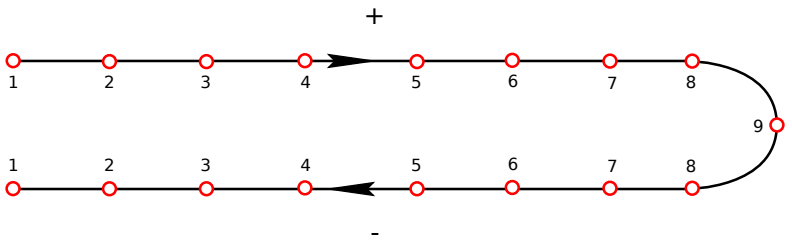

FIGURE 7.2: Illustration of the discrete Keldysh contour: All time points are equidistant. Points with the same Latin index have the same absolute time value, but the time on the lower branch is greater than the one on the upper branch. The point on the tip of the contour is essential for numerical calculations, because it reduces problems concerning singular matrices drastically.

Another issue in the inversion procedure can occur, if the off-diagonal elements ρ_0^{ib} and ρ_0^{bi} of the density matrix vanish. This happens, if the impurity is totally decoupled from the bath for times smaller than t_0. In that case $\hat{V}$ becomes also ill conditioned. This problem can be cured by introducing an infinitesimally small hopping parameter for times smaller than t_0.

7.3 Dual perturbation theory on the Keldysh contour

In this section we will generalize the dual perturbation theory to the case of non-equilibrium systems. On the one hand this derivation will be a generalization, because we will deal with time-dependent objects, on the other hand it will be less general than the equilibrium dual fermion derivation described in chapter 4, because the present derivation is limited to local problems. This section will be exclusively on the superperturbation method on the Keldysh contour only. A generalization to k-dependent problems is possible and will definitely be a future project. For a more detailed introduction to the dual theory we suggest to read chapter 4 first. In this section we will discuss differences to the equilibrium case, but general remarks to the dual theory will not be repeated. We also stick to the notation used in chapter 4. We start by writing the action of the full system:

$$S^{\mathrm{F}}[c^*, c] = \sum_{tt'} \sum_{ab} c^*_{at} [G^{-1}_{0tt'} - \Delta_{tt'}]_{ab} c_{bt'} + S^{\mathrm{NG}}[c^*, c]. \tag{7.17}$$

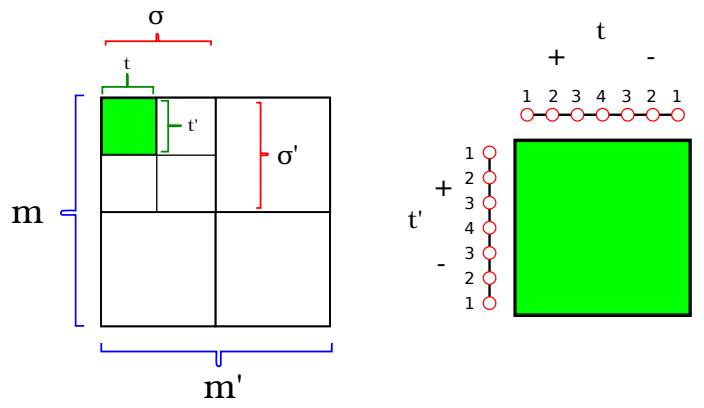

FIGURE 7.3: Structure of a discretized two times matrix on the Keldysh contour. Such a matrix normally depends on 6 indices, where the structure has been defined as follows: The outer indices m, m' are orbital quantum numbers. σ, σ' are spin degrees of freedom, which build 4×4 blocks in the orbital matrix. Each spin block consists of a t t' matrix. The composition of such a time block is depicted on the right side: each time runs along the discretized contour, first along the upper branch $(+)$, then along the lower one $(-)$. To illustrate the time labeling the unfolded contour has been included at each side of the matrix. The Latin numbers along the contour label the absolute time value of each point. Points with same index have the same absolute value, but lie on different branches of the contour. The point number 4 symbolizes the tip of the contour.

To stress that we are working on a time grid, we explicitly write the indices of the time-dependent matrices. Indices for orbital and spin degrees of freedom have been summarized in Latin letters. $S^{\mathrm{NG}}[c^*, c]$ is some local interaction. The reader should note that in the Keldysh theory the action is defined with i in the exponent like in the $T = 0$ equilibrium theory: $Z = \int D[c^*, c] \exp(iS^{\mathrm{F}}[c^*, c])$.
In the next step the hybridization of the reference system $\tilde{\Delta}_{tt'}$ is added and subtracted:

$$S^{\mathrm{F}}[c^*, c] = S^{\mathrm{Ref}}[c^*, c] + \sum_{tt'} \sum_{ab} c^*_{at} [\tilde{\Delta}_{tt'} - \Delta_{tt'}]_{ab} c_{bt'} \tag{7.18}$$

$$S^{\mathrm{Ref}}[c^*, c] = \sum_{tt'} \sum_{ab} c^*_{at} [G^{-1}_{0tt'} - \tilde{\Delta}_{tt'}]_{ab} c_{bt'} + S^{\mathrm{NG}}[c^*, c]. \tag{7.19}$$

Even though the last step seems trivial, it has some major issues, which are not apparent when looking at the formulas. One has to be aware that in the non-equilibrium case the action representation always involves boundary conditions that enter the discrete

matrices as has been shown in example 7.1 and example 7.2. When we add and subtract $\tilde{\Delta}_{tt'}$ and rewrite the action as a part, that we call reference system and a difference, we assume that both systems have the same ρ contribution on the impurity. The other parts of the density matrix are less important, because the differences in these terms will be treated perturbatively by doing an expansion in $\tilde{\Delta}_{tt'} - \Delta_{tt'}$. In the equilibrium case it was not necessary to discuss the boundary conditions of the action, because they were automatically fulfilled when working with Matsubara frequencies.
Now dual variables are introduced via a Hubbard-Stratonovich transformation. The transformation can be written in the following form:

$$e^{c_1^* n_{12} D_{23}^{-1} n_{34} c_4} = \frac{1}{\det D} \int \mathcal{D}[f^*, f] e^{-f_1^* D_{12} f_2 + f_1^* n_{12} c_2 + c_1^* n_{12} f_2} \tag{7.20}$$

with the following definitions for n and D:

$$\left.\begin{aligned} n &= i g_{12}^{-1} \\ D &= i g_{12}^{-1} [\tilde{\Delta} - \Delta]_{23}^{-1} g_{34}^{-1} \end{aligned}\right\} \rightarrow n_{12} D_{23}^{-1} n_{34} = i[\tilde{\Delta} - \Delta]_{14}. \tag{7.21}$$

After some straightforward algebra the partition function can be brought into the following form, which contains dual and c-fermions:

$$Z = \exp\left(i S^{\mathrm{Ref}}[c^*, c] + i \sum_{tt'} \sum_{ab} c_{at}^* [\tilde{\Delta} - \Delta] c_{bt'} \right) \tag{7.22}$$

$$= Z_f \exp\left(i \left\{ f_1^* [-g^{-1} (\tilde{\Delta} - \Delta)^{-1} g^{-1}]_{12} f_2 + f_1^* g_{12}^{-1} c_2 + c_1^* g_{12}^{-1} f_2 + S^{\mathrm{Ref}}[c^*, c] \right\} \right) \tag{7.23}$$

$$= Z_f \exp(i S^{\mathrm{F}}[c^*, c, f^*, f]), \tag{7.24}$$

with

$$Z_f = \det(-ig[\tilde{\Delta} - \Delta]g). \tag{7.25}$$

Analogous to the equilibrium case, the action can be split into three parts: Two parts, which contain either c-fermions or dual variables, and a part that describes the coupling of the first two and consequently contains a mixture of both variables:

$$S^{\mathrm{F}}[c^*, c, f^*, f] = S^{\mathrm{Ref}}[c^*, c] + S^{\mathrm{C}}[c^*, c, f^*, f] - f_1^* [g^{-1} (\tilde{\Delta} - \Delta)^{-1} g^{-1}]_{12} f_2, \tag{7.26}$$

with:

$$S^{\mathrm{C}}[c^*, c, f^*, f] = f_1^* g_{12}^{-1} c_2 + c_1^* g_{12}^{-1} f_2. \tag{7.27}$$

In the last equation we have combined temporal, orbital and spin indices into numbers. To integrate out the c-fermion part, the following defining equation for the dual interaction potential $\mathcal{V}$ is introduced:

$$\begin{aligned}\int \exp\big(i(S^{\mathrm{Ref}}[c_{\mathbf{i}}^*, c_{\mathbf{i}}] + S^{\mathrm{C}}[c_{\mathbf{i}}^*, c_{\mathbf{i}}, f_{\mathbf{i}}^*, f_{\mathbf{i}}])\big)\mathcal{D}[c_{\mathbf{i}}^*, c_{\mathbf{i}}] \\ \stackrel{!}{=} \mathcal{Z}_{\mathrm{Ref}} \exp\big(i(-\sum_{12} f_1^* g_{12}^{-1} f_2 + \mathcal{V}[f^*, f])\big).\end{aligned} \tag{7.28}$$

The c-fermions are integrated out by choosing the dual potential in such a way that the last equation holds. This is done by series expansion of both sides and by comparison of the different orders. For the left hand side of Eq. (7.28) we get:

$$\begin{aligned}\int \exp(i(S^{\mathrm{Ref}}[c_{\mathbf{i}}^*, c_{\mathbf{i}}] + S^{\mathrm{C}}[c_{\mathbf{i}}^*, c_{\mathbf{i}}, f_{\mathbf{i}}^*, f_{\mathbf{i}}]))\mathcal{D}[c_{\mathbf{i}}^*, c_{\mathbf{i}}] \\ = \sum_n \langle \frac{i^n}{n!} (f_1^* g_{12}^{-1} c_2 + c_1^* g_{12}^{-1} f_2)^n \rangle_{\mathrm{Ref}}\end{aligned} \tag{7.29}$$

$$= 1 - i f_1^* g_{12}^{-1} f_2 + \frac{1}{4} g_{11'}^{-1} g_{33'}^{-1} \chi_{1'2'3'4'} g_{2'2}^{-1} g_{4'4}^{-1} f_1^* f_2 f_3^* f_4 \pm \dots \tag{7.30}$$

In order to expand the right hand side, the following ansatz for $\mathcal{V}[f^*, f]$ is chosen:

$$\mathcal{V}[f^*, f] = c_{12}^2 f_1^* f_2 + c_{1234}^4 f_1^* f_2 f_3^* f_4 + \dots . \tag{7.31}$$

Finally, the right-hand side can be brought into the following form:

$$\begin{aligned}\exp\big(i(-f_1^* g_{12}^{-1} f_2 + \mathcal{V}[f_{\mathbf{i}}^*, f_{\mathbf{i}}])\big) = 1 + i\big(-f_1^* g_{12}^{-1} f_2 + c_{12}^2 f_1^* f_2 \\ + c_{1234}^4 f_1^* f_2 f_3^* f_4 + \dots\big) - \frac{1}{2!}\big(f_1^* g_{12}^{-1} f_2 f_3^* g_{34}^{-1} f_4 + \dots\big) - \frac{i}{3!} \dots .\end{aligned} \tag{7.32}$$

Now both sides are compared order by order to fix the unknown coefficients c^{n}. One can easily see that because both sides already contain the same quadratic part, c_{12}^2 has

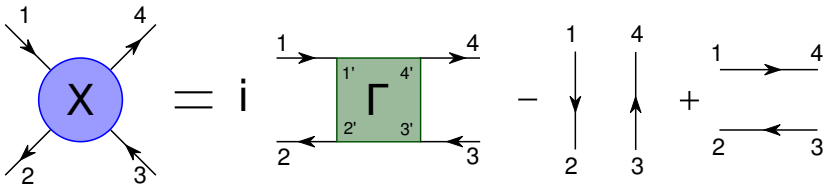

FIGURE 7.4: Composition of the two-particle Green's function. The two main building blocks are the fully irreducible vertex part and the trivial reducible part, consisting of two fermionic propagators.

to be zero. For c^4_{1234} one gets:

$$ic^4_{1234} = \frac{1}{4} g^{-1}_{11'} g^{-1}_{33'} \chi_{1'2'3'4'} g^{-1}_{2'2} g^{-1}_{4'4} + \frac{1}{2} g^{-1}_{12} g^{-1}_{34}. \tag{7.33}$$

The last term can be symmetrized:

$$\begin{aligned}
\frac{1}{2} g^{-1}_{12} g^{-1}_{34} f^*_1 f_2 f^*_3 f_4 &= \frac{1}{4} g^{-1}_{12} g^{-1}_{34} (2 f^*_1 f_2 f^*_3 f_4) && (7.34)\\
&= \frac{1}{4} g^{-1}_{12} g^{-1}_{34} (f^*_1 f_2 f^*_3 f_4 - f^*_1 f_4 f^*_3 f_2) && (7.35)\\
&= \frac{1}{4} [g^{-1}_{12} g^{-1}_{34} - g^{-1}_{14} g^{-1}_{32}] f^*_1 f_2 f^*_3 f_4 && (7.36)\\
&= \frac{1}{4} g^{-1}_{11'} g^{-1}_{33'} (g_{1'2'} g_{3'4'} - g_{1'4'} g_{3'2'}) g^{-1}_{2'2} g^{-1}_{4'4}, && (7.37)
\end{aligned}$$

which leads to the following final result:

$$\begin{aligned}
c^4_{1234} &= -\frac{i}{4} g^{-1}_{11'} g^{-1}_{33'} (\chi_{1'2'3'4'} + g_{1'2'} g_{3'4'} - g_{1'4'} g_{3'2'}) g^{-1}_{2'2} g^{-1}_{4'4} && (7.38)\\
&= -\frac{i}{4} g^{-1}_{11'} g^{-1}_{33'} (\chi_{1'2'3'4'} - \chi^0_{1'2'3'4'}) g^{-1}_{2'2} g^{-1}_{4'4} && (7.39)\\
&= \frac{1}{4} \gamma_{1234}, && (7.40)
\end{aligned}$$

with

$$\chi^0_{1'2'3'4'} = g_{14} g_{32} - g_{12} g_{34}. \tag{7.41}$$

The reader should notice that in the non-equilibrium case the definition of the vertex part is different from the equilibrium case. To illustrate the differences, Fig. 7.4 shows the definition of the vertex in the Keldysh theory. The definition for the equilibrium

vertex is shown in Fig. 3.7 in Chapter 3. With the final result for the first term of the dual potential, the dual action can be written as follows:

$$S^{\mathrm{d}}[f^*, f] = f_1^*(G_0^{\mathrm{d}})_{12}^{-1} f_2 + \frac{\gamma_{1234}}{4} f_1^* f_2 f_3^* f_4 + \dots \tag{7.42}$$

with the following definition of the bare dual Green's function:

$$G_0^{\mathrm{d}} = -g[g + (\tilde{\Delta} - \Delta)^{-1}]^{-1} g. \tag{7.43}$$

Our aim is to retrieve an expression for the lowest order diagram of the dual theory on the Keldysh contour. This is done by expanding the expression for the dual Green's function in terms of the dual potential. The Green's function is defined as follows:

$$G^{\mathrm{D}} = -i \int D[f^*, f] f_1 f_2^* e^{iS^{\mathrm{d}}[f^*, f]}. \tag{7.44}$$

The action is given by $S^{\mathrm{d}}[f^*, f] = S_0^{\mathrm{D}}[f^*, f] + \mathcal{V}[f^*, f]$, so that the lowest order of the Green's function reads:

$$G^{\mathrm{D}} \approx G_0^{\mathrm{D}} - i \int f_1 f_2^* i\mathcal{V} e^{iS_0^{\mathrm{D}}} D[f^*, f] \tag{7.45}$$

$$= G_0^{\mathrm{D}} + \int f_1 f_2^* \frac{\gamma_{1'2'3'4'}}{4} f_{1'}^* f_{2'} f_{3'}^* f_{4'} e^{iS_0^{\mathrm{D}}} D[f^*, f]. \tag{7.46}$$

The integral is solved via Wick theorem. Summation over all 4 contractions yields in the final result:

$$G_{12}^{\mathrm{D}} \approx G_{012}^{\mathrm{D}} - i\gamma_{1'2'3'4'} G_{011'}^{\mathrm{D}} G_{02'2}^{\mathrm{D}} G_{04'3'}^{\mathrm{D}}. \tag{7.47}$$

A graphical interpretation of latter equation in terms of diagrams is shown in Fig. 7.5. After calculating an approximation to the dual propagator the result can be exactly transformed back to c-fermions using the following expression:

$$G = (\tilde{\Delta} - \Delta)^{-1} + [g(\tilde{\Delta} - \Delta)]^{-1} G^d [(\tilde{\Delta} - \Delta) g]^{-1} \tag{7.48}$$

Here g is the Green's function in terms of c-fermions and g^d the dual propagator. A derivation of this relation can be found in appendix A.

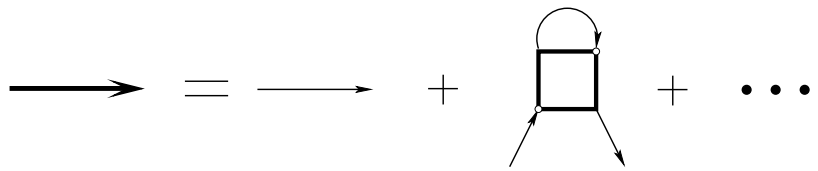

FIGURE 7.5: Illustration of the lowest order contributions to the Keldysh Green's function: The full dual propagator can be approximated by the bare dual propagator plus the first diagram with external lines.

7.4 Calculating one and two particle Green's function in the exact diagonalization scheme

In the last section it has become clear that the key ingredients to construct the superperturbation theory are the one and two particle Green's function of the reference system. In the following we will give the formulas of those quantities in the Lehmann representation. We start with the one particle Green's function. This quantity depends on two times and two indices:

$$G_{\alpha\beta}(t,t') = -i\langle T_C c_\alpha(t) c_\beta^\dagger(t')\rho_0\rangle. \tag{7.49}$$

To derive the spectral representation, identity matrices are inserted between the operators, and the time-evolution operator is written in its diagonal form:

$$\begin{aligned} G_{\alpha\beta}(t,t') = \frac{1}{Z}\sum_{o,i,j,k} & - i\langle o|i\rangle\langle i|c_\alpha|j\rangle\langle j|c_\beta^\dagger|k\rangle\langle k|o\rangle e^{-\beta E_o} e^{i[E_i t + E_j(t'-t) - E_k t']}\cdot\theta_C(t-t') \\ & + i\langle o|i\rangle\langle i|c_\beta^\dagger|j\rangle\langle j|c_\alpha|k\rangle\langle k|o\rangle e^{-\beta E_o} e^{i[E_i t' + E_j(t-t') - E_k t]}\cdot\theta_C(t'-t). \end{aligned} \tag{7.50}$$

Here $|o\rangle$ labels the eigenvectors of the auxiliary Hamiltonian H_0, which describes the system before the perturbation at t_0. Z is the partition function corresponding to the density matrix ρ_0. t and t' are times on the Keldysh contour, which means that the

theta functions are defined as follows:

$$\theta_C(t'-t) = \begin{cases} 0 & \text{if } t > t' \\ 1 & \text{if } t < t', \end{cases} \tag{7.51}$$

where the relation symbols order the times along the contour, as explained in Fig. 7.1. The formal definition of the two particle Green's function is given by the following expression:

$$\chi_{\alpha\beta\gamma\delta}(t_1,t_2,t_3,t_4) = \langle T_C c_\alpha(t_1) c^\dagger_\beta(t_2) c_\gamma(t_3) c^\dagger_\delta(t_4) \rho_0 \rangle \tag{7.52}$$

$$= \langle T_C O_1 O_2 O_3 O_4 \rho_0 \rangle. \tag{7.53}$$

Here it was necessary to introduce abbreviations for the operators, in order to rewrite the time-ordered product as sum over all possible permutations multiplied by a theta function in the four time arguments:

$$\begin{aligned} \chi_{\alpha\beta\gamma\delta}(t_1,t_2,t_3,t_4) = & \sum_{\pi\in S_n} (-1)^\pi \theta_C(t_{\pi_1} > t_{\pi_2} > t_{\pi_3} > t_{\pi_4}) \\ & \times \sum_{o,i,j,k,l,m} \langle o|i\rangle\langle i|O_{\pi_1}|j\rangle\langle j|O_{\pi_2}|k\rangle\langle k|O_{\pi_3}|l\rangle\langle l|O_{\pi_4}|m\rangle\langle m|o\rangle \\ & \times e^{i[E_i(t_{\pi_1}) + E_j(t_{\pi_2}-t_{\pi_1}) + E_k(t_{\pi_3}-t_{\pi_2}) + E_l(t_{\pi_4}-t_{\pi_3}) + E_m(-t_{\pi_4})]} \\ & \times e^{-\beta E_o}/Z. \end{aligned} \tag{7.54}$$

The reader should notice that for a given time combination only one permutation contributes to the final result. This situation is quite different from the equilibrium case where an explicit summation over all permutations was required to obtain a representation of the two-particle Green's function on Matsubara frequencies.

Numerical considerations Even though the formulas for the spectral representations look quite simple, their numerical evaluation is a challenging task. In the following we would like to describe where the numerical difficulties arise in comparison to the equilibrium case.

The most apparent issue is that the numerical description of time-dependent phenomena

requires the discretization of a formal continuous time argument. By choosing a finite time step Δt, a discretion error is introduced to the problem. To overcome this issue, it is necessary to perform the limit Δt to zero. Consequently several calculations for different grid sizes have to be performed in order to do an extrapolation to the continuous time limit. Additionally, there is no cyclic invariance on the real time axis. Consequently, all quantities depend on one more time argument than in the equilibrium theory. The Green's function is a matrix in two times and the two particle Green's function depends on four times. The combination of the systematic discretization errors and the additional time argument leads to large time matrices, which need a great amount of computer memory. In the case of the two particle Green's function the demand on computer memory is so huge that it can not be stored on a VLM[2] machine with 250 Gb memory. If the two particle Green's function is required during a simulation, it has to be recalculated each time. In the equilibrium case the numerical effort is by far smaller. All quantities depend on less time arguments and there exists a natural discretization of the problem: the Matsubara formalism. Matsubara frequencies are by construction discrete and in most cases the calculation of a few function values on small frequencies is enough because the high energy tail only contains trivial information.

Furthermore, the computation of a Green's function matrix element for a given time combination is more expensive in the non-equilibrium case than in the equilibrium one. Because the expectation value is constructed as a trace over the initial density matrix, two more identity matrices have been inserted in the spectral representation of the one and two particle Green's function. In the equilibrium case the calculation of the single particle Green's function requires a loop over N^2 indices, where N is the dimension of the Hilbert space. The same calculation in a non-equilibrium situation requires a loop over N^4 indices.

Because of the numerical requirements of a non-equilibrium simulation, the developed computer code has been highly optimized. It contains all optimizations mentioned in section 3.1.2 and has been additionally improved by precalculating all non-zero matrix elements of the two particle Green's function in Eq. (7.54). This procedure makes the calculation of the vertex part very efficient during the computation of the first diagram. Nevertheless, all simulations were highly demanding and it was necessary to parallelize

[2]VLM- Very Large Memory.

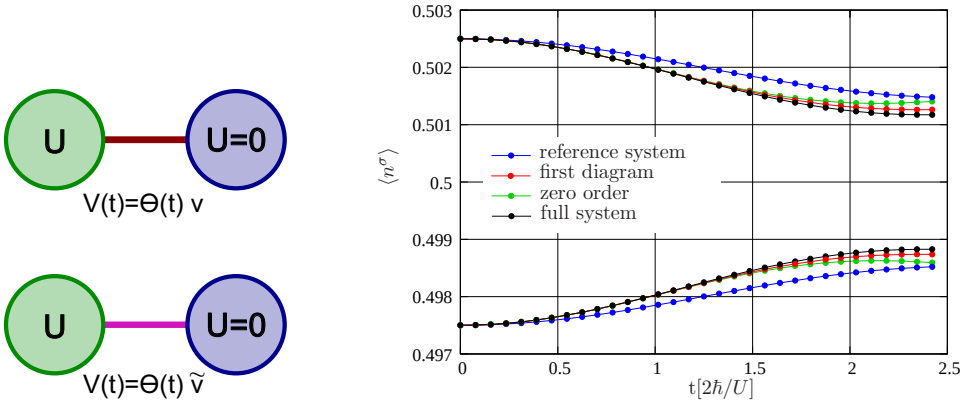

FIGURE 7.6: First test of the superperturbation method on the Keldysh contour. (a) the model under consideration consists of one interacting site coupled to one bath site (upper left picture). The time dependence consists of a sudden switch in the hopping amplitude from an infinitesimally small value to a non-zero one. The reference system is prepared in the same way, but the hopping is switched to a lower value (lower left picture). (b) Plot of $n^\sigma(t)$ for the full system, the reference system and different degrees of approximation. The zero-order curve corresponds to a dual theory without any diagram, the first-order curve to a solution including the first diagram. Both curves are shifted from the reference solution towards the exact result. The data points corresponding to the solution with the first diagram are in good agreement with the solution of the full system. The calculations have been done for the following parameters: $\beta = 5$, $U = 2$, $v = 0.5$, $\tilde{v} = 0.4$, $B = 0.001$.

the code. The following results were obtained on a machine with 32 processors and 250 GB RAM. The total computation time was of the order of 24 hours for a single task.

7.5 A first test

As a first test the time evolution of an exactly solvable model was calculated. Figure 7.6(a) shows the model under consideration. The full system consists of an interacting site coupled to one additional bath site. At time t_0 the system is prepared in such a way that both sites are half filled and the spin degeneracy on the interacting site is lifted via a small magnetic field. Both sites are coupled with an infinitesimally small coupling. The time dependence of the full system consists of a sudden switch in the hopping amplitude

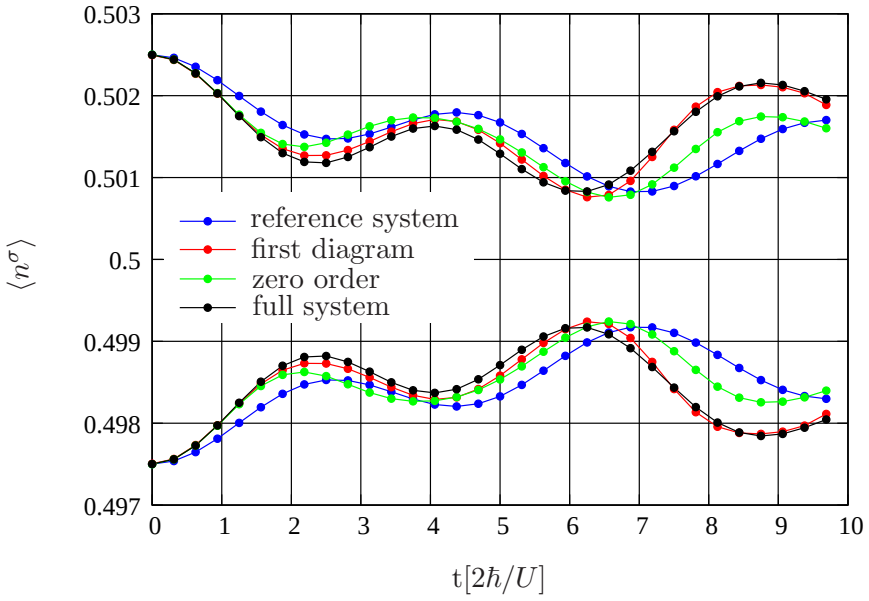

FIGURE 7.7: The plot shows the same calculation as in Fig. 7.6(b), but for longer times.

to a non-zero value.

The reference system, which is used as a starting point for the perturbation expansion, is modeled in the same way, but the hopping is switched to a different value. Fig. 7.6(b) shows the time dependence of the occupation number on the interacting site for small times. The black dotted curve is the exact time evolution of the full system, the blue curve is the time evolution of the reference system. The green and red data points show different expansion orders in the dual potential. The green points correspond to a dual theory without any diagram, the red curve to the solution including the first diagram. As one can see, both approximations improve the solution of the reference system towards the solution of the full system and the order of the curves is as expected: The solution including the first diagram gives the best improvement. Fig. 7.7 shows the time evolution of the system for longer times. The superperturbation theory remains in quite good agreement with the exact result.

To overcome the systematic discretization error in the time argument, several simulations for different grid sizes have been performed and the limit to a continuous time

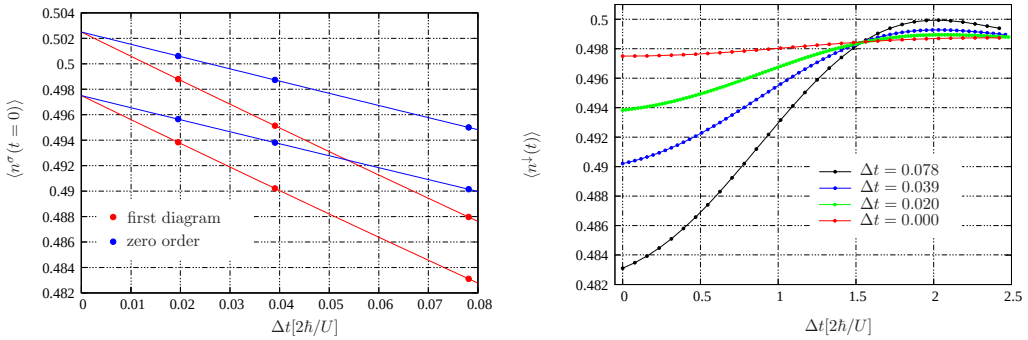

(a) (b)

FIGURE 7.8: Dependence of the grid size on the final result. (a) Regression curve for the $n^\sigma(t=0)$ point of Fig. 7.7. In this case a quadratic regression has been performed. (b) Plot of $n^\sigma(t)$ for different Δt. The dependence of the result on Δt is quite strong. The reason for this behavior is that the effect of the initial magnetic field is very small, so that a high precession in the final result is needed to see the small effect.

variable has been done numerically by quadratic regression. The final result can be expanded into a Taylor series in Δt around the continuous solution:

$$n^\sigma(t,\Delta t)|_{\Delta t=0} \approx n^\sigma(t,0) + a\cdot\Delta t + b\cdot(\Delta t)^2 \pm \ldots. \tag{7.55}$$

The three constants a, b and the solution for a continuous time, $n^\sigma(t,0)$, have been calculated by quadratic regression. The procedure is depicted in Fig. 7.8(a) for the time point $t=0$. Here the dependence on Δt is almost linear, but the quadratic regression was necessary to resolve the effect of the small initial magnetic field. The differences in $n^\downarrow(t)$ for different Δt are shown in Fig. 7.8(b).

7.6 Outlook

In this chapter it has been demonstrated that the dual perturbation theory is general enough to treat time dependent phenomena. Illustrated for the superperturbation method it was shown, that all formulas can be generalized in terms of the Keldysh formalism.

The presented work has many possibilities for future generalizations and extensions.

As indicated in Chapter 4, it is possible to generalize the described theory to treat k-dependent lattice problems like in the VLA approach. To do so, it is necessary to formulate the VLA on the Keldysh contour and to include at least the first two diagrams into the dual self-energy, because an approximation including only the first diagram will still be local. Such a scheme would be the first extension of the DMFT to a non-equilibrium situation and a great breakthrough in the field.
Additionally, a great future challenge will be the description of multi-orbital systems. Here the total number of sites in the reference system is a real limitation of the approach. Even though our computer code is highly optimized, it is not possible to treat more than 4 sites in total for a long end time. The reason for this constraint is twofold: On the one hand the Hilbert space grows exponentially with the size of the reference system, on the other hand the continuous time argument requires more and more computer memory if larger end times are desired.
Both problems can be circumvented by more sophisticated numerical algorithms, which have not been implemented yet. The complication of a huge Hilbert space can be treated in a Krylov-like scheme, where the time evolution operator $\exp(-iHt)$ is approximated as described in section 3.1.3. This procedure will allow the calculation of real-time correlation functions for higher system sizes of the order of 10 sites in total. Such a solver is the topic of the ongoing diploma thesis of Nadine Weißfahl.
The continuous time argument and the accompanying discretion error can be cured by a transformation to a discrete basis set for continuous functions. This idea was first discussed in the diploma thesis of Lewin Boehnke for the equilibrium case and goes back to an idea of Olivier Parcollet. At the moment a publication is in preparation. Such a discrete basis is formed by Legendre polynomials, which are the solution of the following differential equation:

$$\frac{d}{dt}\left[(1-t^2)\frac{d}{dt}P_l(t)\right] + l(l+1)P_l(t) = 0. \tag{7.56}$$

These functions are complete on the interval $I_l = [-1, 1]$, but can also be a basis for functions on arbitrary intervals, because two intervals can be mapped on each other by a linear transformation. Figure 7.9 shows the first 6 Legendre polynomials on the interval I_l. The expansion of a function $f(t)$ in Legendre Polynomials has the following form:

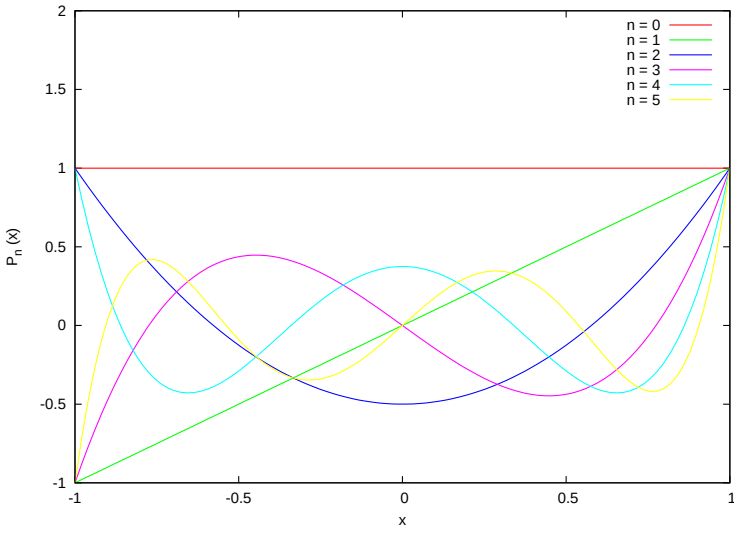

FIGURE 7.9: First 6 Legendre polynomials.

$$f(t) = \sum_{l=0}^{\infty} c_l P_l(t). \tag{7.57}$$

In which the coefficients can be calculated by the following integral:

$$c_l = \frac{2l+1}{2} \int_{-1}^{1} dt f(t) P_l(t). \tag{7.58}$$

The l dependent prefactor in front of the integral is an additional normalization factor, which is required because the polynomials are orthogonal but not orthonormal. The great advantage of the Legendre basis set is that the basis is countable by construction and no artificial discretization is needed when describing continuous functions. In this sense the Legendre basis is comparable to Matsubara frequencies, which are also discrete. The only systematic error enters at the point, where the number of Legendre polynomials is truncated in the description of a function. This kind of approximation is well known from the Matsubara case, where the high energy tail contains very low information and is normally also cut. In the Legendre case it can be shown that the expansion coefficients drop exponentially if the function under consideration is continuous. For the Keldysh Green's function this means that the matrix dimension in Legendre coefficients can be

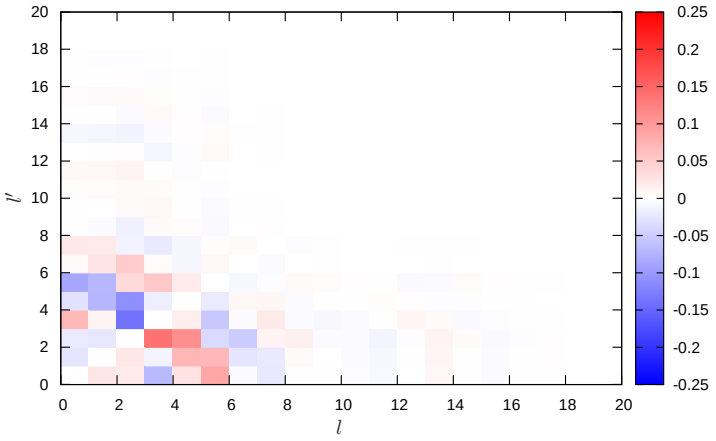

FIGURE 7.10: $+-$ block of the Keldysh Green's function in the Legendre basis. Because the $+-$ block does not contain a jump on the diagonal, the Legendre coefficients drop exponentially fast to zero.

decreased drastically in comparison to a discrete time description. In the following some preliminary results are presented. Figure 7.10 shows the real part of the $+-$ block of the Keldysh Green's function in the Legendre basis. As one can see, the absolute value of the matrix elements drops very quickly and for indices larger than 18 the matrix elements are nearly zero. The data has been calculated by directly evaluating an expression for the $+-$ Green's function in Legendre coefficients in its spectral representation:

$$G^{+-}_{\alpha\beta}(l,l') = \sum_{0,i,j,k} \langle 0|i\rangle\langle i|c^\dagger_\beta|j\rangle\langle j|c_\alpha|k\rangle\langle k|0\rangle e^{-\beta E_0} A^l_{jk} A^{l'}_{ij}. \tag{7.59}$$

The factors A^l_{jk} and $A^{l'}_{ij}$ are the Legendre coefficients of the exponential factors in Eq. (7.50). They can be easily evaluated by applying a recursion formula.

To illustrate the power of the method, the time dependence of the occupation number was extracted from the Keldysh Green's function in Legendre polynomials and compared with the exact result calculated within the Lehmann representation of the expectation value $n^\sigma(t)$. Figure 7.11 shows the results. In the upper left plot the exact time evolution (black dots) is compared with different orders of truncation in the Legendre basis. As one can see, even a small matrix size like 15×15 gives good results. The figure to the right shows a detailed zoom of the left one. The small differences in the curves for

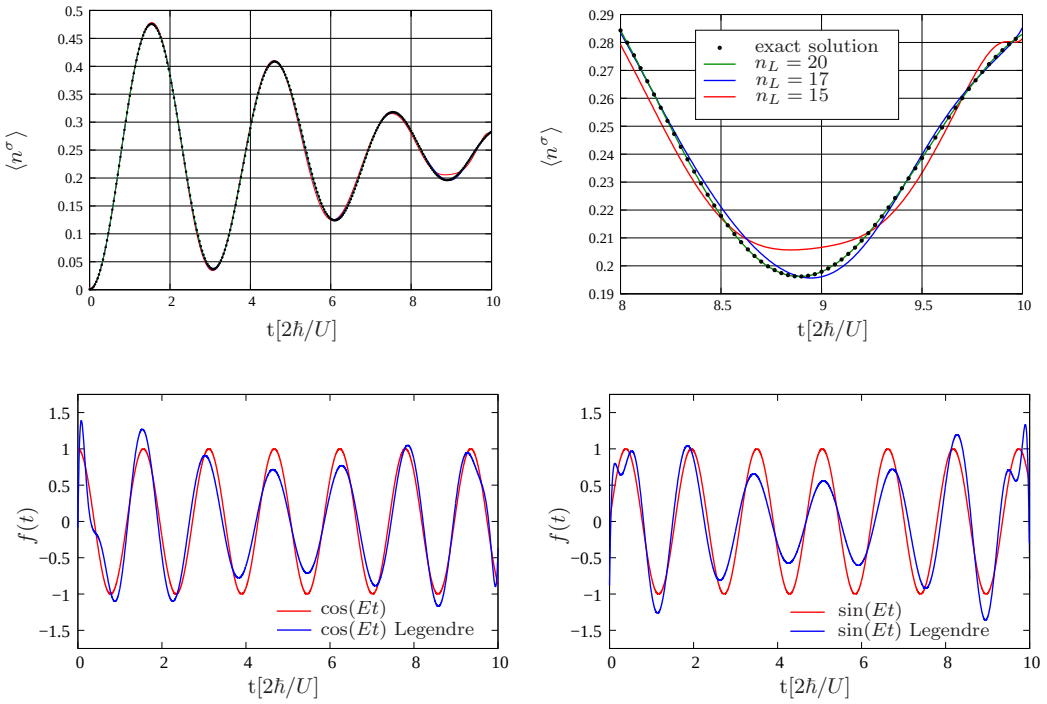

FIGURE 7.11: *upper left:* Comparison of the time evolution of the density $n(t)$, calculated in the Legendre basis for different cutoffs and transformed back, with the exact result. *upper right:* detailed view of left picture. If the number of used Legendre coefficients is larger than 20, the back transform can't be distinguished from the exact result. *lower row:* Real part and imaginary part of the exponential $\exp(iEt)$ for the largest energy difference (E = 4.03) and its representation through Legendre polynomials up to order $n_l = 20$. The maximal order is clearly insufficient for an accurate representation, even though the total Green's function is well reproduced.

different Legendre cutoffs are visible here, but a total number of 20×20 coefficients is enough to exactly describe the time evolution of the system. If the time argument would have been discretized in the standard way, the matrix would have been of the order 120×120. The absolute memory gain is enormous.

The surprising thing about the expansion in Legendre polynomials is that even though the Green's function can be described by a few coefficients, these coefficients are not sufficient to model every exponential factor in the standard spectral representation in Eq. (7.50) up to the same precession one is able to reach for the total Green's function. The figures in the lower row show the time evolution for the exponential $\exp(iEt)$ with

the highest Energy in the test system. As one can see the deviation from its Legendre representation is quite large, even though the whole Green's function is well described by the same number of coefficients. This implies that the transformation to the Legendre basis set works as some kind of filter, which is able to exclude the effect of high frequency contributions to the final result.

Up to now, only the $+-$ block of the single particle Green's function has been calculated using its spectral representation in Legendre polynomials. A generalization to the Green's function on the whole contour is still needed, but it is in principle no problem. One issue might be that the whole Green's function includes discontinuities on the diagonal, which are caused by the anti-commuting behavior of the fermionic operators. It is well known that the description of such a jump in terms of a Legendre basis can increase the number of needed coefficients, but is still possible on a modern computer. One might argue that the representation of the Green's function in the Legendre basis including the jump on the diagonal might be as complicated as working with the discretized scheme introduced at the beginning of the chapter. But the opposite is the case: The real performance gain will not be the storage of the single particle Green's function, but the evaluation of the first diagram. This calculation involves the computation of the vertex, which has no discontinuity, because the jumps of the two particle Green's function cancel out with those of the trivial part. This implies that the the sum over the fermion loop in the first diagram can be accomplished with exponentially few coefficients, which is an enormous speed gain in comparison to the standard discretization described in this chapter.

Chapter 8

Conclusions

The intention of this thesis was to generalize the dual fermion approach to a broader scope. Therefore, several new algorithms for the treatment of strongly correlated systems have been introduced. The key idea of all these new methods is to approximate a large interacting fermionic system by a smaller exactly solvable system, which has been optimized for the physical situation at hand. The dual perturbation theory then allows to formulate a series expansion around this reference system. Because the reference system itself already contains much of the essential physics, this kind of perturbative approximation is better suited for the investigation of phase transitions than standard perturbation theories such as the weak- or strong-coupling expansion.
In the second chapter the prototype of such a reference system, the Anderson impurity model, was introduced. Despite of its zero-dimensional character, the model is able to describe rich physics, because local quantum fluctuations are fully taken into account. A very important application of the AIM, the DMFT, is reviewed at the end of the chapter.
The success of the AIM as a starting point for the investigation of strongly correlated systems is based on the availability of a huge number of very efficient solvers for the model. In the third chapter we therefore discuss the technical basis of the dual approach: efficient impurity solvers. A brief review of the exact diagonalization and several quantum Monte Carlo approaches is given.
In order to demonstrate that all approaches described in this thesis are based on the

same fundamental idea, we gave a general derivation of the dual fermion approach for the equilibrium case in chapter 4. Based on this derivation the differences between all described schemes have been discussed.

The first example, the superperturbation solver for the Anderson impurity model, has been discussed in chapter 5. Here an impurity problem with a continuous energy spectrum in the bath is approximated by a discrete reference system, which can be solved using exact diagonalization. It was shown that the SPERT is exact in the weak- and strong-coupling regime and additionally allows to converge exponentially fast to the exact result by increasing the number of bath sites. Based on an investigation of the Kondo problem, it was shown that a Kondo like peak can be found in the lowest order approximation by taking into account just a single bath site. A comparison with NRG results revealed that although a quasi-particle peak at the Fermi level can be reproduced, the typical exponential scaling of the Kondo temperature is not reproduced by this lowest order approximation. Nevertheless, a good description of the singlet formation in the magnetic susceptibility at low temperatures was obtained, if the reference system itself has a singlet ground state.

Additionally, it was shown that the approach allows to directly calculate the density of states on the real axis. A non-causality problem, which forms at low temperatures in the vicinity of poles in the reference system, was alleviated by generalizing a recently developed renormalization scheme. Furthermore, a first multi orbital test calculation was presented.

An efficient approximation for correlated lattices, the variational lattice approach has been introduced in Chapter 6. In this case the reference system is also given by a discrete Anderson impurity problem. In comparison to the CTQMC implementation, the VLA offers a much more efficient numerical treatment of correlated lattices. Applying this scheme it was possible to determine the phase diagram of the Mott metal-insulator transition in two dimensions. In comparison to an earlier CDMFT study on a 4 site plaquette it was shown that the critical U is increased from $U_C^{\mathrm{CDMFT}} = 6.05$ to $U_C^{\mathrm{VLA}} = 6.4 \pm 0.1$. The reason for this increase is that the VLA takes into account long-ranged spatial correlations, which break the perfect singlet formation, which is possible in the CDMFT on a plaquette. Since the results of the VLA contain no stochastic noise, the approach offers the possibility to perform an analytic continuation using Padé. Applying this technique

it was possible to show that the pseudogap opens directly on the Fermi surface in the bad metal regime. A high resolution analysis of the band structure has not been possible in the standard CTQMC implementation of dual fermion, because of the insufficient resolution of MAXENT.
At the end of the thesis it was demonstrated that the dual fermion ansatz is not limited to the equilibrium case. In chapter 7 the method was generalized to non-equilibrium phenomena by formulating the theory in the Keldysh framework. Taking the superperturbation as an example, it was shown that the method is numerically feasible and first benchmark calculations have been presented. At the end of the chapter a possible extension in terms of Legendre polynomials has been discussed.

Summarizing the results of the previous chapters, we have demonstrated that the dual fermion approach is a fairly general method and can be interpreted as a kind of superperturbation theory. Here "super" means that the perturbation expansion is performed around a non-trivial exactly solvable starting point.
In principle, for all presented approaches two possible extensions are imaginable: An improvement of the exact diagonalization impurity solver or an extension of the order of dual diagrams taken into account. The first improvement would allow to extend the described approaches to the investigation of multi-orbital system. In order to do this a formulation involving a Krylov solver would be necessary but could be accomplished very easily. The second generalization, an increase in dual diagrams, could be applied in cases, where an increase in the number of bath sites does not suffice. Such a case is the investigation of the Kondo scaling. Here a FLEX or Parquet approach would be useful. The method with the widest future applicability is the superperturbation solver for the non-equilibrium case. Because other solvers suffer from great drawbacks, such as the dynamic phase problem, the SPERT could be of great help in this fast developing field of physics.

Appendix A

Connection between G^{d} and G

In this section an exact relation between the dual Green's function for f-fermions and its counterpart for c-fermions is established in terms of the Keldysh formalism. To derive this connection, we start by introducing a differential identity for the c-Green's function. This is done by revisiting the exact relation between the action formulation in dual and c-space:

$$Z = \int \exp(iS^{\mathrm{F}}[c^*, c])D[c^*, c] = Z_f \int \exp(iS^{\mathrm{F}}[f^*, f, c^*, c])D[f^*, f, c^*, c], \tag{A.1}$$

with $Z_f = \det[-ig(\tilde{\Delta} - \Delta)g]$. Now the lefthand site of latter equation is written in its full form and the term $\Delta^{ab}_{tt'}$ is reinterpreted as a source field.

$$Z = \int D[c^*, c] \exp\left(i\left\{ \sum_{tt'} \sum_{ab} c^*_{at}[(G^0_{tt'})^{-1} - \Delta_{tt'}]_{ab} c_{bt'} + S^{\mathrm{NG}} \right\}\right). \tag{A.2}$$

A functional differentiation with respect to $\Delta^{ab}_{tt'}$ yields:

$$\frac{\delta Z[\Delta]}{\delta \Delta_{ab}} = \frac{\delta}{\delta \Delta_{ab}} \int D[c^*, c] \exp(iS^{\mathrm{F}}[c^*, c]) \tag{A.3}$$

$$= -i \int D[c^*, c] c^*_a c_b \exp(iS^{\mathrm{F}}[c^*, c]) \tag{A.4}$$

$$= -Z g_{ba}. \tag{A.5}$$

The desired connection for the c-Green's function is consequently given by:

$$g = -\frac{1}{Z}\frac{\delta Z[h]}{\delta \Delta}. \tag{A.6}$$

To derive a functional connection between the dual Green's function g^d and g the differential operator $-1/Z(\delta/\delta\Delta)$ is applied to the righthand site of eq. (A.1). Special attention has to be given to Z_f, which also contains Δ:

$$-\frac{1}{Z}\frac{\delta Z}{\delta \Delta} = -\frac{1}{Z}\Bigg[\underbrace{\frac{\delta Z_f}{\delta \Delta}\frac{Z}{Z_f}}_{\mathrm{A}} + \underbrace{Z_f \frac{\delta}{\delta \Delta}\left(\frac{Z}{Z_f}\right)}_{B}\Bigg], \tag{A.7}$$

with $Z/Z_f = \int \exp(iS^{\mathrm{D}}[c^*, c, f^*, f])D[c^*, c, f^*, f]$. In the next step the quantities A and B are evaluated. For the computation of A the following relation for the differential of a determinant is needed: $d\det(C) = \det(C)\,\mathrm{Tr}\{\, C^{-1}dC\,\}$.

$$\frac{Z_f}{Z}A_{ml} = \frac{\delta Z_f}{\delta \Delta} = \frac{\delta}{\delta \Delta_{lm}}\det(-ig(\tilde{\Delta} - \Delta)g) \tag{A.8}$$

$$= -Z_f\,\mathrm{Tr}\{\,[g^{-1}(\tilde{\Delta} - \Delta)^{-1}]_{fa'}g^{-1}_{a'b'}g_{b'b}\frac{\delta \Delta_{bc}}{\delta \Delta_{lm}}g_{cd}\,\} \tag{A.9}$$

$$= -Z_f[g^{-1}(\tilde{\Delta} - \Delta)^{-1}]_{fb}\frac{\delta \Delta_{bc}}{\delta \Delta_{lm}}g_{cf} \tag{A.10}$$

$$= -Z_f g^{-1}_{ff'}[(\tilde{\Delta} - \Delta)^{-1}]_{f'l}g_{mf} \tag{A.11}$$

$$= -Z_f(\tilde{\Delta} - \Delta)^{-1}_{ml} \tag{A.12}$$

The second term can be elaborated with an expression for the derivative of an inverse matrix: $\partial A^{-1}/\partial a_{lm} = -A^{-1}\partial A/\partial a_{lm}A^{-1}$.

$$B_{ml} = Z_f\frac{\delta}{\delta \Delta_{lm}}\iint D[f^*, f, c^*, c]\exp(iS^{\mathrm{Ref}} + iS^{\mathrm{SC}} + if_1^*[-g^{-1}(\tilde{\Delta} - \Delta)^{-1}g^{-1}])_{12}f_2 \tag{A.13}$$

$$= Z_f\iint D[f^*, f, c^*, c]\exp(iS^{\mathrm{F}})f_a^*\frac{\delta}{\delta \Delta_{lm}}\{-i[g^{-1}(\tilde{\Delta} - \Delta)^{-1}g^{-1}]_{ab}f_b\} \tag{A.14}$$

$$= Z_f\iint D[f^*, f, c^*, c]\exp(iS^{\mathrm{F}})i\{f_a^*[g^{-1}(\tilde{\Delta} - \Delta)^{-1}]_{al}[(\tilde{\Delta} - \Delta)^{-1}g^{-1}]_{mb}f_b\} \tag{A.15}$$

$$= -Z(\tilde{\Delta} - \Delta)^{-1} g^{-1} g^d g^{-1} (\tilde{\Delta} - \Delta)^{-1} \tag{A.16}$$

$$= -Z\Big[g(\tilde{\Delta} - \Delta)]^{-1} g^d [(\tilde{\Delta} - \Delta)g]^{-1}\Big]_{ml} \tag{A.17}$$

If the reults for A and B are inserted back in Eq. (A.7) one yields in the desired connection between the dual and the c-Green's funtion:

$$g = (\tilde{\Delta} - \Delta)^{-1} + [g(\tilde{\Delta} - \Delta)]^{-1} g^d [(\tilde{\Delta} - \Delta)g]^{-1} \tag{A.18}$$

Bibliography

[1] P. W. Anderson. Localized magnetic states in metals. *Physical Review*, 124(1): 41–&, 1961.

[2] A. C. Hewson. *The Kondo Problem to Heavy Fermions*. Cambridge Studies in Magnetism, 2003.

[3] P. Werner, A. Comanac, L. de' Medici, M. Troyer, and A. J. Millis. Continuous-time solver for quantum impurity models. *Physical Review Letters*, 97(7), 2006.

[4] A. N. Rubtsov and A. I. Lichtenstein. Continuous-time quantum monte carlo method for fermions: Beyond auxiliary field framework. *Jetp Letters*, 80(1):61–65, 2004.

[5] M. Caffarel and W. Krauth. Exact diagonalization approach to correlated fermions in infinte dimensions - mott transition and superconductivity. *Physical Review Letters*, 72(10):1545–1548, 1994.

[6] A. Georges, G. Kotliar, W. Krauth, and M. Rozenberg. Dynamical mean-field theory of strongly correlated fermion systems and the limit of infinite dimensions. *Reviews of Modern Physics*, 68(1):13–125, 1996.

[7] A. I. Lichtenstein and M. I. Katsnelson. Ab initio calculations of quasiparticle band structure in correlated systems: Lda++ approach. *Physical Review B*, 57 (12):6884–6895, 1998.

[8] K. Held. Electronic structure calculations using dynamical mean field theory. *Advances In Physics*, 56(6):829–926, 2007.

[9] G. Kotliar, S. Y. Savrasov, K. Haule, V. S. Oudovenko, O. Parcollet, and C. A. Marianetti. Electronic structure calculations with dynamical mean-field theory. *Reviews of Modern Physics*, 78(3):865–951, 2006.

[10] W. Metzner and D. Vollhardt. Correlated lattice fermions in d=infinity dimensions. *Physical Review Letters*, 62(3):324–327, 1989.

[11] T. Maier, M. Jarrell, T. Pruschke, and M. H. Hettler. Quantum cluster theories. *Reviews of Modern Physics*, 77(3):1027–1080, 2005.

[12] H. A. Bethe. Statistical theory of superlattices. *Proceedings of the Royal Society of London. Series A, Mathematical and Physical Sciences*, 150(871):552–575, 1935.

[13] C. Lanczos. An iteration method for the solution of the eigenvalue problem of linear differential and integral operators. *J. Res. Nat. Bur. Standards*, 45(4):255–282, 1950.

[14] S. Yamada, T. Imamura, and M. Machida. 16.447 tflops and 159-billion-dimensional exact-diagonalization for trapped Fermion-Hubbard model on the Earth Simulator. In *Proceedings of the 2005 ACM/IEEE conference on Supercomputing*, page 44. IEEE Computer Society, 2005.

[15] B. Gough. *GNU Scientific Library Reference Manual - Third Edition*. Network Theory Ltd., 2009.

[16] E. Koch, G. Sangiovanni, and O. Gunnarsson. Sum-rules and bath-parametrization for quantum cluster theories. *Phys. Rev. B*, 78(11):115102, 2008.

[17] W. H. Press. *Numerical recipes in C*. Cambridge University Press, 2nd ed., v2.0 edition, 1992.

[18] A. Ralston and P. Rabinowitz. *A first course in numerical analysis*. Dover Publications, Mineola, NY, 2nd ed edition, 2001.

[19] J. Stoer and R. Bulirsch. *Introduction to numerical analysis*, volume 12. Springer, New York, 3rd ed edition, 2002.

[20] E. Anderson, Z. Bai, C. Bischof, S. Blackford, J. Demmel, J. Dongarra, J. Du Croz, A. Greenbaum, S. Hammarling, A. McKenney, and D. Sorensen. *LAPACK Users' Guide*. Society for Industrial and Applied Mathematics, Philadelphia, PA, third edition, 1999.

[21] C. Moler and C. Van Loan. Nineteen dubious ways to compute the exponential of a matrix, twenty-five years later. *Siam Review*, 45(1):3–49, 2003.

[22] M. Hochbruck and C. Lubich. On krylov subspace approximations to the matrix exponential operator. *Siam Journal On Numerical Analysis*, 34(5):1911–1925, 1997.

[23] A. M. Laeuchli and P. Werner. Krylov implementation of the hybridization expansion impurity solver and application to 5-orbital models. *Physical Review B*, 80(23), 2009.

[24] D. P. Landau and K. Binder. *A guide to Monte-Carlo simulations in statistical physics*. Cambridge University Press, Cambridge, 2009.

[25] W. von der Linden. A quantum Monte Carlo approach to many-body physics. *Physics Reports*, 220:53 – 162, 1992.

[26] D. M. Ceperley. Path integrals in the theory of condensed helium. *Rev. Mod. Phys.*, 67:279–355, 1995.

[27] W. M. C. Foulkes, L. Mitas, R. J. Needs, and G. Rajagopal. Quantum Monte Carlo simulations of solids. *Rev. Mod. Phys.*, 73:33–83, 2001.

[28] Z. E. Dell and S. V. Franklin. The buffon-laplace needle problem in three dimensions. *Journal of Statistical Mechanics-Theory and Experiment*, 2009.

[29] I. Abbas, J. Rovira, and J. CasanovaS. Clinical trial optimization: Monte carlo simulation markov model for planning clinical trials recruitment. *Contemporary Clinical Trials*, 28(3):220–231, 2007.

[30] B. L. Hammond, W. A. Lester, and P. J. Reynolds. *Monte Carlo methods in ab initio quantum chemistry*, volume v. 1. World Scientific, Singapore, 1994.

[31] C. Z. Mooney. *Monte Carlo simulation*, volume no. 07-116. Sage Publications, Thousand Oaks, Calif., 1997.

[32] R. E. Bellman. *Dynamic programming*. Princeton University Press, Princeton, 1957.

[33] J. W. Negele and H. Orland. *Quantum many-particle systems*. Perseus Books, Reading, MA, 1998.

[34] M. Troyer and U. J. Wiese. Computational complexity and fundamental limitations to fermionic quantum monte carlo simulations. *Physical Review Letters*, 94(17), 2005.

[35] A. A. Markov. Classical text in translation - an example of statistical investigation of the text eugene onegin concerning the connection of samples in chains. *Science In Context*, 19(4):591–600, 2006.

[36] N. Metropolis, A. W. Rosenbluth, M. N. Rosenbluth, A. H. Teller, and E. Teller. Equation of state calculations by fast computing machines. *Journal of Chemical Physics*, 21(6):1087–1092, 1953.

[37] W. K. Hastings. Monte-carlo sampling methods using markov chains and their applications. *Biometrika*, 57(1):97–&, 1970.

[38] J. E. Hirsch and R. M. Fye. Monte-carlo method for magnetic-impurities in metals. *Physical Review Letters*, 56(23):2521–2524, 1986.

[39] M. Jarrell. Hubbard-model in infinite dimensions - a quantum monte-carlo study. *Physical Review Letters*, 69(1):168–171, 1992.

[40] K. Held, A. K. McMahan, and R. T. Scalettar. Cerium volume collapse: Results from the merger of dynamical mean-field theory and local density approximation. *Physical Review Letters*, 87(27), 2001.

[41] M. I. Katsnelson and A. I. Lichtenstein. First-principles calculations of magnetic interactions in correlated systems. *Physical Review B*, 61(13):8906–8912, 2000.

[42] A. I. Lichtenstein, M. I. Katsnelson, and G. Kotliar. Finite-temperature magnetism of transition metals: An ab initio dynamical mean-field theory. *Physical Review Letters*, 87(6), 2001.

[43] J. E. Hirsch. Discrete hubbard-stratonovich transformation for fermion lattice models. *Physical Review B*, 28(7):4059–4061, 1983.

[44] J. E. Hirsch. Erratum: Discrete hubbard-stratonovich transformation for fermion lattice models. *Phys. Rev. B*, 29(7):4159, 1984.

[45] H. F. Trotter. On the product of semi-groups of operators. *Proceedings of the American Mathematical Society*, pages 545–551, 1959.

[46] M. Suzuki. Relationship between d-dimensional quantal spin systems and (d+ 1)-dimensional ising systems—equivalence, critical exponents and systematic approximants of the partition function and spin correlations—. *Progress of Theoretical Physics*, 56(5):1454–1469, 1976.

[47] J. Sherman and W. J. Morrison. Adjustment of an inverse matrix corresponding to a change in one element of a given matrix. *Annals of Mathematical Statistics*, 21(1):124–127, 1950.

[48] N. Blumer. Numerically exact green functions from hirsch-fye quantum monte carlo simulations, 2007.

[49] N. Blumer. Multigrid hirsch-fye quantum monte carlo method for dynamical mean-field theory. 2008.

[50] J. Yoo, S. Chandrasekharan, R. K. Kaul, D. Ullmo, and H. U. Baranger. On the sign problem in the hirsch-fye algorithm for impurity problems. *Journal of Physics A-Mathematical and General*, 38(48):10307–10310, 2005.

[51] A. N. Rubtsov, V. V. Savkin, and A. I. Lichtenstein. Continuous-time quantum monte carlo method for fermions. *Physical Review B*, 72(3), 2005.

[52] P. Werner and A. J. Millis. Hybridization expansion impurity solver: General formulation and application to kondo lattice and two-orbital models. *Physical Review B*, 74(15), 2006.

[53] N. V. Prokofev, B. V. Svistunov, and I. S. Tupitsyn. Exact quantum monte carlo process for the statistics of discrete systems. *Jetp Letters*, 64(12):911–916, 1996.

[54] E. Gull, P. Werner, A. Millis, and M. Troyer. Performance analysis of continuous-time solvers for quantum impurity models. *Physical Review B*, 76(23), 2007.

[55] E. Gull. *Continuous-Time Quantum Monte Carlo Algorithms for Fermions*. PhD thesis, ETH ZURICH, 2008.

[56] H. Hafermann. *Numerical Approaches to Spatial Correlations in Strongly Interacting Fermion Systems*. PhD thesis, Universiät Hamburg, 2009.

[57] H. Tasaki. The hubbard model - an introduction and selected rigorous results. *Journal of Physics-Condensed Matter*, 10(20):4353–4378, 1998.

[58] N. W. Ashcroft and N. D. Mermin. *Solid state physics*. Holt, Rinehart and Winston, New York, 1976.

[59] A. N. Rubtsov. Small parameter for lattice models with strong interaction. *Arxiv preprint cond-mat/0601333*, 2006.

[60] A. N. Rubtsov, M. I. Katsnelson, and A. I. Lichtenstein. Dual fermion approach to nonlocal correlations in the hubbard model. *Physical Review B*, 77(3), 2008.

[61] A. N. Rubtsov, M. I. Katsnelson, A. I. Lichtenstein, and A. Georges. Dual fermion approach to the two-dimensional hubbard model: Antiferromagnetic fluctuations and fermi arcs. *Physical Review B*, 79(4), 2009.

[62] H. Lee, G. Li, and H. Monien. Hubbard model on the triangular lattice using dynamical cluster approximation and dual fermion methods. *Physical Review B*, 78(20), 2008.

[63] H. Hafermann, M. Kecker, S. Brener, A. N. Rubtsov, M. I. Katsnelson, and A. I. Lichtenstein. Dual fermion approach to high-temperature superconductivity. *Journal of Superconductivity and Novel Magnetism*, 22(1):45–49, 2009.

[64] H. Hafermann, G. Li, A. N. Rubtsov, M. I. Katsnelson, A. I. Lichtenstein, and H. Monien. Efficient perturbation theory for quantum lattice models. *Physical Review Letters*, 102(20), 2009.

[65] H. Hafermann, C. Jung, S. Brener, M. I. Katsnelson, A. N. Rubtsov, and A. I. Lichtenstein. Superperturbation solver for quantum impurity models. *Epl*, 85(2), 2009.

[66] A. A. Abrikosov, L. P. Gorkov, and I. E. Dzialoshinskiĭ. *Methods of quantum field theory in statistical physics*. Dover Publications, New York, rev. english ed. edition, 1963.

[67] N. E. Bickers, D. J. Scalapino, and S. R. White. Conserving approximations for strongly correlated electron-systems - bethe-salpeter-equation and dynamics for the two-dimensional hubbard-model. *Physical Review Letters*, 62(8):961–964, 1989.

[68] N. E. Bickers and D. J. Scalapino. Conserving approximations for strongly fluctuating electron-systems .1. formalism and calculational approach. *Annals of Physics*, 193(1):206–251, 1989.

[69] N. E. Bickers and S. R. White. Conserving approximations for strongly fluctuating electron-systems .2. numerical results and parquet extension. *Physical Review B*, 43(10):8044–8064, 1991.

[70] G. Baym and L. P. Kadanoff. Conservation laws and correlation functions. *Physical Review*, 124(2):287–&, 1961.

[71] G. Baym. Self-consistent approximations in many-body systems. *Physical Review*, 127(4):1391–&, 1962.

[72] S. Brener, H. Hafermann, A. N. Rubtsov, M. I. Katsnelson, and A. I. Lichtenstein. Dual fermion approach to susceptibility of correlated lattice fermions. *Physical Review B*, 77(19), 2008.

[73] S. Pairault, D. Senechal, and A. M. S. Tremblay. Strong-coupling expansion for the hubbard model. *Physical Review Letters*, 80(24):5389–5392, 1998.

[74] S. Pairault, D. Senechal, and A. M. S. Tremblay. Strong-coupling perturbation theory of the hubbard model. *European Physical Journal B*, 16(1):85–105, 2000.

[75] T. D. Stanescu and G. Kotliar. Strong coupling theory for interacting lattice models. *Physical Review B*, 70(20), 2004.

[76] S. K. SARKER. A new functional integral formalism for strongly correlated fermi systems. *Journal of Physics C-Solid State Physics*, 21(18):L667–L672, 1988.

[77] D. Boies, C. Bourbonnais, and A. M. S. Tremblay. One-particle and 2-particle instability of coupled luttinger liquids. *Physical Review Letters*, 74(6):968–971, 1995.

[78] X. Dai, K. Haule, and G. Kotliar. Strong-coupling solver for the quantum impurity model. *Physical Review B*, 72(4), 2005.

[79] K. Yosida and K. Yamada. Perturbation expansion for the anderson hamiltonian. *Progress of Theoretical Physics Supplement*, 46:244–255, 1970.

[80] K. Yosida and Yamada K. Perturbation expansion for the anderson hamiltonian. iii. *Progress of Theoretical Physics*, 53(5):1286–1301, 1975.

[81] H. Keiter and J. C. Kimball. Diagrammatic perturbation technique for the anderson hamiltonian and relation to the s-d exchange hamiltonian. *International Journal of Magnetism*, 1:233–251, 1971.

[82] H. Park, K. Haule, and G. Kotliar. Cluster Dynamical Mean Field Theory of the Mott Transition. *Physical Review Letters*, 101(18):186403–+, 2008.

[83] I. S. Krivenko, A. N. Rubtsov, M. I. Katsnelson, and A. I. Lichtenstein. Analytical approximation for single-impurity Anderson model. *Soviet Journal of Experimental and Theoretical Physics Letters*, 91:319–325, 2010.

[84] G. Kotliar and D. Vollhardt. Strongly correlated materials: Insights from dynamical mean-field theory. *Physics Today*, 57(3):53–59, 2004.

[85] V. I. Anisimov, A. I. Poteryaev, M. A. Korotin, A. O. Anokhin, and G. Kotliar. First-principles calculations of the electronic structure and spectra of strongly correlated systems: dynamical mean-field theory. *Journal of Physics Condensed Matter*, 9:7359–7367, 1997.

[86] G. Kotliar, S. Y. Savrasov, K. Haule, V. S. Oudovenko, O. Parcollet, and C. A. Marianetti. Electronic structure calculations with dynamical mean-field theory. *Reviews of Modern Physics*, 78(3):865, 2006.

[87] G. D. Mahan. *Many-particle physics*. Kluwer Academic/Plenum Publishers, New York, 3rd ed edition, 2000.

[88] P. W. Anderson. *The Theory of Superconductivity in the High-Cuprates*. Princeton University Press, Princeton, 1997.

[89] S. Sachdev. *Quantum phase transitions*. Cambridge Univ Pr, 2001.

[90] D. J. Scalapino. The case for dx2 - y2 pairing in the cuprate superconductors. *Physics Reports*, 250(6):329 – 365, 1995.

[91] A. I. Lichtenstein and M. I. Katsnelson. Antiferromagnetism and d-wave superconductivity in cuprates: A cluster dynamical mean-field theory. *Phys. Rev. B*, 62 (14):R9283–R9286, 2000.

[92] V. V. Mazurenko, A. I. Lichtenstein, M. I. Katsnelson, I. Dasgupta, T. Saha-Dasgupta, and V. I. Anisimov. Nature of insulating state in $nav2o5$ above charge-ordering transition: A cluster dynamical mean-field study. *Phys. Rev. B*, 66(8): 081104, 2002.

[93] Gabriel Kotliar, Sergej Y. Savrasov, Gunnar Pálsson, and Giulio Biroli. Cellular dynamical mean field approach to strongly correlated systems. *Phys. Rev. Lett.*, 87(18):186401, 2001.

[94] M. Potthoff. Self-energy-functional approach: Analytical results and the Mott-Hubbard transition. *The European Physical Journal B*, 36(3):335–348, 2003.

[95] A. Toschi, A. A. Katanin, and K. Held. Dynamical vertex approximation: A step beyond dynamical mean-field theory. *Physical Review B (Condensed Matter and Materials Physics)*, 75(4):045118, 2007.

[96] C. Slezak, M. Jarrell, Th Maier, and J. Deisz. Multi-scale extensions to quantum cluster methods for strongly correlated electron systems, 2006.

[97] D. Goldhaber-Gordon, H. Shtrikman, D. Mahalu, D. Abusch-Magder, U. Meirav, and M. A. Kastner. Kondo effect in a single-electron transistor. *Nature*, 391(6663): 156–159, 1998.

[98] H. Kishida, M. Ono, K. Miura, H. Okamoto, M. Izumi, T. Manako, M. Kawasaki, Y. Taguchi, Y. Tokura, T. Tohyama, K. Tsutsui, and S. Maekawa. Large third-order optical nonlinearity of cu-o chains investigated by third-harmonic generation spectroscopy. *Physical Review Letters*, 87(17), 2001.

[99] L. Hackermueller, U. Schneider, M. Moreno-Cardoner, T. Kitagawa, T. Best, S. Will, E. Demler, E. Altman, I. Bloch, and B. Paredes. Anomalous expansion of attractively interacting fermionic atoms in an optical lattice. *Science*, 327 (5973):1621–1624, 2010.

[100] M. Wagner. Expansions of nonequilibrium green-functions. *Physical Review B*, 44 (12):6104–6117, 1991.

[101] A. Kamenev and A. Levchenko. Keldysh technique and non-linear σ-model: basic principles and applications. *Advances in Physics*, 58:197–319, 2009.

Danksagung

An dieser Stelle möchte ich mich recht herzlich bei all jenen bedanken, die zum Gelingen dieser Arbeit beigetragen haben und mich in den vergangenen 3 Jahren auf die eine oder andere Art unterstützt haben.
Meinen besonderen Dank möchte zu Anfang an meinen Betreuer Alexander Lichtenstein richten. Für das Bereitstellen eines sehr interessanten Themas, sehr gute Arbeitsbedingungen, aber auch für gute und warmherzige Ratschläge möchte ich ihm meinen aufrichtigen Dank aussprechen. Durch viele interessante Diskussionen und die Möglichkeit an Konferenzen in aller Welt teilzunehmen hat er nicht nur zum Erfolg dieser Arbeit beigetragen, sondern auch meinen Horizont erweitert.
Bei Frank Lechermann bedanke ich mich für das zügige Erstellen des Zweitgutachtens und das Generieren diverser LDA Hamiltonians. Des Weiteren möchte ich mich bei all jenen bedanken, die mich wissenschaftlich auf meinem Weg begleitet haben. Insbesondere danke ich Alexey Rubtsov für viele hilfreiche Diskussionen und die Einladung auf eine wundervolle Wolga Konferenz. Auch seinen Studenten Igor Krivenko und Andrey Antipov danke ich recht herzlich für den offenen Austausch von Computer Code, aber auch für die netten Abende, die wir zusammen in Moskau und Hamburg verbracht haben.
Gleiches gilt auch für Philipp Werner und Emanuel Gull, die mich gerade zu Beginn meiner Arbeit beim Umgang mit diversen Monte Carlo Programmen unterstützt haben. Besonders danke ich Philipp, der mich bei meinen ersten Gehversuchen in exakter Diagonalisierung begleitet hat.
Besonders möchte ich auch Erik Koch danken, der es in 15 Minuten geschafft hat, mich in die fortgeschrittenen Geheimnisse exakter Diagonalisierung einzuweihen. Diese 15 Minuten haben mir sehr viel Arbeit erspart, wofür ich sehr dankbar bin.
Desweiteren danke ich Frithjof Anders für das Bereitstellen von NRG Daten und seine erhellenden Kommentare zum Kondo scaling.
Auf meinen Reisen bin ich immer wieder sehr freundlich aufgenommen worden und mir wurde jede Hilfe entgegen gebracht, die ich benötigte. Besonders danke ich Alexander Shick für eine gute Zeit in Prag und Christoph Piefke, der mich in die französischen Alpen begleitet hat.
Während eines dreijährigen Projektes ist man nicht nur auf fachliche Hilfe angewiesen.

Insbesondere der gute Kontakt zu meinen Kollegen hat mich immer wieder motiviert und meine Stimmung oben gehalten. Ich bedanke mich an dieser Stelle bei allen Mitgliedern der Gruppe magno für ihre Unterstützung und das Übernehmen diverser Prüfungsbeisitze. Insbesondere bedanke ich mich bei Aljoscha Wilhelm und Alexander Lieder, die mich am Ende meiner Arbeit bei der Fertigstellung diverser Projekte unterstützt haben. Auch Tim Wehling sei an dieser Stelle für diverse "geliehene" Zuckerwürfel gedankt. Für eine Einweisung in die verbotenen Tricks von LaTeX und diverse Erläuterungen zur Bundesliga Tabelle bedanke ich mich recht herzlich bei Björn Vogt.
Besonderen Dank schulde ich an dieser Stelle auch Hartmut Hafermann, der mich mit Rat und Tat bei all meinen Projekten unterstützt hat. Einen besonderen Dank hat sich auch Sergey Brener verdient, der mich während meiner Arbeit immer beim Finden diverser Fehler in Programmen unterstützt hat und der mit Aussagen wie "Warum dauert das invertieren einer Matrix solange?" zu der guten Performance meiner Codes beigetragen hat.
Bedanken möchte ich mich auch bei allen Mitgliedern des Instituts die mir mit wertvollem Rat beiseite gestanden haben. Ich danke insbesondere Michael Potthoff für wertvolle Diskussionen bezüglich Lanczos und die Form der Keldysh Kontour. Herrn Scharnberg danke ich für eine spannende Wanderung durch die Heide mit anschließendem Kaffee und Kuchen.
Besonders danke ich auch Bodo Krause-Kyora für die Betreung bei allen computerrelevanten Fragen. Ich möchte an dieser Stelle auch den immer freundlichen Menschen der Verwaltung danken, die mich bei vielen bürokratischen Vorgängen unterstützt haben. Insbesondere danke ich hier Juan Mercado, der immer wieder ein hohes Maß an Verständnis für die bürokratischen Unzulänglichkeiten junger Doktoranden aufbringt und mich sehr stark bei der Verlängerung meines Vertrages unterstützt hat. Besonderen Dank möchte ich in dieser Sache auch an die Mitarbeiter des Sekretariats, Frau Sen und Frau Schmidtke richten.
Für das Korrekturlesen meiner Arbeit bedanke ich mich recht herzlich bei Jindrich Kolorenc, Oleg Peil und Sergey Schuwalow.
Ich möchte mich bei all meinen Freunden für ihre Unterstützung bedanken und für das Verständnis, dass ich mich im letzten halben Jahr etwas rar gemacht habe. Besonderen

Dank richte ich hier an meine beiden Spielrunden, bei denen ich herrliche Abende verbracht habe und an die Waldsportguppe Norderstedt sowie die Karate Abteilung des Tura, die für meine körperliche Fitness gesorgt haben.
Meiner Familie und insbesondere meinen Eltern danke ich für ihre stete Unterstützung in meinen Leben und die vielen guten Worte, die mich immer motiviert haben. Ein besonderer Dank gilt auch meiner zukünftigen Frau Ina, die im letzten Jahr unendlich viel Geduld mit mir hatte und sehr viel Rücksicht geübt hat. Ohne ihre stete Motivation wäre mir die Arbeit sehr viel schwerer gefallen.

Im Hamburger Spätsommer *Christoph Jung*